The VVV survey: a window to the inner Galactic globular clusters

Javier Alonso-García

Pontificia Universidad Católica

The VVV infrared GC catalog

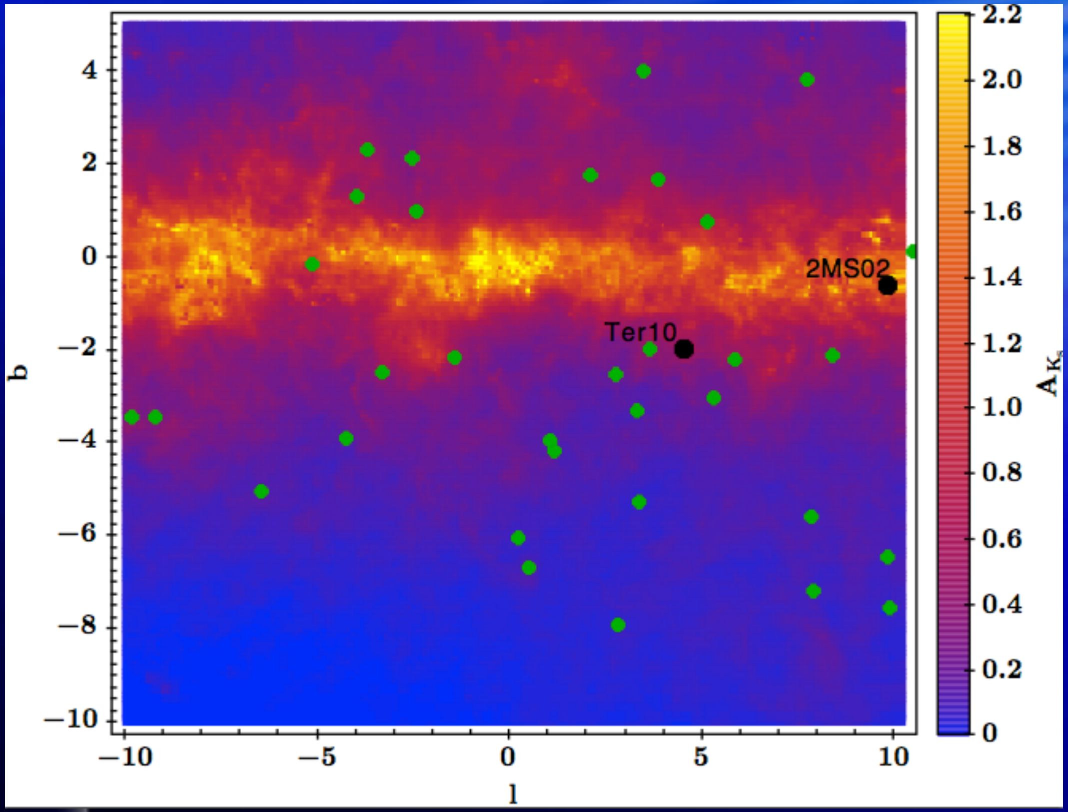

- 36 inner Galaxy GCs in Harris catalog
- Half metal-poor (-1.7<[Fe/H]<-1), half metal-rich (-1<[Fe/H<-0.1)

2MASS-GC02 Terzan 10

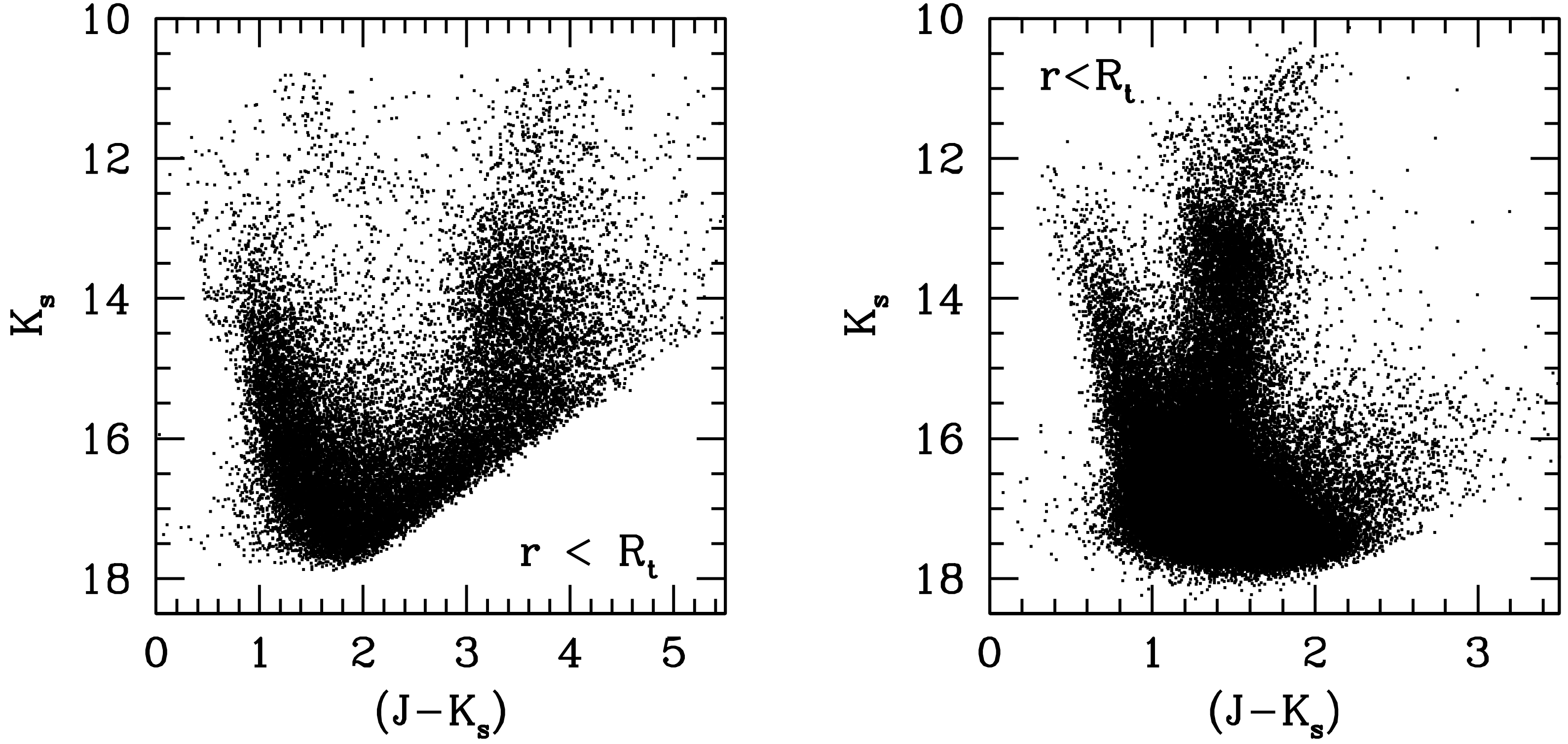

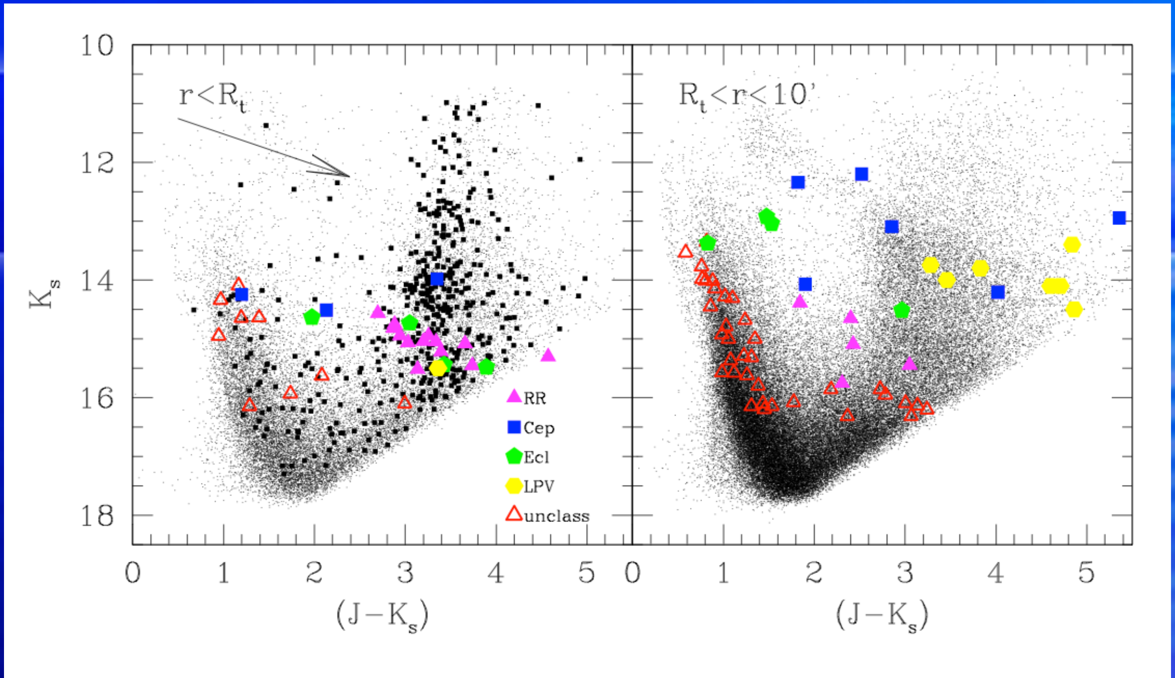

2MASS-GC02

42 epochs

Inside R_{tidal}
32 variables
(13 RRLyrae)

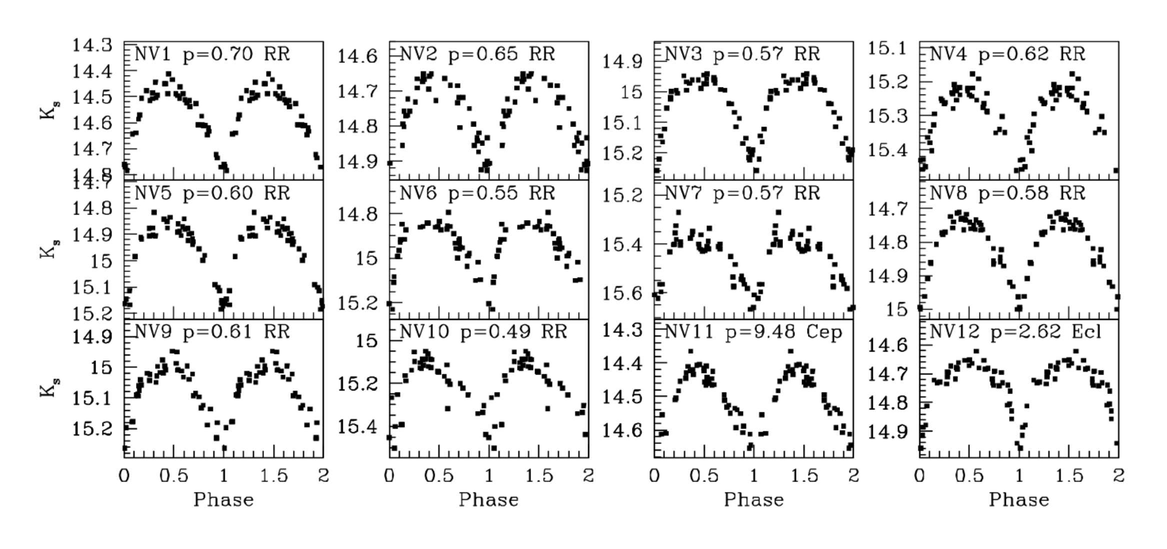

Terzan 10

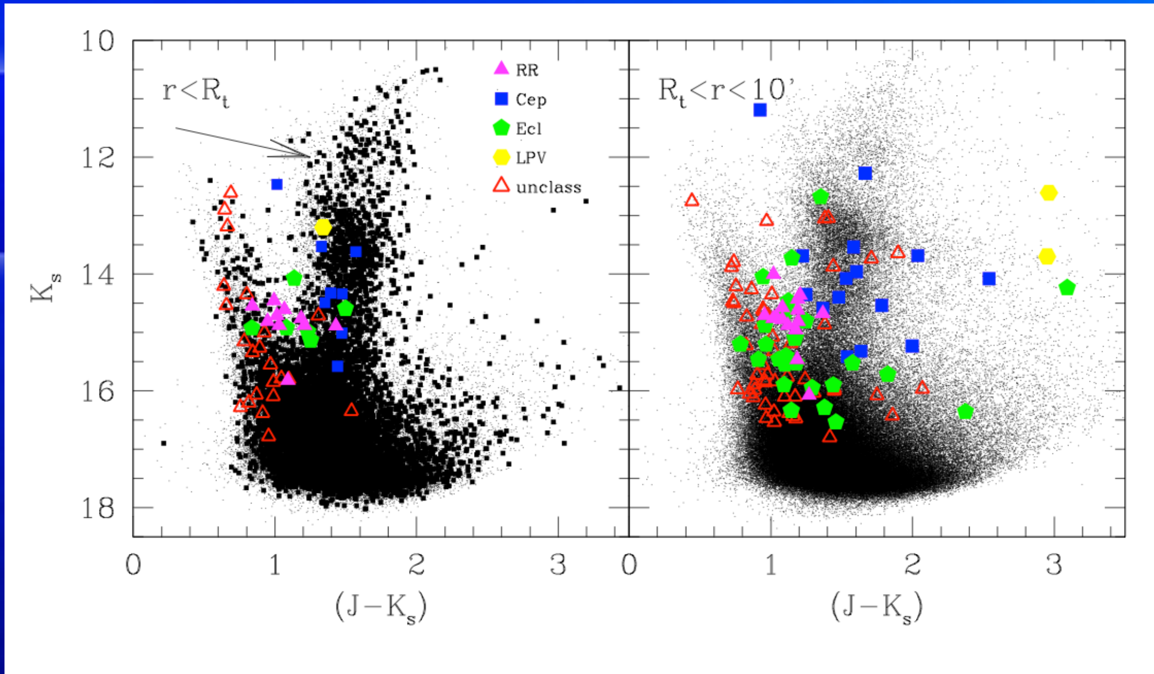

101 epochs

Inside R_{tidal}
48 variables
(10 RRLyrae)

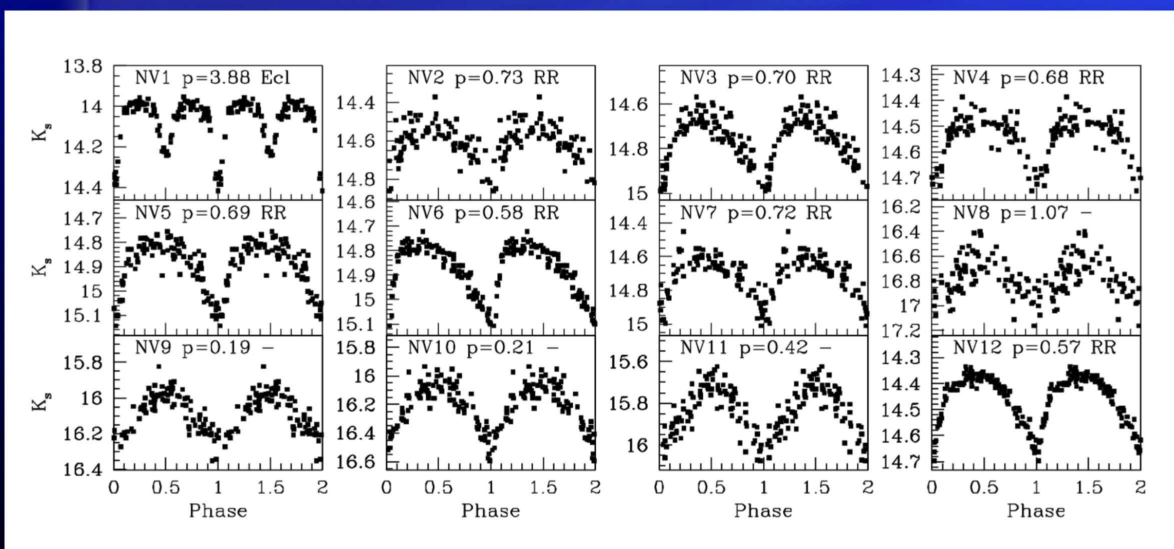

2MASS-GC02

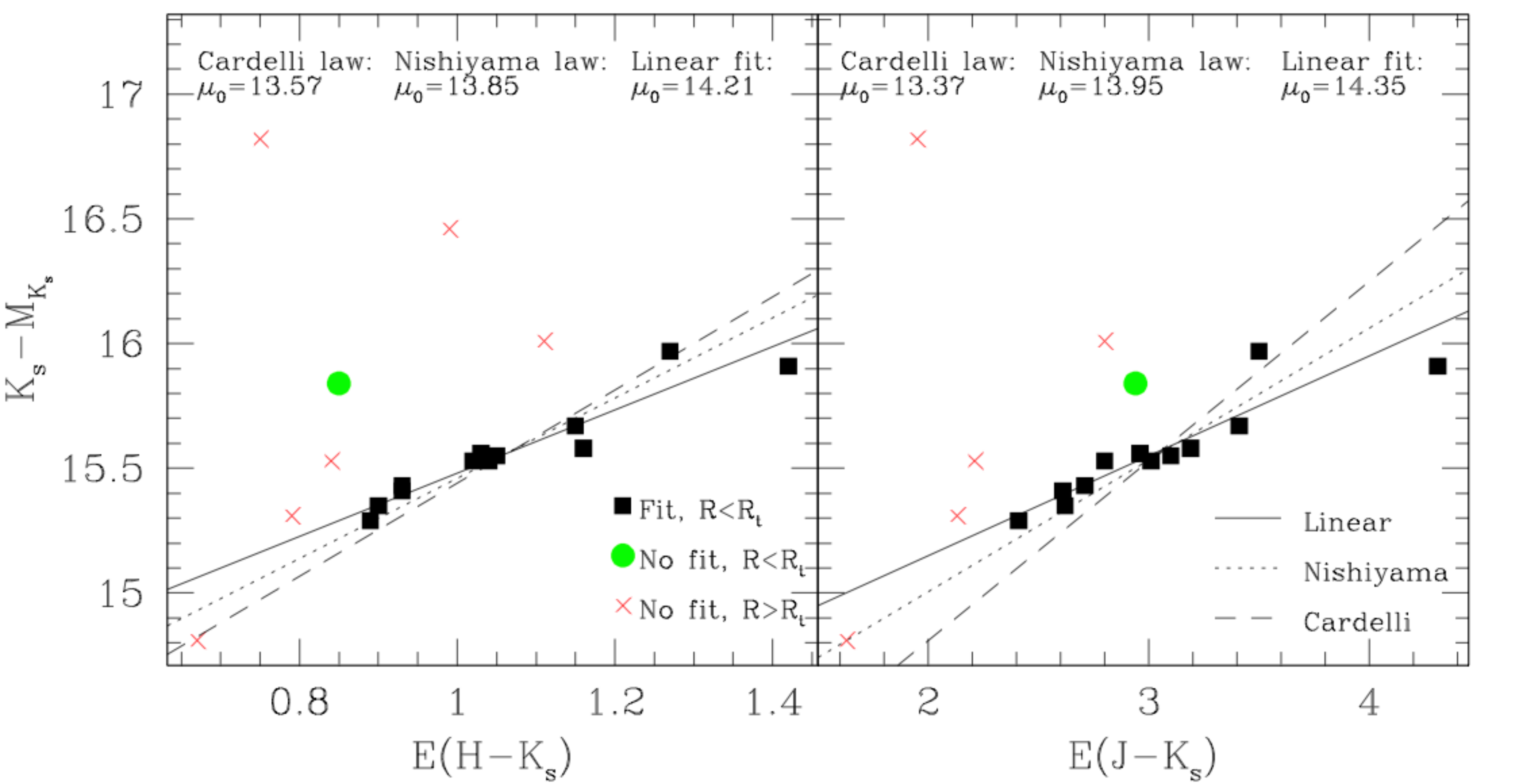

Cardelli law: μ_0=13.57
Nishiyama law: μ_0=13.85
Linear fit: μ_0=14.21
Cardelli law: μ_0=13.37
Nishiyama law: μ_0=13.95
Linear fit: μ_0=14.35
Fit, R<R$_t$
No fit, R<R$_t$
No fit, R>R$_t$
Linear
Nishiyama
Cardelli
17
16.5
16
15.5
15
0.8
1
1.2
1.4
2
3
4
$K_s - M_{K_s}$
$E(H-K_s)$
$E(J-K_s)$

Terzan 10

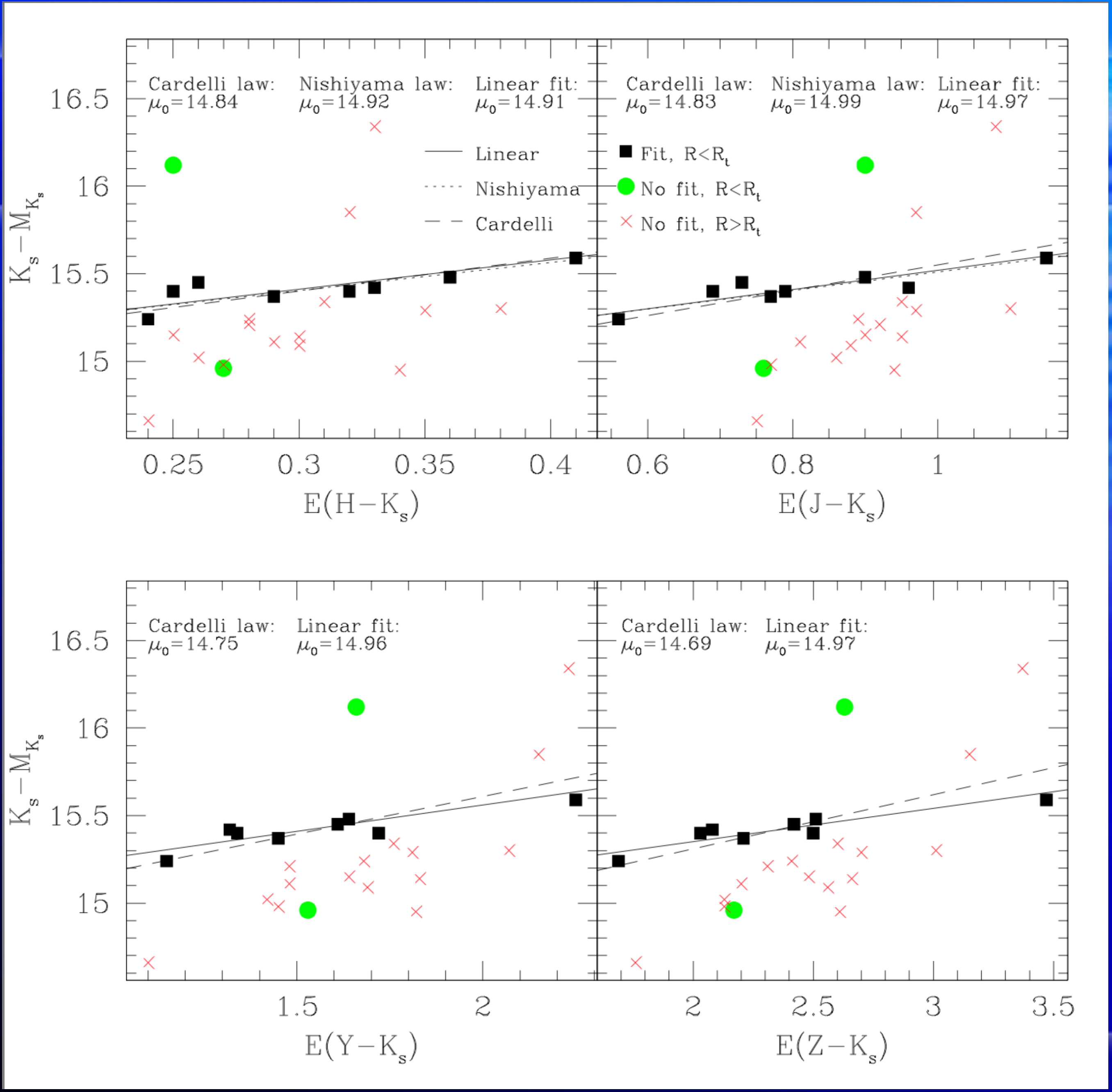

Cardelli law: μ_0=14.84
Nishiyama law: μ_0=14.92
Linear fit: μ_0=14.91
Linear
Nishiyama
Cardelli
$K_s - M_{K_s}$
E(H−K_s)
Cardelli law: μ_0=14.83
Nishiyama law: μ_0=14.99
Linear fit: μ_0=14.97
Fit, R<R_t
No fit, R<R_t
No fit, R>R_t
E(J−K_s)
Cardelli law: μ_0=14.75
Linear fit: μ_0=14.96
E(Y−K_s)
Cardelli law: μ_0=14.69
Linear fit: μ_0=14.97
E(Z−K_s)

Extinctions

	2MASS-GC02	Terzan 10	Nishiyama09	Cardelli89
$A_{K_s}/E(H-K_s)$	1.27±0.18±0.23	$1.67\pm0.28^{-0.06}_{-0.31}$	1.61±0.04	1.87
$A_{K_s}/E(J-K_s)$	0.40±0.08±0.13	0.55±0.06±0.08	0.528±0.015	0.72
$A_{K_s}/E(Y-K_s)$	···	0.30±0.05±0.09	···	0.43
$A_{K_s}/E(Z-K_s)$	···	0.19±0.03±0.07	···	0.31

Distances

	$R_{\odot,\mathrm{Harris96}}$ (kpc)	$R_{GC,\mathrm{Harris96}}$[1] (kpc)	$E(B-V)_{\mathrm{Harris96}}$	$R_{\odot,\mathrm{derived}}$ (kpc)	$R_{GC,\mathrm{derived}}$[1] (kpc)	$E(J-K_s)_{\mathrm{derived}}$
2MASS-GC02	4.9	-3.2	5.16	$7.1\pm0.5\pm0.9$	$-1.6\pm0.2\pm^{0.6}_{0.2}$	2.92
Terzan 10	5.8	-2.3	2.40	$9.8\pm0.2\pm0.5$	$+2.0\pm0.2\pm0.4$	0.82

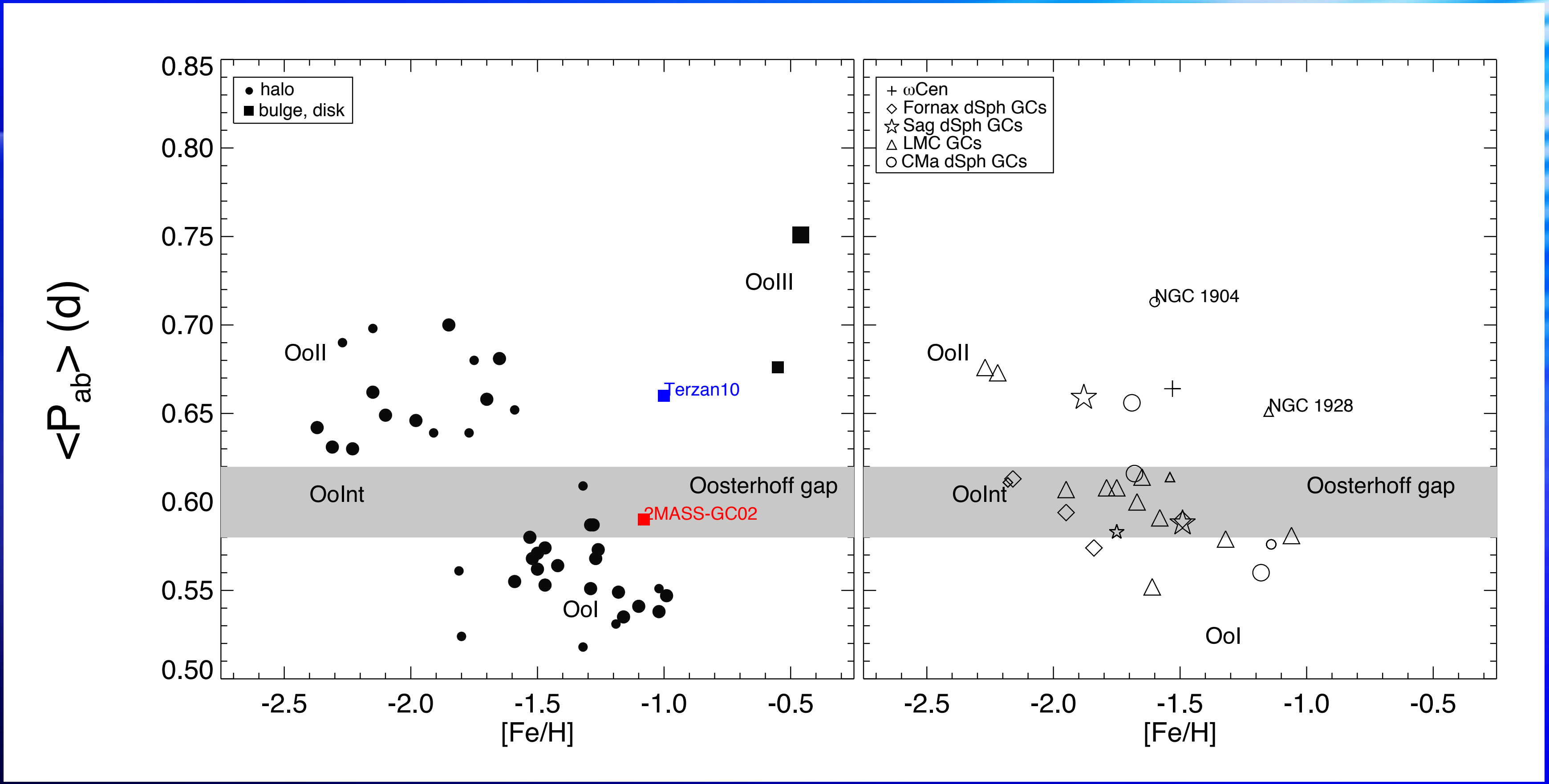

2MASS-GC02: <P>=0.59d [Fe/H] = -1.08

Terzan 10: <P>= 0.66d [Fe/H] = -1.00

Distance determination to Omega Centauri with optical and NIR photometry of RR Lyrae

Vittorio Francesco Braga[1,2]

UNIVERSITA' degli STUDI di ROMA
TOR VERGATA

SAPIENZA
UNIVERSITÀ DI ROMA

Bono G.[1], Stetson P.B.[3], Dall'Ora M.[4], Marconi M.[4], Coppola G.[4], Ferraro I.[5], Buonanno R.[1], Iannicola G.[5], Neeley J.[6], Marengo M.[6], CRRP collaboration[7]

(1) Università di Roma Tor Vergata, Italy (2) Università di Roma Sapienza, Italy (3) NRC-DAO, Victoria, Canada (4) Osservatorio Astronomico di Capodimonte, Italy, (5) Osservatorio Astronomico di Roma, Italy (6) Iowa State University, USA (7) Carnegie Observatories, USA

Why RR Lyr?

- Population II... Population II everywhere (Spirals: Halo, bulge, thick disk; Ellipticals)
- Independent check on other methods (Cepheid PL relation, TRGB, MS fitting, ZAHB fitting...)
- By-product: Galactic bulge 3D structure, old population tracer

Why IR?

- Lower extinction
- Lower systematics due to reddening law
- Theoretically lower metallicity effects ☠

Why GCs?

- Same distance, reddening, age, metallicity (NOT Omega Cen)
- Homogeneous metallicity scales (*Zinn&West, 1984*, *Carretta et al. 2009*)
- Homogeneous age scales (*Salaris&Weiss, 2002, Marin-Franch et al. 2009, VandenBerg et al. 2013*)
- ...not a homogeneous distance scale

Period-Luminosity (PL) and Period-Wesenheit (PW) relations

$$M_K = a + b * \log P$$

Observed NIR PL
Longmore et al. (1986)

$$M_K = a + b * \log P + c * \log Z$$

Theoretical PLZ
Bono et al. (2001,2003)

$$M_X = a_X + b_X * \log P + c_X * \log Z$$

Theoretical PLZ
Catelan et al. (2004)

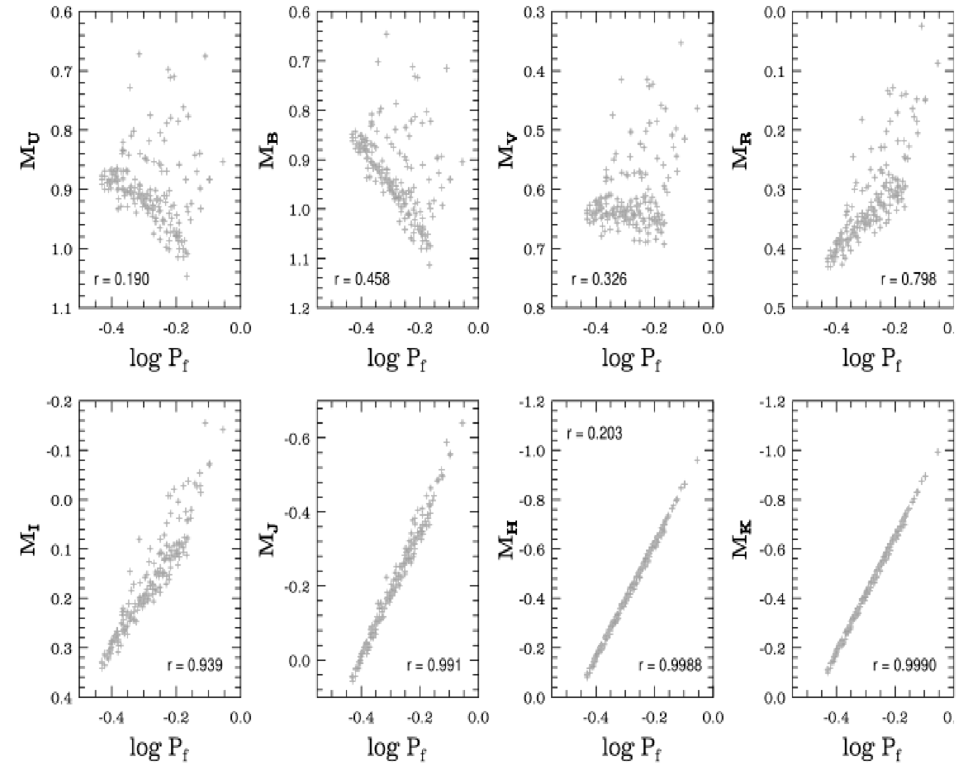

Catelan et al. (2004)

Wesenheit magnitude: reddening independent!

$$W_{YZ}^{X} = X - \left(\frac{A_Y}{A_X} - \frac{A_Z}{A_X}\right)^{-1} (Y - Z)$$

Omega Centauri

DM_0 [mag]	13.70±0.06	(1)
[Fe/H]	[-2.2,-0.9]	(2,3)
Reddening law	Cardelli et al. 1989	(4)
E(B-V)	0.11±0.02	(1)
R_V	3.1	(4)
RRL number	192	(5)

(1) Del Principe et al. (2006); (2) Rey et al. (2000); (3) Sollima et al. (2006); (4) Cardelli et al. (1989); (5) Kaluzny et al. (2004)

New photometry for RRL; highest number of RRL; metallicity spread

Omega Cen data and analysis

BVI photometry: ESO/Danish 1.54m over 6 years + other over 21 years. Up to ~1700 phase points per light curve

JK photometry: Del Principe et al. (2006) and references therein

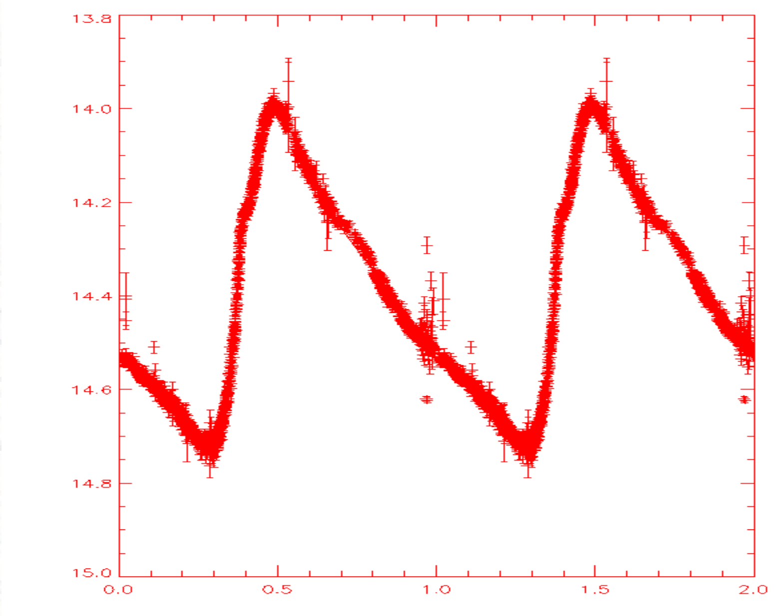

Period measure

- Lomb-Scargle variant
- Phase dispersion minimization

Mean magnitude estimate

- Average over spline fit
- Average over template fit (K band)
- Average over phase points (badly sampled)

PLZ and PWZ calibration: Pulsation models from *Marconi et al. (2014, in preparation)*

Empirical PLZ and PWZ relations

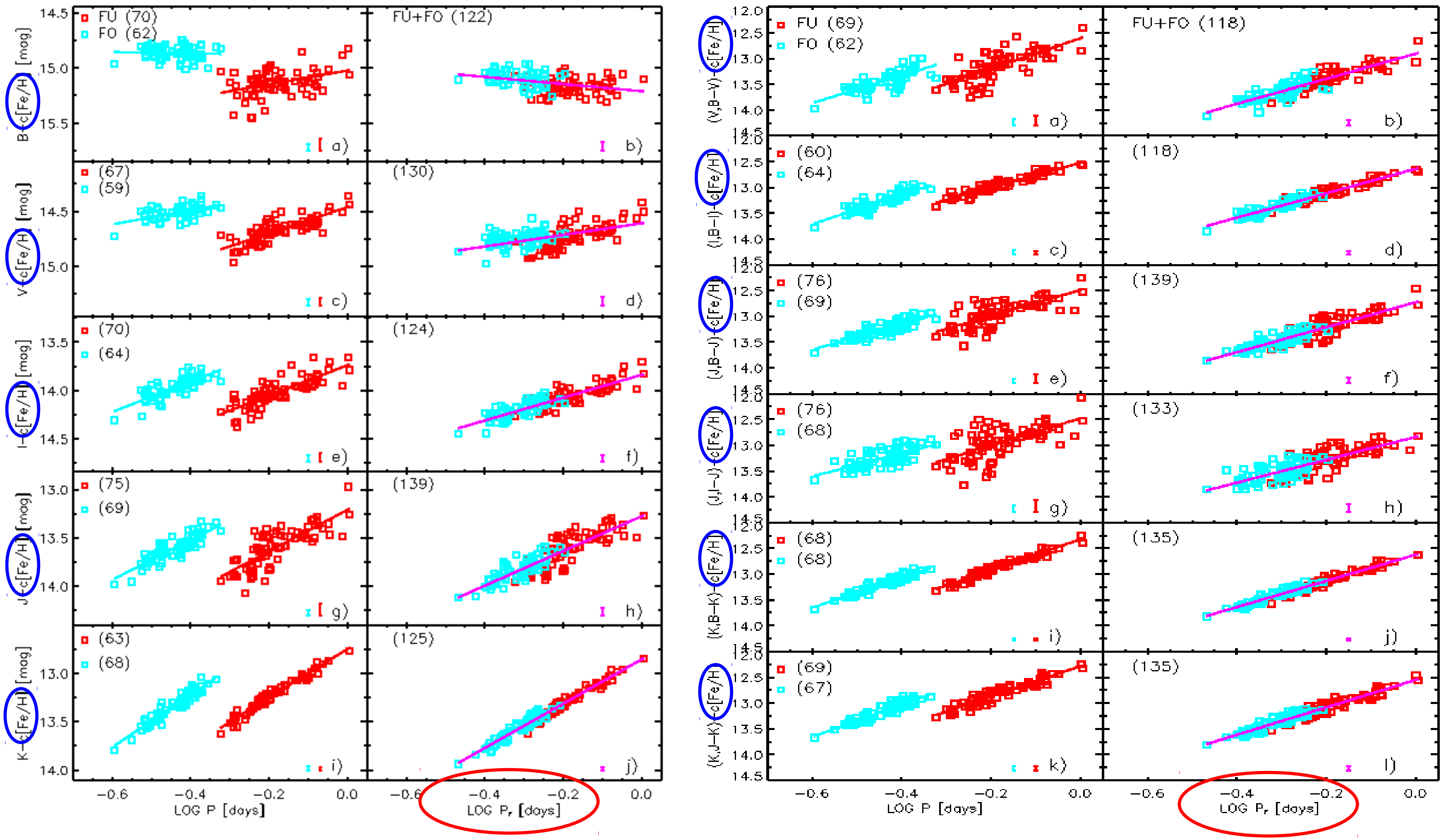

FO period is fundamentalized: $\log P_F = \log P + 0.127$

Subtracted metallicity term

Distance modulus estimate

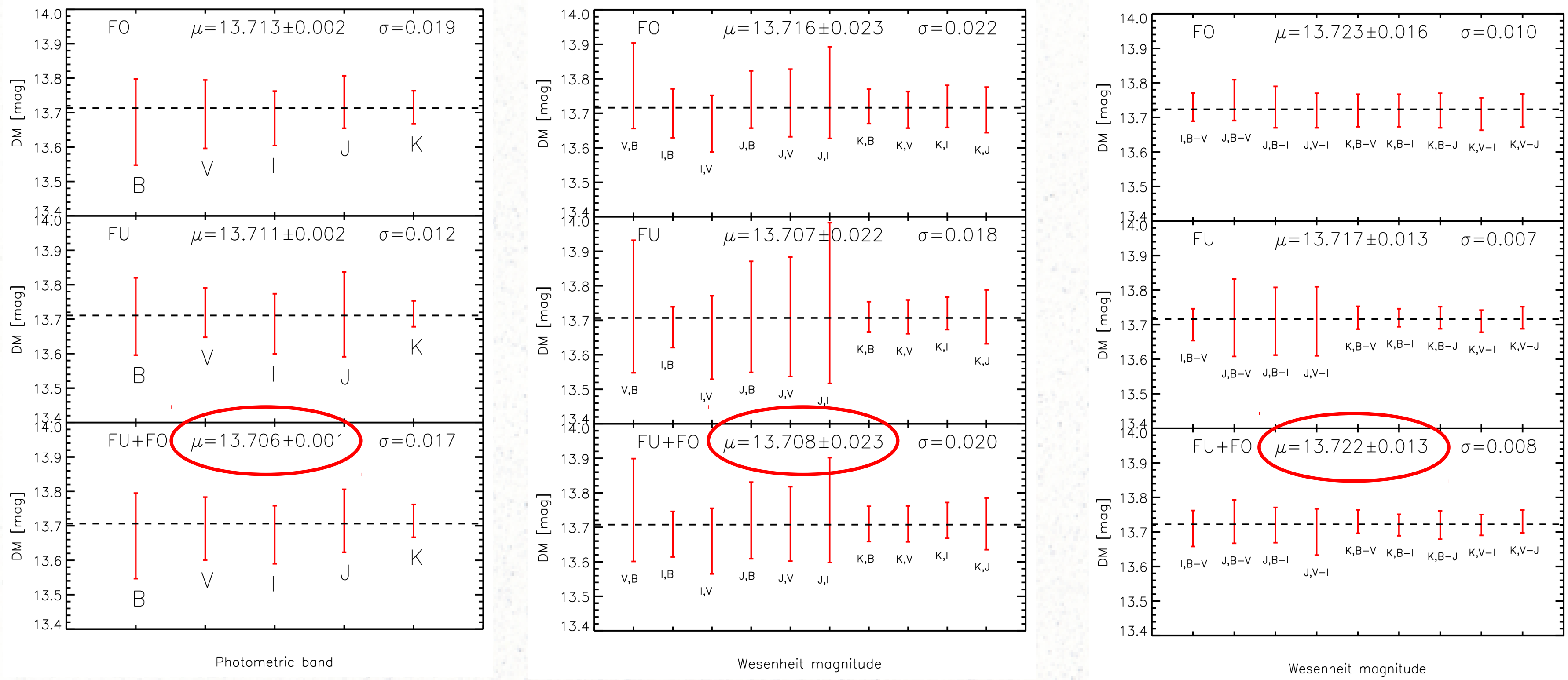

μ=13.711 ± 0.005 ± 0.003 mag

Agreement with literature
- Del Principe et al. (2006): 13.70 (RRL JK PLZ relation)
- Thompson et al. (2001): 13.64 (eclipsing binaries)
- Kiron et al. (2011): 13.60 (W UMa stars)

Metallicity correction does matter and is going in the right way!

Probing the Circumnuclear Stellar Populations of Starburst Galaxies in the Near-infrared

Poster #5

Natacha Zanon Dametto

PhD student at Institute of Physics of UFRGS (Porto Alegre, Brazil)

Advisor:
Rogério Riffel

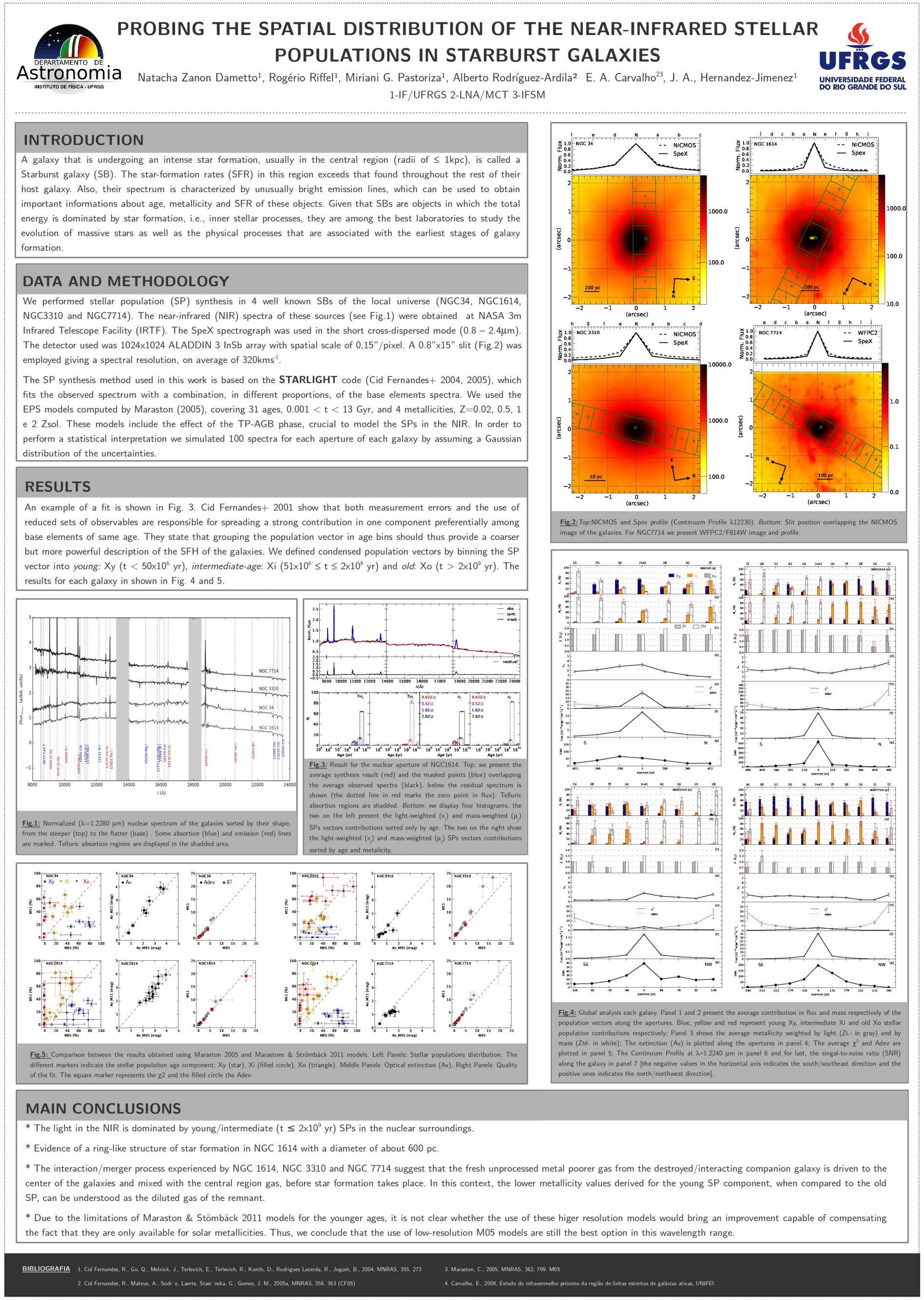

MAIN GOAL

Analyze the spacial distribution of the stellar populations (SPs), in the NIR, of 4 well known Starburst Galaxies, by means of SP fitting.

NGC 34

NGC 1614

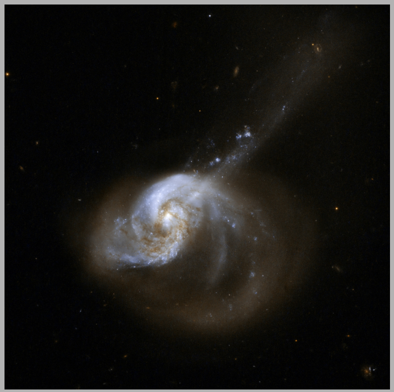

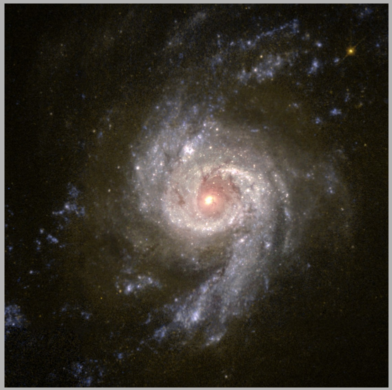

NGC 3310

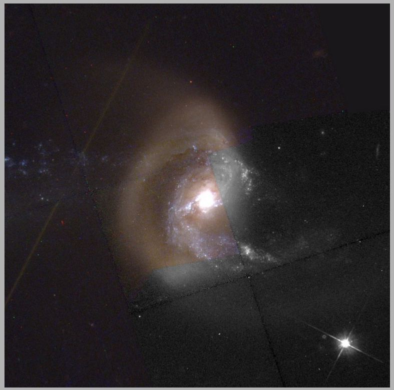

NGC 7714

MAIN GOAL

Analyze the spacial distribution of the stellar populations (SPs), in the NIR, of 4 well known Starburst Galaxies, by means of SP fitting.

THE DATA

The near-infrared (NIR) spectra of these sources were obtained at NASA 3m Infrared Telescope Facility (IRTF). The SpeX spectrograph was used in the short cross-dispersed mode (0.8 – 2.4mm). The average spectral resolution was 320kms^{-1}.

NGC 34

NGC 1614

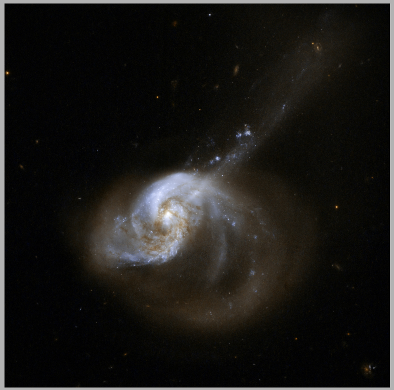

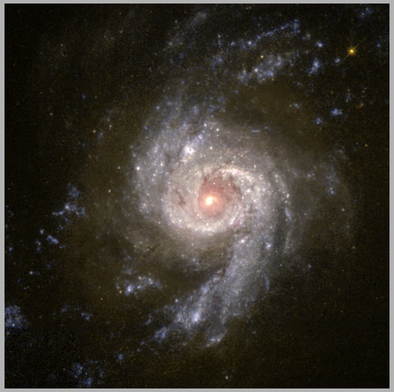

NGC 3310

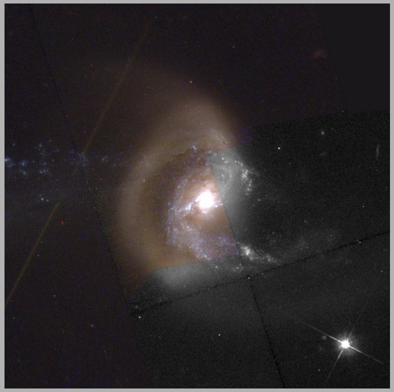

NGC 7714

MAIN GOAL

Analyze the spacial distribution of the stellar populations (SPs), in the NIR, of 4 well known Starburst Galaxies, by means of SP fitting.

THE DATA

The near-infrared (NIR) spectra of these sources were obtained at NASA 3m Infrared Telescope Facility (IRTF). The SpeX spectrograph was used in the short cross-dispersed mode (0.8 – 2.4mm). The average spectral resolution was $320kms^{-1}$.

METHODOLOGY

The SP synthesis method used in this work is based on the STARLIGHT code (Cid Fernandes+ 2004, 2005).

*EPS models computed by Maraston (2005).

NGC 34

NGC 1614

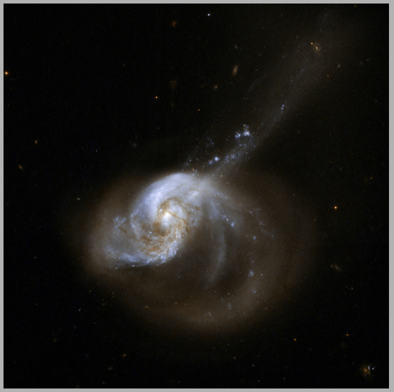

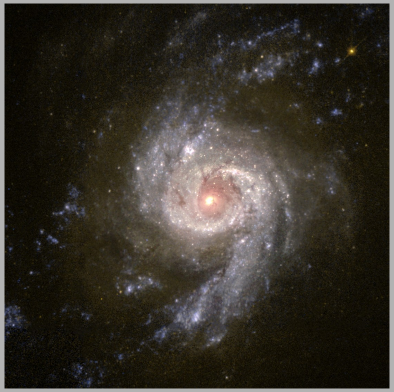

NGC 3310

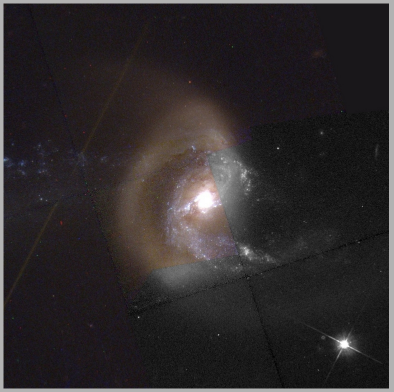

NGC 7714

MAIN RESULTS

* The light in the NIR is dominated by young/intermediate (t ≤ $2x10^9$ yr) SPs in the nuclear surroundings.

NGC 1614

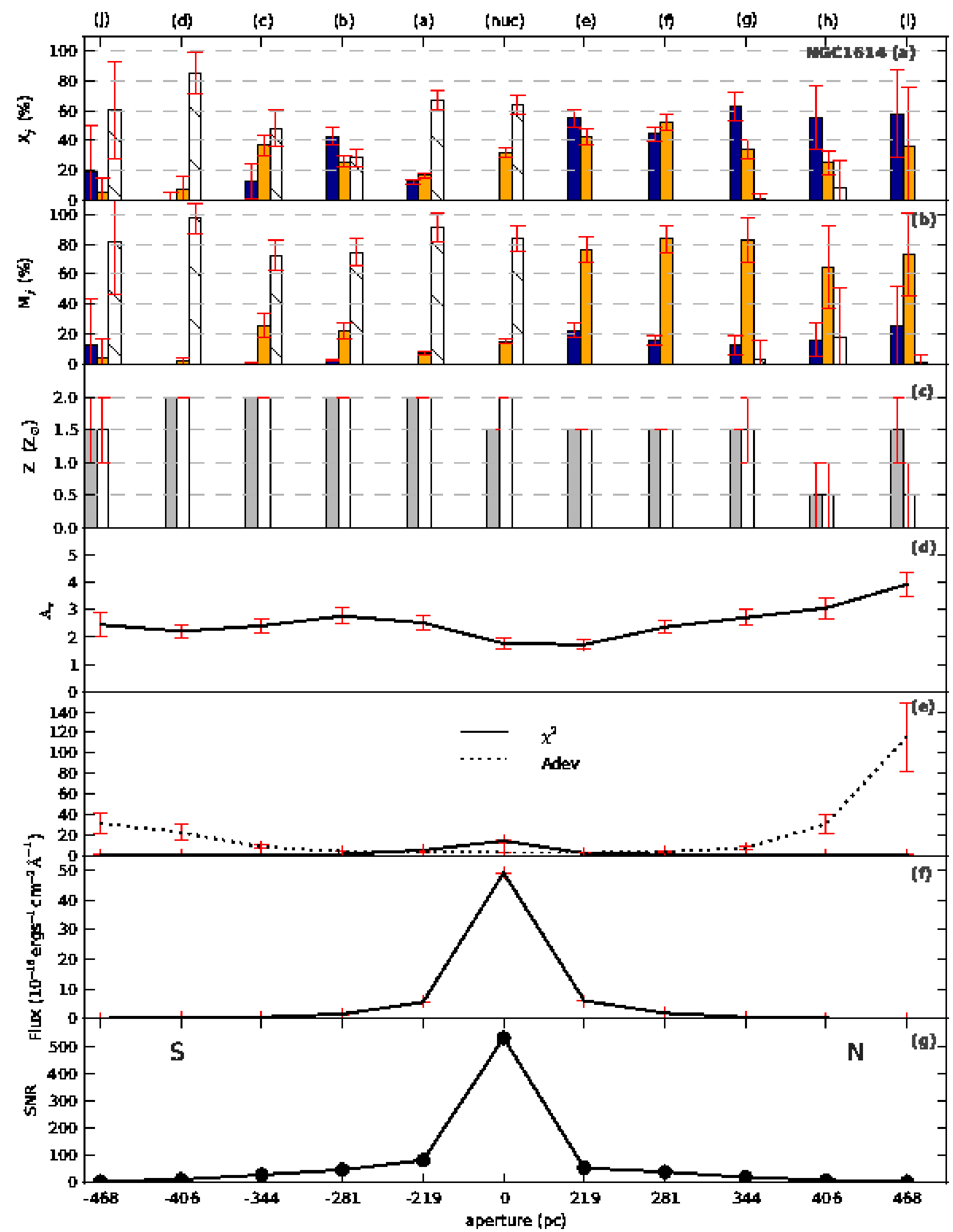

MAIN RESULTS

* The light in the NIR is dominated by young/intermediate (t ≤ 2x10^9 yr) SPs in the nuclear surroundings.

* Evidence of a ring-like structure of star formation in NGC 1614 with a diameter of about 600 pc.

NGC 1614

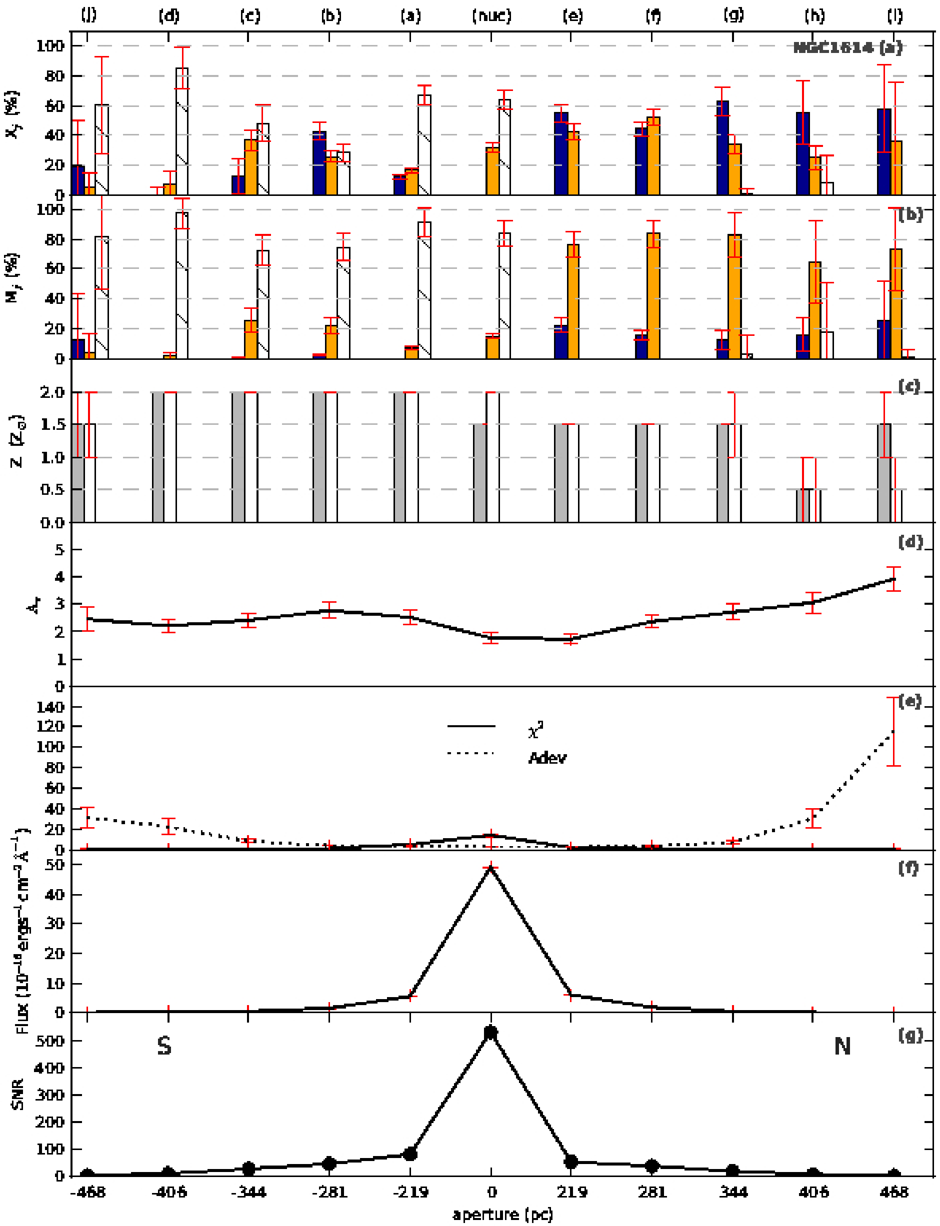

MAIN RESULTS

* The light in the NIR is dominated by young/intermediate (t ≤ 2×10^9 yr) SPs in the nuclear surroundings.

* Evidence of a ring-like structure of star formation in NGC 1614 with a diameter of about 600 pc.

* The lower metallicity values derived for the young SP component, when compared to the old SP, can be understood as the diluted gas of the remnant (interaction/merger process).

NGC 1614

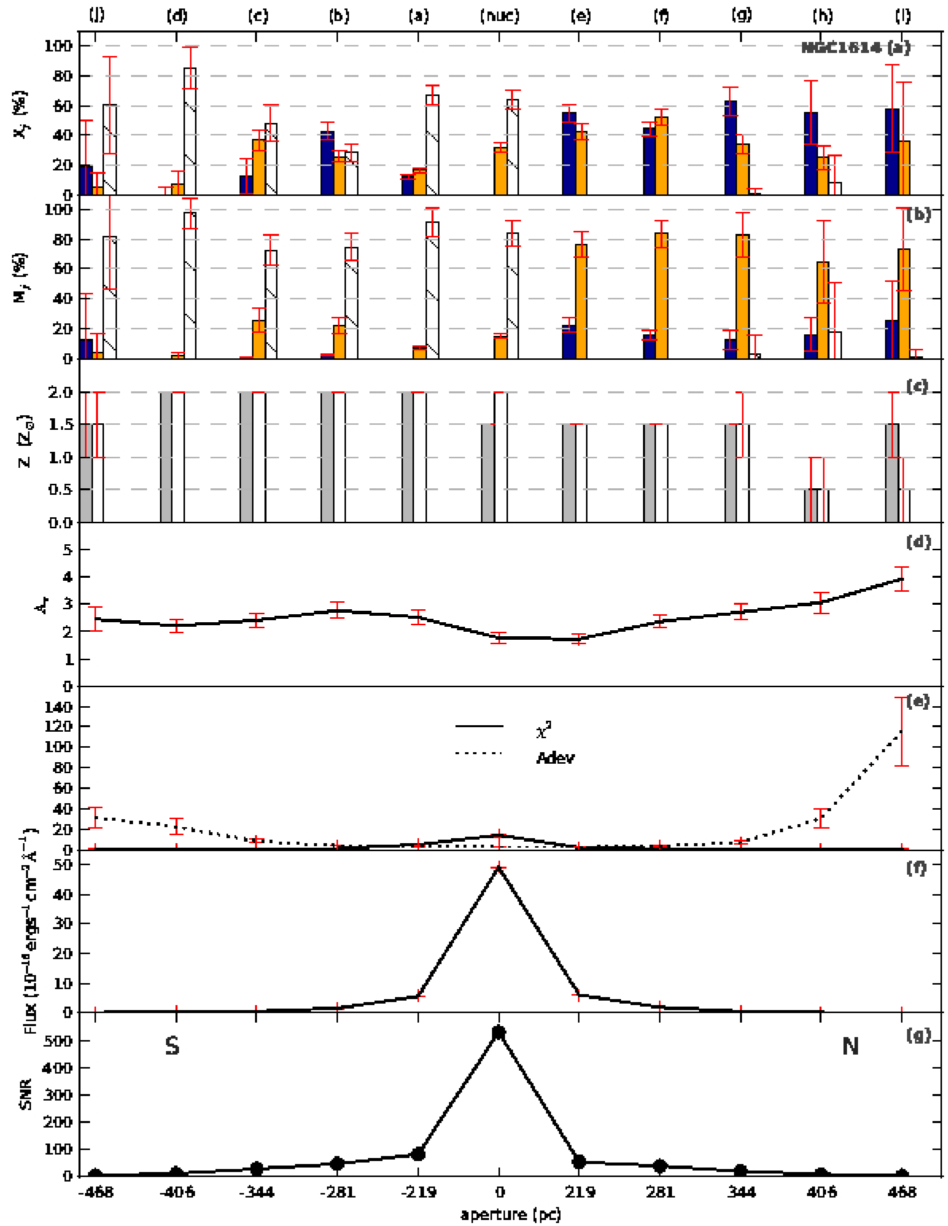

MAIN RESULTS

* The light in the NIR is dominated by young/intermediate ($t \leq 2x10^9$ yr) SPs in the nuclear surroundings.

* Evidence of a ring-like structure of star formation in NGC 1614 with a diameter of about 600 pc.

* The lower metallicity values derived for the young SP component, when compared to the old SP, can be understood as the diluted gas of the remnant (interaction/merger process).

* Due to the limitations of Maraston & Stömbäck 2011 models for the younger ages, we conclude that the use of low-resolution M05 models are still the best option in this wavelength range.

NGC 1614

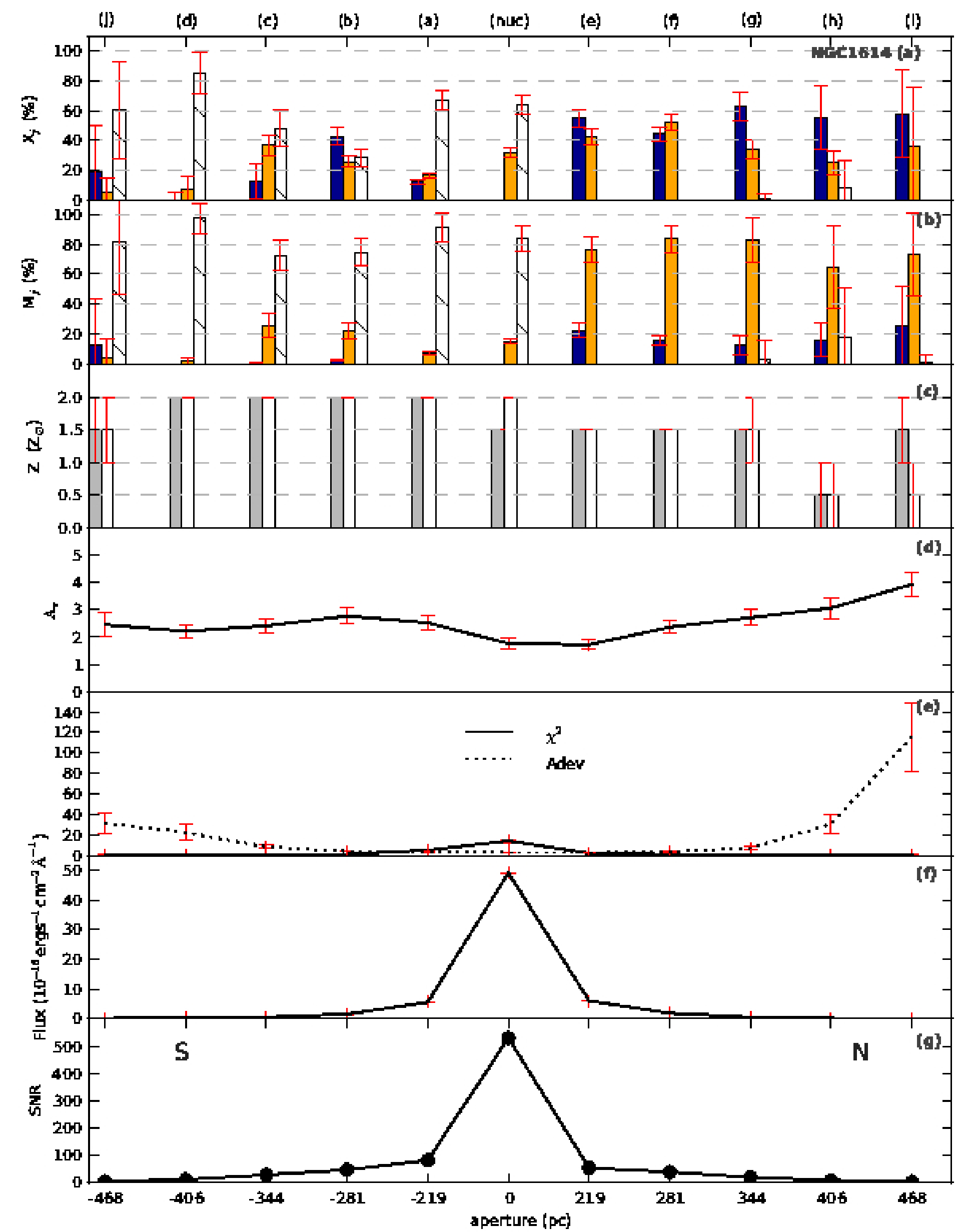

For more informations:

Poster #5

Thanks for the attention!

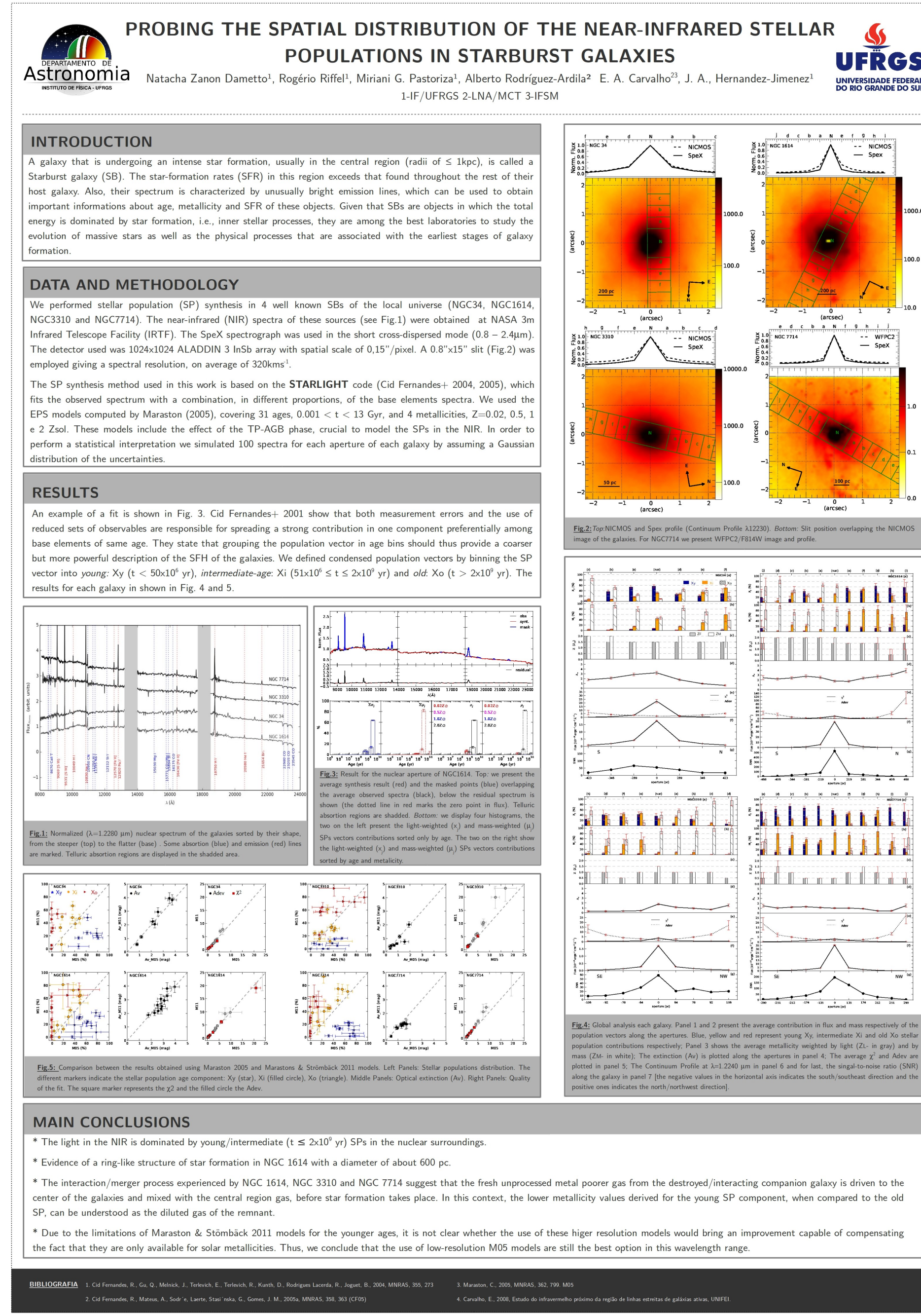

PROBING THE SPATIAL DISTRIBUTION OF THE NEAR-INFRARED STELLAR POPULATIONS IN STARBURST GALAXIES

Natacha Zanon Dametto[1], Rogério Riffel[1], Miriani G. Pastoriza[1], Alberto Rodríguez-Ardila[2] E. A. Carvalho[23], J. A., Hernandez-Jimenez[1]
1-IF/UFRGS 2-LNA/MCT 3-IFSM

INTRODUCTION

A galaxy that is undergoing an intense star formation, usually in the central region (radii of ≤ 1kpc), is called a Starburst galaxy (SB). The star-formation rates (SFR) in this region exceeds that found throughout the rest of their host galaxy. Also, their spectrum is characterized by unusually bright emission lines, which can be used to obtain important informations about age, metallicity and SFR of these objects. Given that SBs are objects in which the total energy is dominated by star formation, i.e., inner stellar processes, they are among the best laboratories to study the evolution of massive stars as well as the physical processes that are associated with the earliest stages of galaxy formation.

DATA AND METHODOLOGY

We performed stellar population (SP) synthesis in 4 well known SBs of the local universe (NGC34, NGC1614, NGC3310 and NGC7714). The near-infrared (NIR) spectra of these sources (see Fig.1) were obtained at NASA 3m Infrared Telescope Facility (IRTF). The SpeX spectrograph was used in the short cross-dispersed mode (0.8 – 2.4µm). The detector used was 1024x1024 ALADDIN 3 InSb array with spatial scale of 0,15"/pixel. A 0.8"x15" slit (Fig.2) was employed giving a spectral resolution, on average of 320kms^{-1}.

The SP synthesis method used in this work is based on the **STARLIGHT** code (Cid Fernandes+ 2004, 2005), which fits the observed spectrum with a combination, in different proportions, of the base elements spectra. We used the EPS models computed by Maraston (2005), covering 31 ages, $0.001 < t < 13$ Gyr, and 4 metallicities, Z=0.02, 0.5, 1 e 2 Zsol. These models include the effect of the TP-AGB phase, crucial to model the SPs in the NIR. In order to perform a statistical interpretation we simulated 100 spectra for each aperture of each galaxy by assuming a Gaussian distribution of the uncertainties.

RESULTS

An example of a fit is shown in Fig. 3. Cid Fernandes+ 2001 show that both measurement errors and the use of reduced sets of observables are responsible for spreading a strong contribution in one component preferentially among base elements of same age. They state that grouping the population vector in age bins should thus provide a coarser but more powerful description of the SFH of the galaxies. We defined condensed population vectors by binning the SP vector into *young*: Xy ($t < 50\times10^6$ yr), *intermediate-age*: Xi ($51\times10^6 \leq t \leq 2\times10^9$ yr) and *old*: Xo ($t > 2\times10^9$ yr). The results for each galaxy in shown in Fig. 4 and 5.

Fig.1: Normalized (λ=1.2280 µm) nuclear spectrum of the galaxies sorted by their shape, from the steeper (top) to the flatter (base) . Some absorption (blue) and emission (red) lines are marked. Telluric absorption regions are displayed in the shadded area.

Fig.2: *Top:* NICMOS and Spex profile (Continuum Profile λ12230). *Bottom:* Slit position overlapping the NICMOS image of the galaxies. For NGC7714 we present WFPC2/F814W image and profile.

Fig.3: Result for the nuclear aperture of NGC1614. Top: we present the average synthesis result (red) and the masked points (blue) overlapping the average observed spectra (black), below the residual spectrum is shown (the dotted line in red marks the zero point in flux). Telluric absorption regions are shadded. *Bottom:* we display four histograms, the two on the left present the light-weighted (x_j) and mass-weighted (μ_j) SPs vectors contributions sorted only by age. The two on the right show the light-weighted (x_j) and mass-weighted (μ_j) SPs vectors contributions sorted by age and metalicity.

Fig.4: Global analysis each galaxy. Panel 1 and 2 present the average contribution in flux and mass respectively of the population vectors along the apertures. Blue, yellow and red represent young Xy, intermediate Xi and old Xo stellar population contributions respectively; Panel 3 shows the average metallicity weighted by light (ZL- in gray) and by mass (ZM- in white); The extinction (Av) is plotted along the apertures in panel 4; The average χ^2 and Adev are plotted in panel 5; The Continuum Profile at λ=1.2240 µm in panel 6 and for last, the singal-to-noise ratio (SNR) along the galaxy in panel 7 [the negative values in the horizontal axis indicates the south/southeast direction and the positive ones indicates the north/northwest direction].

Fig.5: Comparison between the results obtained using Maraston 2005 and Marastons & Strömbäck 2011 models. Left Panels: Stellar populations distribution. The different markers indicate the stellar population age component: Xy (star), Xi (filled circle), Xo (triangle). Middle Panels: Optical extinction (Av). Right Panels: Quality of the fit. The square marker represents the χ2 and the filled circle the Adev.

MAIN CONCLUSIONS

* The light in the NIR is dominated by young/intermediate ($t \leq 2\times10^9$ yr) SPs in the nuclear surroundings.

* Evidence of a ring-like structure of star formation in NGC 1614 with a diameter of about 600 pc.

* The interaction/merger process experienced by NGC 1614, NGC 3310 and NGC 7714 suggest that the fresh unprocessed metal poorer gas from the destroyed/interacting companion galaxy is driven to the center of the galaxies and mixed with the central region gas, before star formation takes place. In this context, the lower metallicity values derived for the young SP component, when compared to the old SP, can be understood as the diluted gas of the remnant.

* Due to the limitations of Maraston & Stömbäck 2011 models for the younger ages, it is not clear whether the use of these higer resolution models would bring an improvement capable of compensating the fact that they are only available for solar metallicities. Thus, we conclude that the use of low-resolution M05 models are still the best option in this wavelength range.

BIBLIOGRAFIA
1. Cid Fernandes, R., Gu, Q., Melnick, J., Terlevich, E., Terlevich, R., Kunth, D., Rodrigues Lacerda, R., Joguet, B., 2004, MNRAS, 355, 273
2. Cid Fernandes, R., Mateus, A., Sodr´e, Laerte, Stasi´nska, G., Gomes, J. M., 2005a, MNRAS, 358, 363 (CF05)
3. Maraston, C., 2005, MNRAS, 362, 799. M05
4. Carvalho, E., 2008, Estudo do infravermelho próximo da região de linhas estreitas de galáxias ativas, UNIFEI.

Dependence of the Habitable Zone* on stellar mass and chemical composition (low mass stars)

Giada Valle

Matteo Dell'Omodarme

Pier Giorgio Prada Moroni

Scilla Degl'Innocenti

(Physics Department, Pisa University)

*the range of distances from a star within which a planet may contain liquid water at its surface

(see e.g. Kasting et al. 1993, Kaltenegger & Sasselov 2011)

Dependence of HZ characteristics on the stellar parameters evaluating the related uncertainties → differential analysis expected robust against changes of the HZ boundary positions by improved planetary climate models.

Analyzed characteristics of the HZ (see Valle et al. 2014)

• d_m (in AU): the distance from the host star at which the habitability is longest
• t_m (in Gyr): the corresponding duration
• W (in AU): the width of the zone for which the habitability lasts one half of the maximum
• I (in AU Gyr): the integral
• the inner, R_i , and outer, R_O , boundaries of the continuously habitable zone (CHZ), for which the habitability lasts at least 4 Gyr*, quantities which are particularly useful to plan a search for life signatures in exoplanet atmospheres (see e.g. Seager & Deming 2010).

* Other choices are possible and values from 1 to 5 Gyr are adopted in the literature (see e.g. Turnbull & Tarter 2003, Buccino et al. 2006)

General rule

The higher is the stellar luminosity the farther is the HZ from the host star, thus the HZ moves farther from the host star when:

- the stellar mass increases
- the stellar original helium content increases
- the stellar original metallicity decreases

Moreover the HZ evolves with time following the stellar luminosity variation

The boundaries of the HZ are defined by suitable values of the planet equilibrium temperature - that is, the temperature of a planet in thermal equilibrium between the radiation absorbed from the star and the one radiated into space – values made available by climatic models (see e.g. Kasting et al. 1993, Selsis et al. 2007, Kopparapu et al. 2013, Leconte et al. 2013).

Models and method

220 stellar evolutionary tracks from the Pre-Main Sequence phase to the helium flash at the red-giant branch tip for stars with masses, M, in the range [0.70 - 1.10] M_{sun}, metallicity , Z, in the range [0.005 - 0.04] and various initial helium contents, Y.

Analytical relations for d_m , t_m , W, R_i and R_O as a function of M, Y and Z, with relative errors of the order of a few percent or lower (analytical relations can be found in Valle et al. 2014).

Stellar models are calculated by means of an updated version of the FRANEC stellar evolutionary code (see e.g. Tognelli et al. 2011, Dell'Omodarme et al. 2012).

On-line tool which allows downloading a stellar track for the chosen mass and chemical composition and obtaining the HZ characteristics at the url:

http://astro.df.unipi.it/stellar-models/HZ/

UNIVERSITÀ DI PISA

Physics Department "E. Fermi"

Habitable Zone calculator

This page hosts an interactive calculator that estimates several feature of the habitable zone (HZ) and of the 4 Gyr continuously habitable zone (CHZ).

A C code is available for download to calculate HZ and CHZ for a number of stars.

If you use the calculator or the code, please acknowledge the following paper:

Valle G., Dell'Omodarme M., Prada Moroni P.G., Degl'Innocenti S. (2013). *Evolution of the habitable zone of low-mass stars. Detailed stellar models and analytical relationships for different mass and chemical compositions.*

Input

The following information are required:

- *M*: the mass of the star in solar unit (range: 0.70 - 1.10 M_{sun}).
- *Metallicity*: the metallicity of the star. Either Z (range: 0.005 - 0.04) or [Fe/H].
- *ΔY/ΔZ*: the helium-to-metal enrichment ratio in the relation Y = 0.2485 + ΔY/ΔZ * Z (range: 1 - 3, standard value = 2).
- T_o: the equilibrium temperature of the outer boundary (range: 169 - 203 K).
- *A*: the albedo of the planet (range: 0.0 - 1.0, Earth = 0.3).

Output

The following information are computed:

- dm (AU): the distance from the host star at which the maximum of habitability occurs.
- tm (Gyr): the duration of the maximum habitability.
- W (AU): the width of the HZ for which the habitability lasts at least one half of the maximum
- Ri (AU): the position of the inner boundary of the CHZ, for which the habitability lasts at least 4 Gyr.
- Ro (AU): the position of the outer boundary of the CHZ, for which the habitability lasts at least 4 Gyr.

Analytical models input

Please provide the required input and press the button "Compute...".

Metallicity: ○ Z ◉ [Fe/H]

M (M_{sun})	Metallicity	ΔY/ΔZ	T_o (K)	A

Compute...

Dependence on the chemical composition

•The HZ and CHZ for high-metallicity stars are closer to the host star than those around low metallicity stars (see also Danchi & Lopez 2013).

• First evaluation of the effect on the CHZ of the helium abundance change ($\Delta Y/\Delta Z$ varied from 3 to 1, see e.g. Pagel & Portinari 1998, Casagrande et al. 2007, Gennaro et al. 2010):
- For the inner CHZ boundary, $\Delta R_i/R_i$ from ~5% (for Z = 0.005) to ~30% (for Z = 0.04).
-For the outer boundary, $\Delta R_O/R_O$ < 12%

Interactions among metallicity, mass and helium content are important in determining the CHZ boundaries

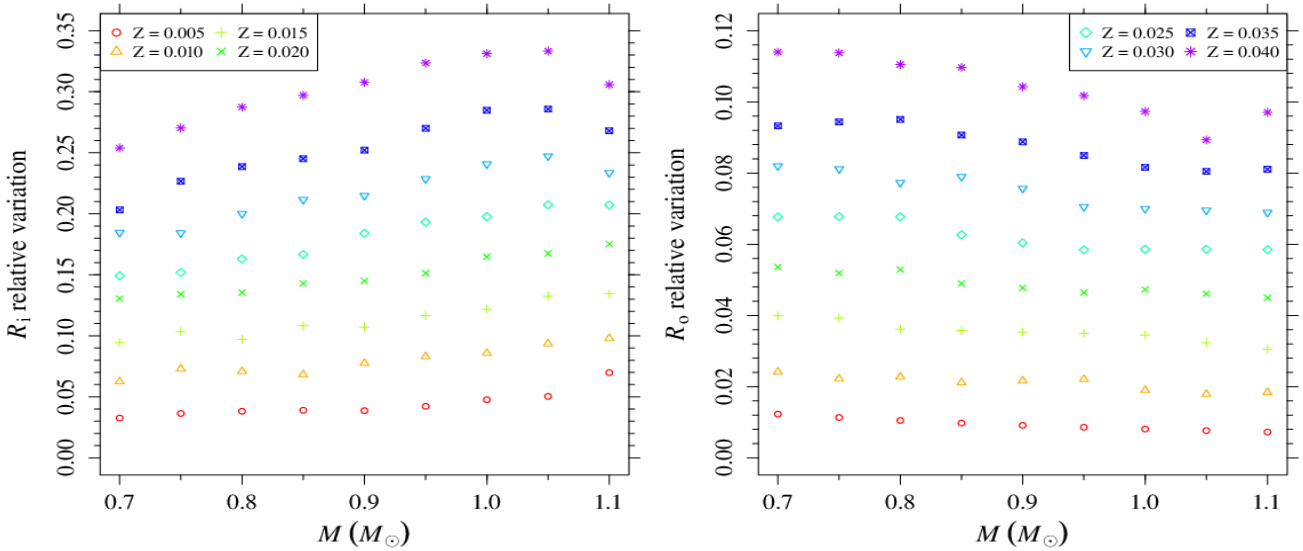

Left panel: relative variation, for a change from $\Delta Y/\Delta Z$= 3 to $\Delta Y/\Delta Z$ = 1, of the CHZ inner boundary as a function of the host star mass for the labeled Z values. Right panel: the same as the left panel, but for the outer CHZ boundary

Sensitivity of CHZ boundaries to mass and metallicity errors

(still not available in the literature)

Errors: $\Delta \log Z$ = 0.1 dex ; ΔM_{star} = 0.05 M_{sun} (see e.g. Basu et al. 2012, Valle et al. 2013).

Monte Carlo simulations (by adopting analytical relations)

- For the inner CHZ boundary, $\Delta R_i/R_i$ from ~ 27% to ~37%
- For the outer CHZ boundary, $\Delta R_O/R_O$ up to ~19%

The contribution of the mass uncertainty is always greater than the one due to the metallicity indetermination and the relative error increases towards low masses and low metallicities.

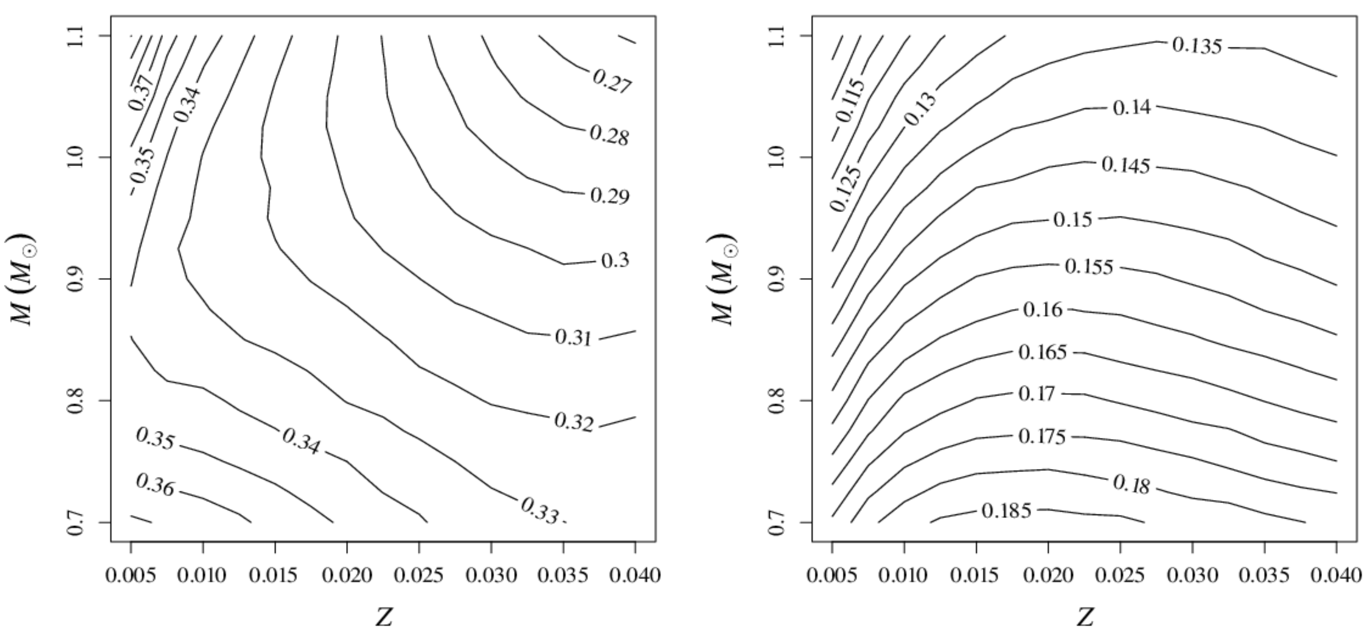

Left panel: contour plot of the relative variation, $\Delta R/R$, of the CHZ internal radius, R_i, due to the simultaneous variation of mass and metallicity of the host star within their uncertainty ranges. Right panel: as in the left panel but for the CHZ outer radius R_O. $\Delta Y/\Delta Z$ = 1 is adopted.

The evaluation of the stellar uncertainty contribution to the overall uncertainty budget for the HZ characteristics plays a crucial role in the search for life signature in exoplanets.

SPECTRAL ENERGY DISTRIBUTIONS OF THE HUBBLE ULTRA DEEP FIELD GALAXIES AT DIFFERENT REDSHIFTS

Umut Emek Demirbozan[1], Mireia Montes[1], Ignacio Trujillo[1]
Instituto de Astrofisica de Canarias, Spain[1]

ABSTRACT

We present spectral energy distributions (SEDs) of the galaxies in the Hubble Ultra Deep Field (HUDF) with a wavelength coverage of 11 filters spanning from the ultraviolet (UV) to the near-infrared. The UV data of HUDF is relatively new and mostly unexplored. Our sample in the HUDF span a range of redshifts from 0.13 up to 5.95 since the HUDF is the deepest image of the universe ever taken. We have used the GOODS/CDF-S spectroscopic redshift compilation to obtain the redshifts of the galaxies and matched 91 galaxies in the HUDF with this spectroscopic redshift catalogue. Therefore, we are able to show how the SEDs of our sample from the HUDF galaxies change with cosmic time. We also compare some of our SEDs with simple stellar population models(SSPs).

SPECTRAL ENERGY DISTRIBUTIONS WITH NEW UV DATA AT DIFFERENT REDSHIFTS

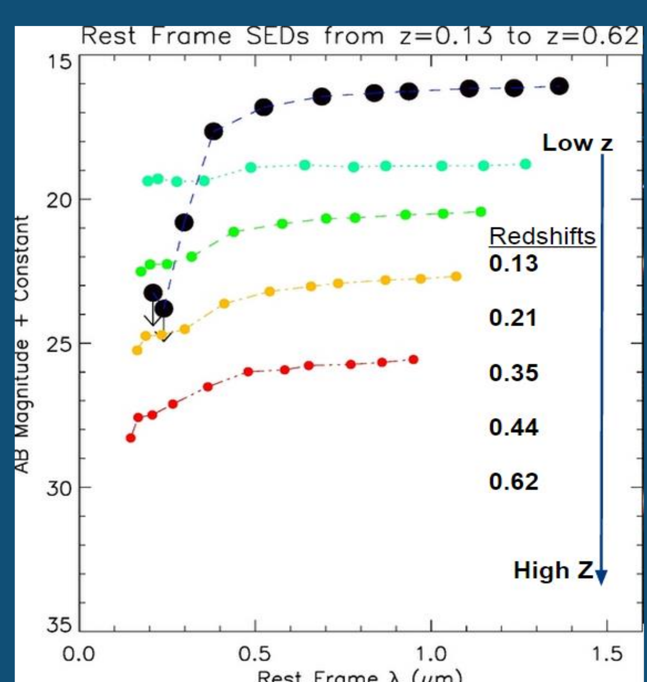

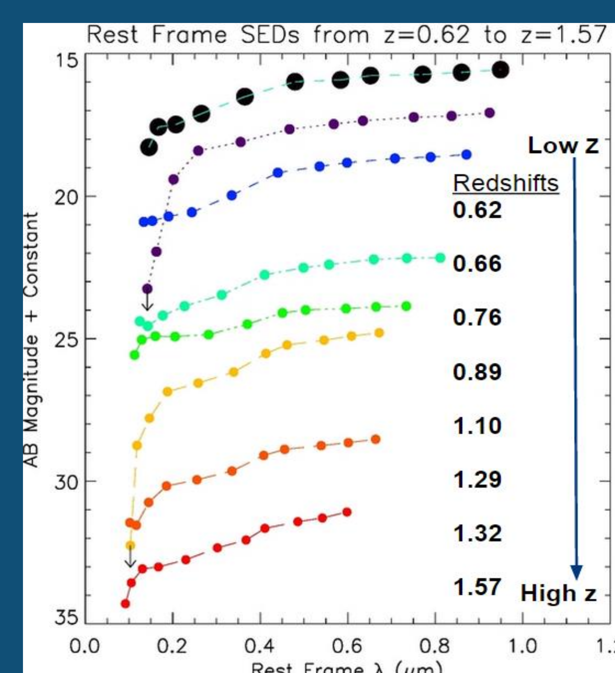

Left: Rest frame SEDs of 5 sample galaxies from z=0.13 to z=0.62. The redshifts of the sample increases from top to bottom. Right: Rest frame SEDs of 8 sample galaxies from z=0.62 to z=1.57. The bottom galaxy at z=0.62 on the left is the top galaxy on the right. The downward arrows on the data mark the upper limit magnitudes.

COMPARISON WITH SIMPLE STELLAR POPULATION MODELS AT DIFFERENT AGES

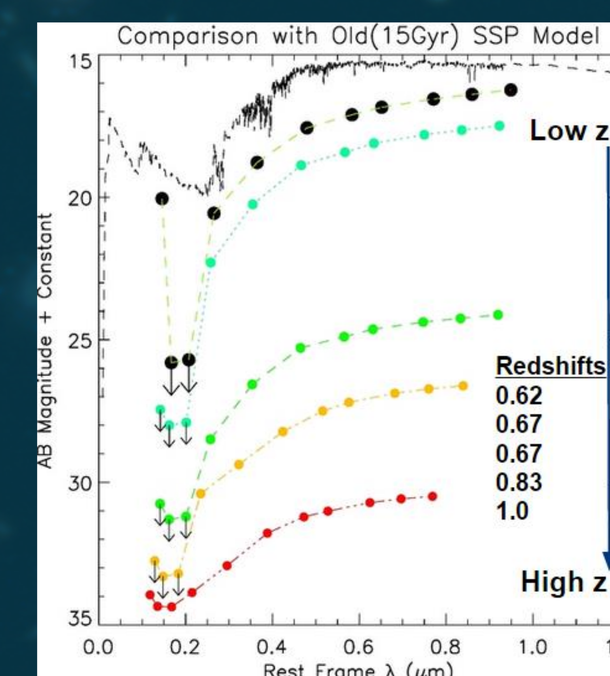

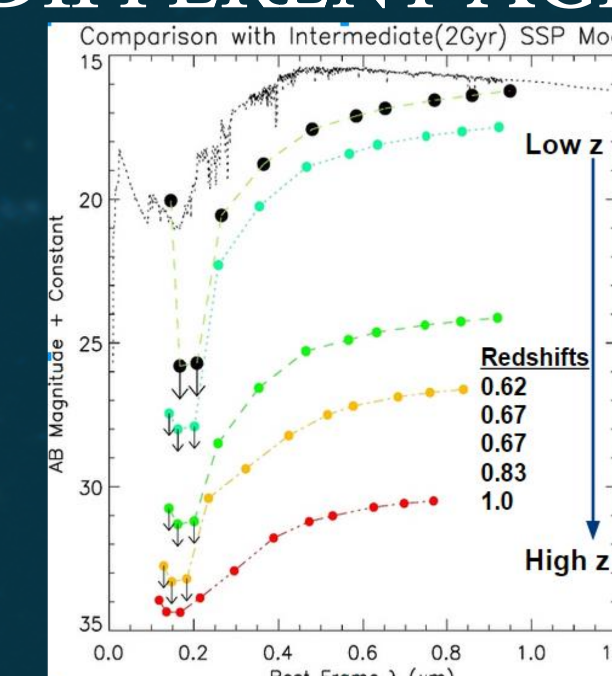

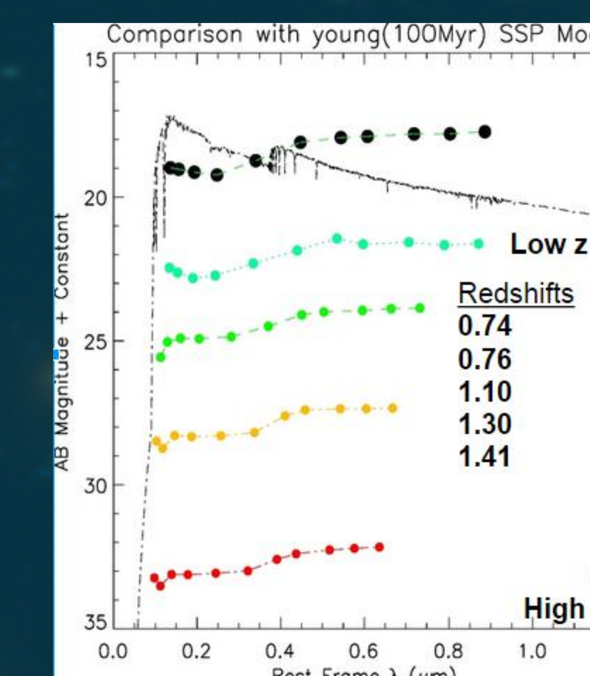

Left: A comparison between 15 Gyr old SSP and 5 sample galaxies at redshifts from z=0.62 to z=1.0. Middle: A comparison between 2 Gyr old SSP and the same sample as on the left. Right: A comparison between 100Myr old SSP and 5 sample galaxies at redshifts from z=0.74 to 1.41. It is seen that the first sample probably aged between 2Gyr and 15Gyr and our second sample consists star-forming galaxies at high redshifts. All of our SSPs are from Bruzual & Charlot (2003).

UV BRIGHT GALAXIES

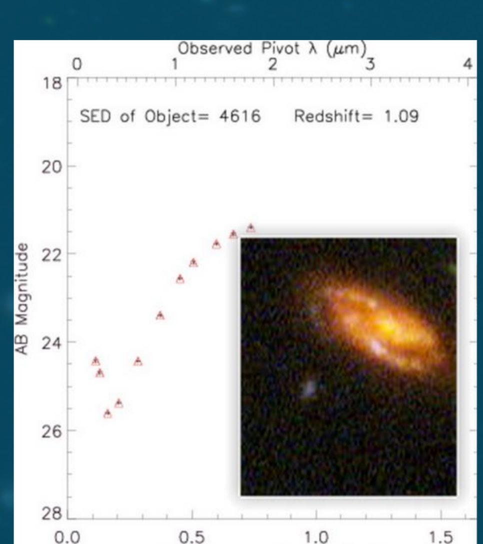

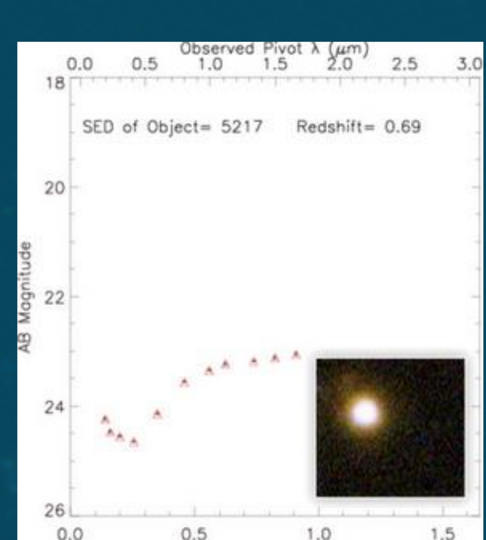

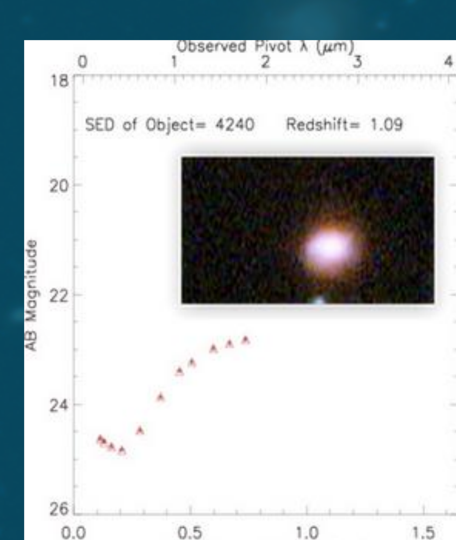

A significant component of our sample has some galaxies which are bright in the UV region. Above we present three random galaxies with bright UV regions from our sample. These galaxies are illustrated with their sample images take from Ultra Deep Field(UDF) Skywalker . We suspect that these bright UV magnitudes might be caused by Lyman-alpha emission from star formation.

METHODS

- **HUDF data is reduced with IDL**
- **Photometry with SExtractor & IDL**
- **We plot SEDs with IDL**
- **We compare some our SEDs with SSPs**

REDSHIFTS OF THE SAMPLE

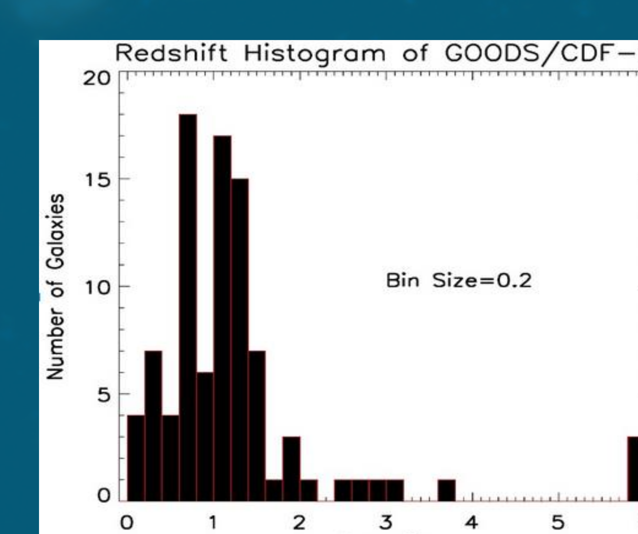

This figure shows the histogram of our matched sample that consists of 91 galaxies. As seen from the figure, most of the galaxies were around redshift z=1.0. This limitation is caused by the number of galaxies in GOODS/CDF-S spectroscopic redshift compilation.

CONCLUSION & FUTURE

We have compiled SEDs for 91 galaxies using the superb imaging of the HUDF. These SEDs include new UV data, complementing the existing optical and near-infrared imaging. This wide wavelength range can help us to understand the properties of stellar populations of the galaxies in detail. We present some SEDs with full coverage of the 11 bands including new UV HUDF data. We have observed that star-forming galaxies are more common at high redshifts in our sample. We also have some galaxies which have bright UV regions that might be from Lyman-alpha emission. In this work, our sample was limited to 91 galaxies which are matched in GOODS/CDF-S spectroscopic redshift compilation with the HUDF. This number remains small as compared to few thousand galaxies in the HUDF. However, with the new generations of space and ground based telescopes such as JWST and E-ELT, we could obtain deeper images that could lead to better SEDs at high redshift and produce larger spectroscopic redshift catalogues with higher redshift confidence which can result in a deeper understanding of the evolution of galaxies across the cosmic time.

Stellar Population Synthesis

a Bayesian approach

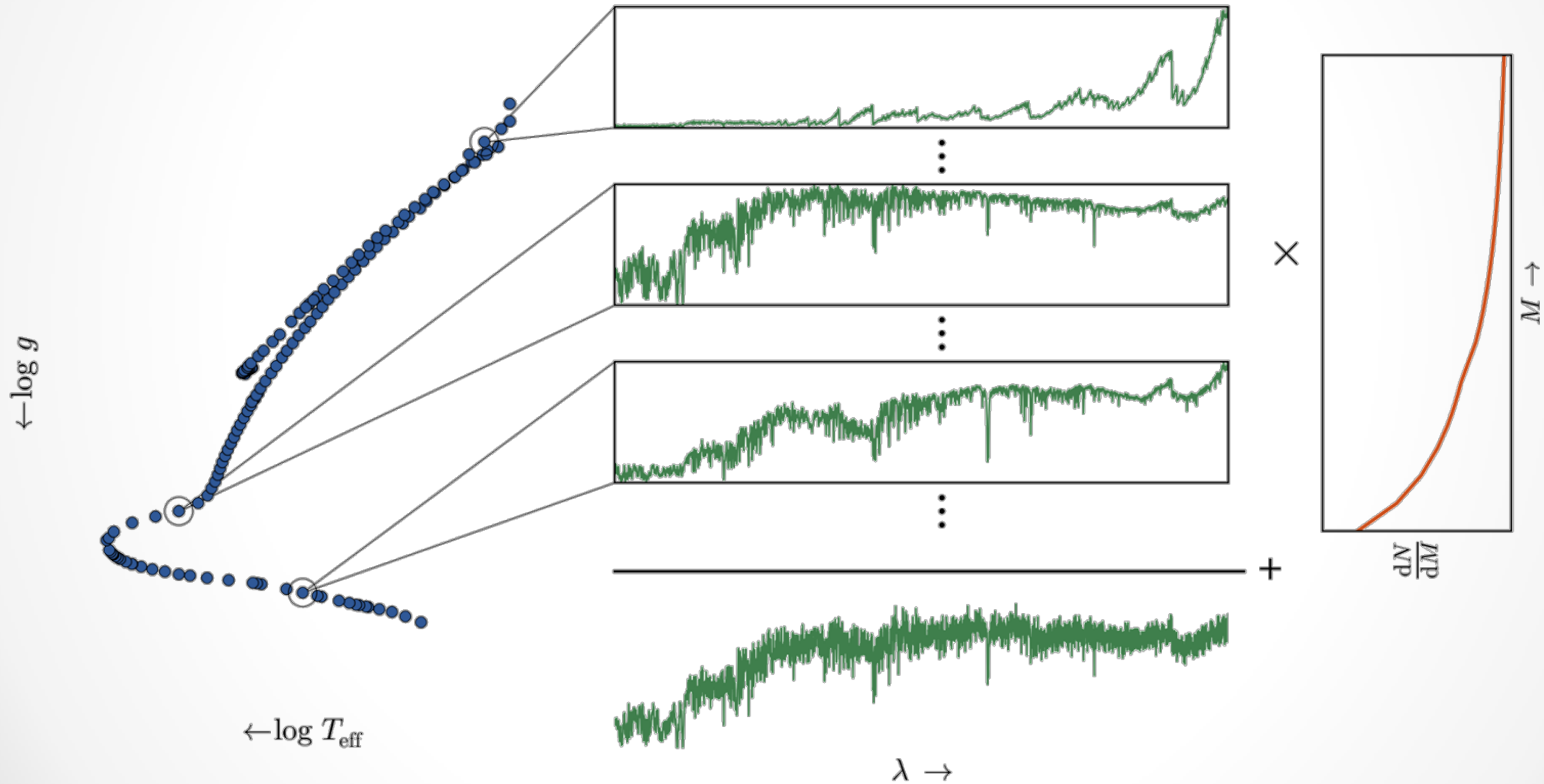

Matthijs Dries, Scott Trager & Léon Koopmans
Kapteyn Astronomical Institute, university of Groningen

Ingredients SPS model

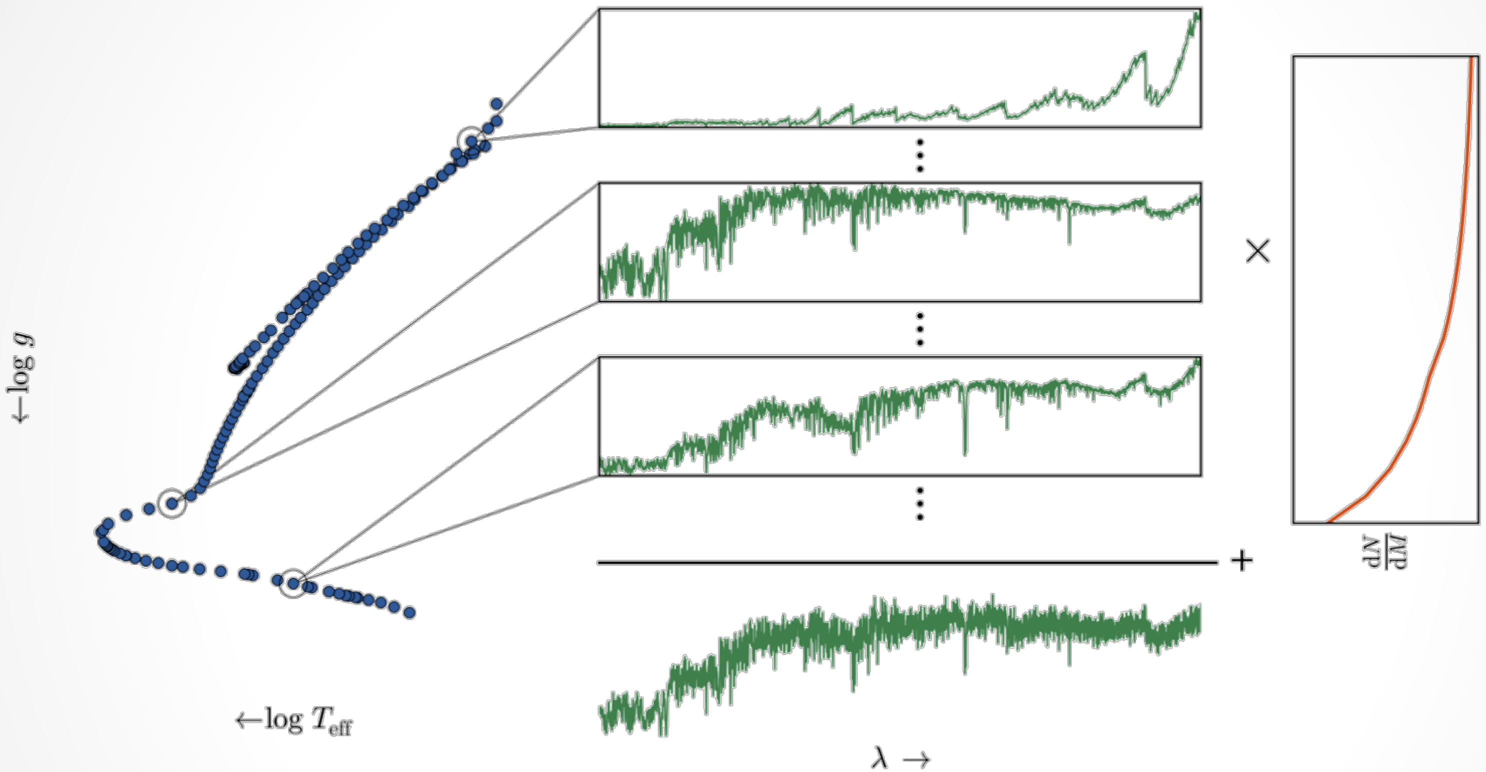

Basic ingredient:

- stellar evolution: isochrones (*Marigo et al. 2008*)
- spectral library: empirical or theoretical *(MILES, XSL)*
- IMF

Bayesian regularization

Posterior $P(H|D) = \frac{P(D|H) \cdot P(H)}{P(D)}$ $\begin{cases} P(D|H) & \text{Likelihood} \\ P(H) & \text{Prior} \\ P(\mathrm{D}) & \text{Evidence} \end{cases}$

galaxy SED = $\sum_i w_i \cdot S_{\lambda,i}$

prior information on e.g. IMF or SFH encapsulated in w_0

goal: reconstruct contributions of stars w_i to galaxy SED

minimize $f = \frac{1}{2}X^2 + \lambda \cdot (w - w_0)^2$

likelihood

regularization parameter

prior

Results

Reconstruction Kroupa galaxy S/N 100

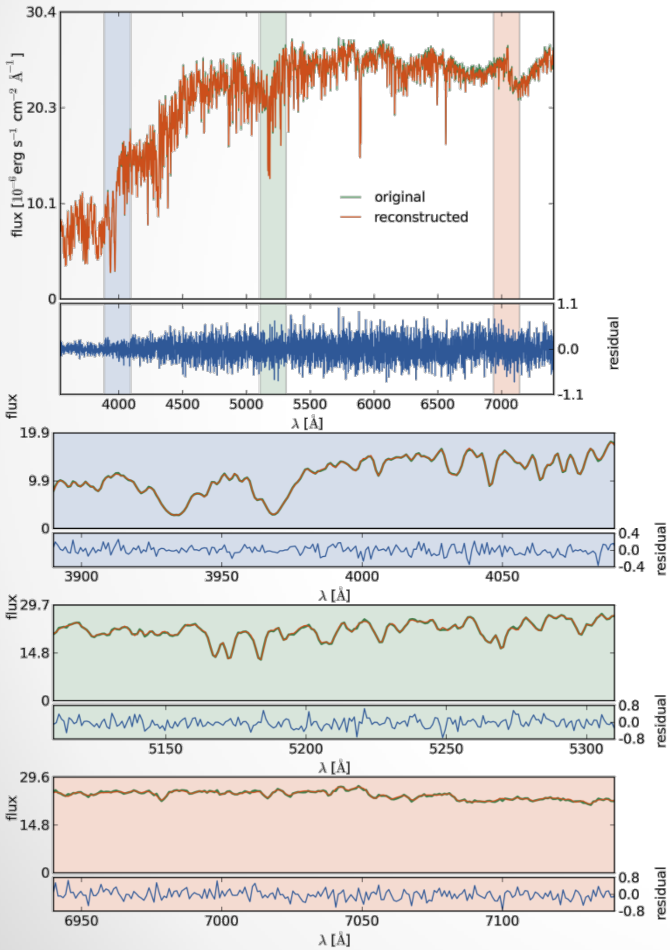

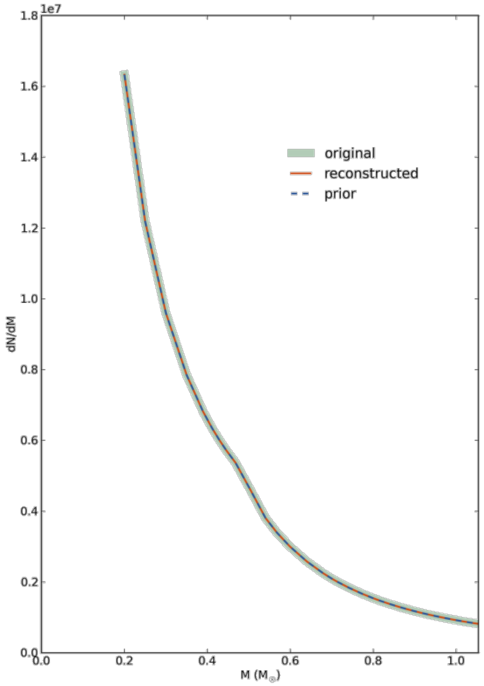

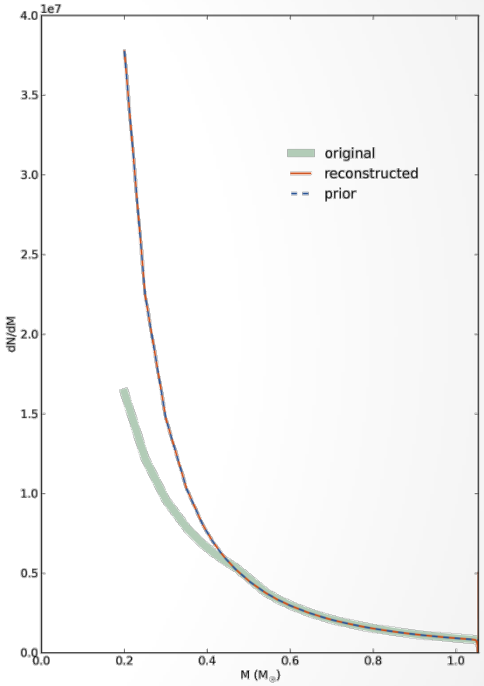

model	Bayesian evidence
Kroupa prior	60350.3
Salpeter prior	60315.0

Stellar Population Synthesis: a Bayesian approach

Matthijs Dries, Scott Trager & Léon Koopmans

Kapteyn Astronomical Institute

1 Abstract

Stellar Population Synthesis (SPS) provides an important link between observational data and theoretical models. In the most simple approach, the Spectral Energy Distribution (SED) of a galaxy is the sum of all the stellar spectra that it contains. Here we discuss a new SPS model based on the MILES library[1], in which we apply Bayesian regularization to reconstruct the SED of a galaxy. With our model we eventually aim to test recent claims of a varying initial mass function in Early-Type Galaxies as a function of galaxy mass / velocity dispersion[2,3].

2 SPS: basic ingredients

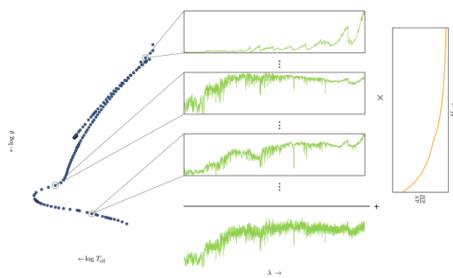

To construct a SPS model we need:

- stellar evolution (isochrones)
- stellar library (either theoretical, empirical or combined)
- initial mass function (IMF)

From these basic ingredients we can create a Single Stellar Population (SSP): a population of stars born at the same time with the same chemical composition.

A real galaxy is however far more complicated, so in addition we may need:

- dust
- star formation history
- chemical evolution
- modelling of uncertain factors: dust, uncertain stellar phases, incompleteness in the data and model ingredients, …

Combining the SSP with the additional ingredients listed above, we can construct a Composite Stellar Population (CSP).

3 Spectrum interpolator

requirement SPS model: stellar spectra at each relevant location in HR diagram. However: coverage of stellar library is limited ⟶ spectrum interpolator:

$$S_\lambda(T_{\rm eff}, \log g, [{\rm Fe/H}])$$

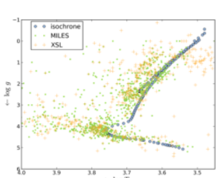

Coverage of HR diagram by both MILES and X-Shooter Spectral Library[4] (XSL).

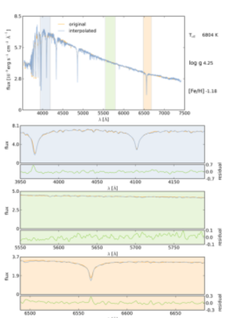

Interpolation of a MILES star. The original star was not part of the interpolation dataset.

4 The model

Bayes' theorem:

$$\textbf{Posterior} \quad P(H|D) = \frac{P(D|H)\cdot P(H)}{P(D)} \quad \begin{cases} P(D|H) & \textbf{Likelihood} \\ P(H) & \textbf{Prior} \\ P(D) & \textbf{Evidence} \end{cases}$$

- **assumption:** SED of a galaxy is a linear combination of stellar spectra, such that:

$$\text{galaxy SED} = \sum_i \boldsymbol{w_i} \cdot \boldsymbol{S_{\lambda,i}}$$

- **goal:** reconstruct individual contributions of stars w_i to galaxy SED
- minimize $f = \underbrace{\tfrac{1}{2}\chi^2}_{\text{likelihood}} + \underbrace{\lambda}_{\text{regularization parameter}} \cdot \underbrace{(w - w_0)^2}_{\text{prior}}$
- Prior information encapsulated in w_0.
- Current version of model only reconstruction of SSP. Ingredients:
  - stellar evolution: *Padova*[5] isochrones
  - stellar library: polynomial interpolator (similar to [6]) based on *MILES* library
  - IMF: variable, model should reconstruct IMF

5 Results

- We create an artificial galaxy spectrum with a **Kroupa** IMF
- To this spectrum we add noise, such that we have **S/N = 20** and **S/N = 100**
- We try to reconstruct IMF by assuming two different priors:
  - IMF is a Kroupa IMF
  - IMF is a Salpeter IMF

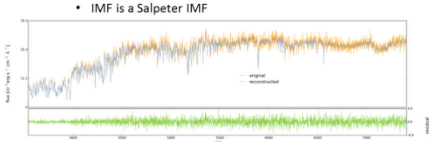

Reconstructed spectrum by assuming a Salpeter prior with S/N = 20.

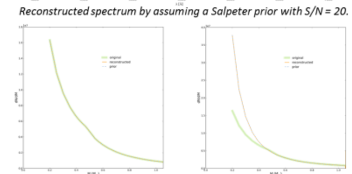

Reconstruction of the IMF by assuming a Kroupa prior (left) and a Salpeter prior (right) for S/N = 100.

- Then we calculate the Bayesian evidence and compare the two models:

prior	Bayesian evidence (S/N = 20)	Bayesian evidence (S/N = 100)
Kroupa	53315.4	60212.1
Salpeter	53313.0	60171.8

Conclusion

- Model is unable to reconstruct IMF if prior is incorrect. Even for S/N = 100, solution follows prior for low-mass end of the IMF.
- However, Bayesian evidence for correct prior model higher than for incorrect prior model. Future models (with XSL) will improve these reconstructions.

References

1. P. Sánchez-Blázquez et al., 2006, MNRAS 371:703
2. M. Cappellari et al., 2012, Nature 484:485
3. C. Conroy & P. van Dokkum, 2012, ApJ 747:69
4. Y. Chen et al., 2011, JPhCS 328:012023
5. P. Marigo et al., 2008, A&A 482:883
6. P. Prugniel, I. Vauglin & M. Koleva, 2011, A&A 531:165

Contact

Matthijs Dries

Kapteyn Astronomical Institute

Email: dries@astro.rug.nl

Poster #12

Bayesian Mass Estimates of the Milky Way

McMaster University

Gwendolyn Eadie, PhD Student
Supervisor: Dr. William Harris
Collaborator: D. Lawrence Widrow
RASPUTIN – Oct. 13-17, 2014

Distant Satellites (Tracers)

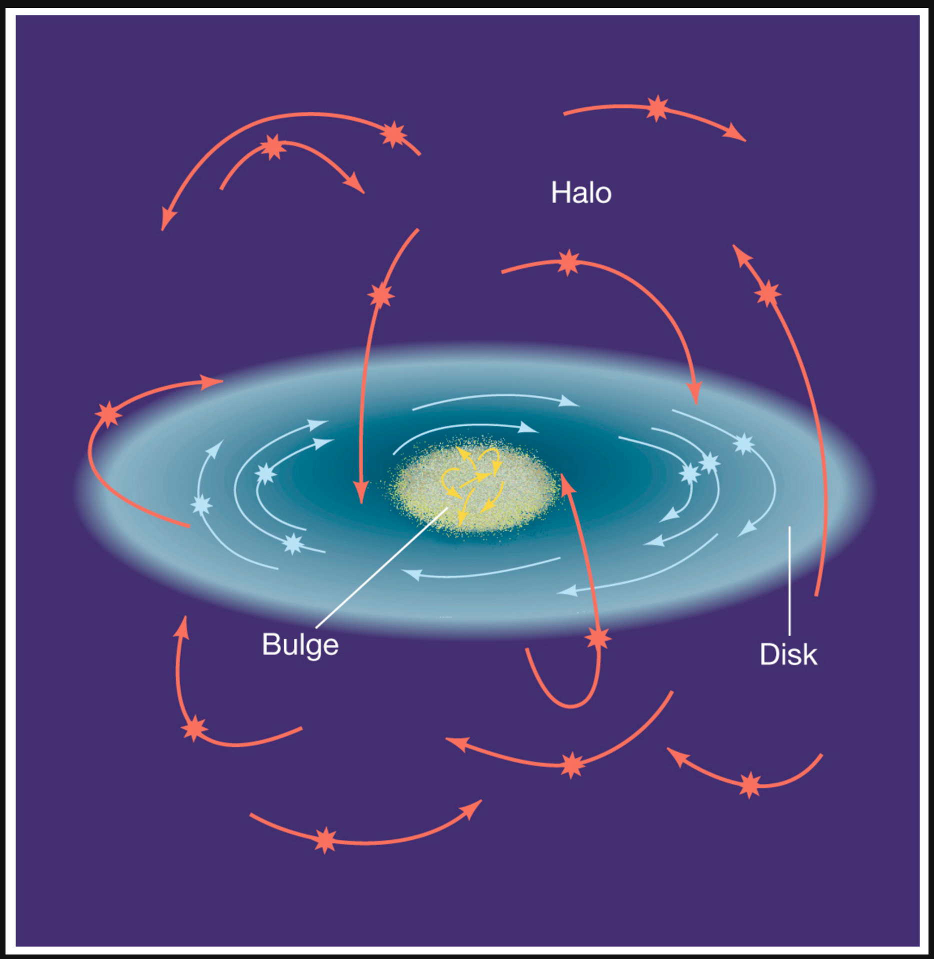

Chaisson & McMillan, *Astronomy*, 2004

- dwarf galaxies
- globular clusters

- *Distance & Speed*

$$\varphi(r) \longrightarrow M(r)$$

Notation

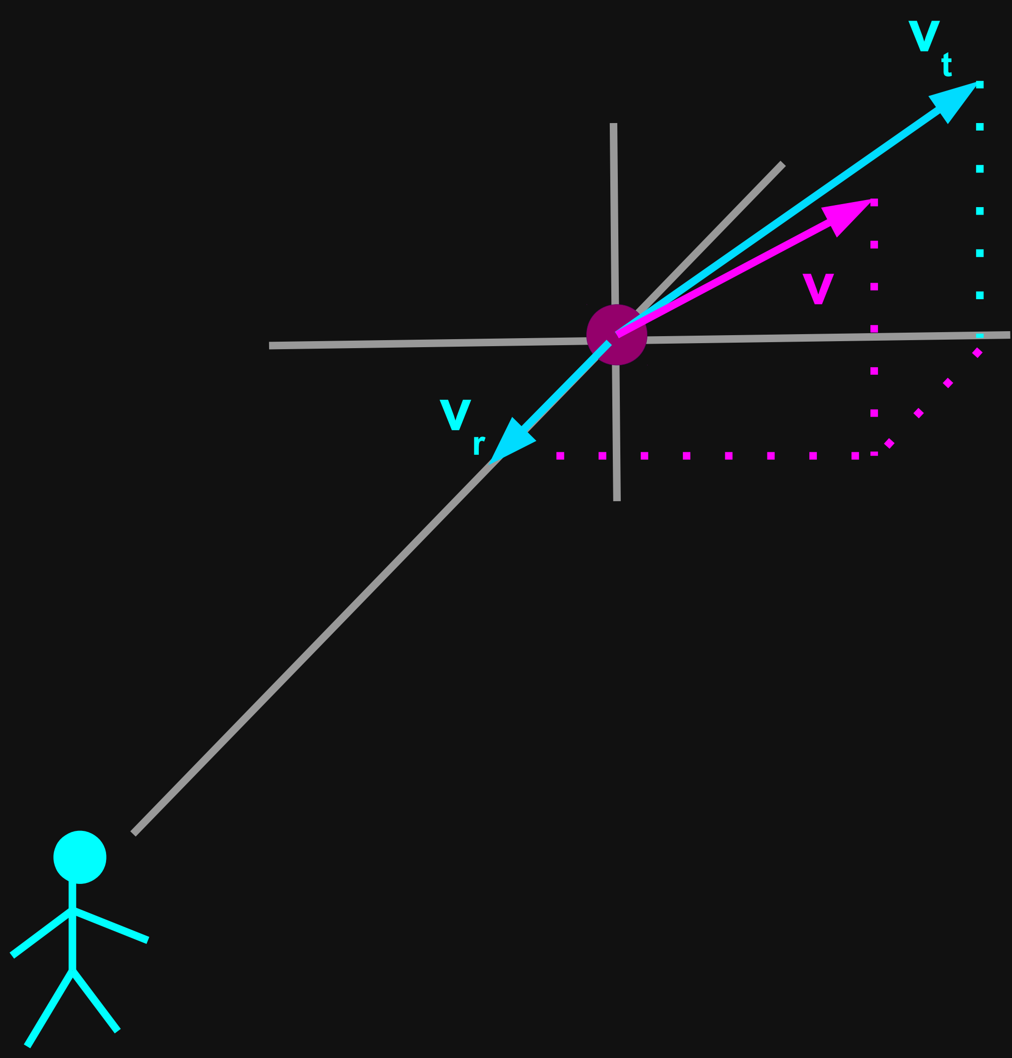

- Kinematic data

$\mathbf{v_r}$ radial velocity

$\mathbf{v_t}$ tangential velocity

$\mathbf{r}$ distance

Bayesian Inference & Incomplete Data

$$p(\boldsymbol{\theta}|y) \propto p(y|\boldsymbol{\theta})\, p(\boldsymbol{\theta})$$

Distribution Function:

$$f(\boldsymbol{r}, \boldsymbol{v}|\boldsymbol{\theta})$$

$$p(\boldsymbol{\theta}|y) \propto \boxed{\prod_{i=1}^{n} f(r_i, \boldsymbol{v}_i|\boldsymbol{\theta})}\, p(\boldsymbol{\theta})$$

posterior distribution

likelihood

priors

some v_t unknown

?

$$v^2 = v_r^2 + v_t^2$$

SOLUTION:

$$p(\boldsymbol{\theta}|y) \propto \prod_{i=1}^{n} f(r_i, v_{r,i})|\boldsymbol{\theta}, \boxed{v_{t,i}})p(\boldsymbol{\theta})\boxed{p(v_{t,i})}$$

unknown v_t's as parameters

M(r) profile credible regions

$$M(r) = M_{tot}\frac{r^2}{(r+a)^2}$$

Hernquist (1990) model

Model - σ^2	$M_{\rm tot}$ ($10^{12} M_\odot$)
H - iso	1.60 ± 0.09
H - OM	1.57 ± 0.09
H - $\beta = 0.5$	1.51 ± 0.08
Jaffe - iso	1.66 ± 0.10

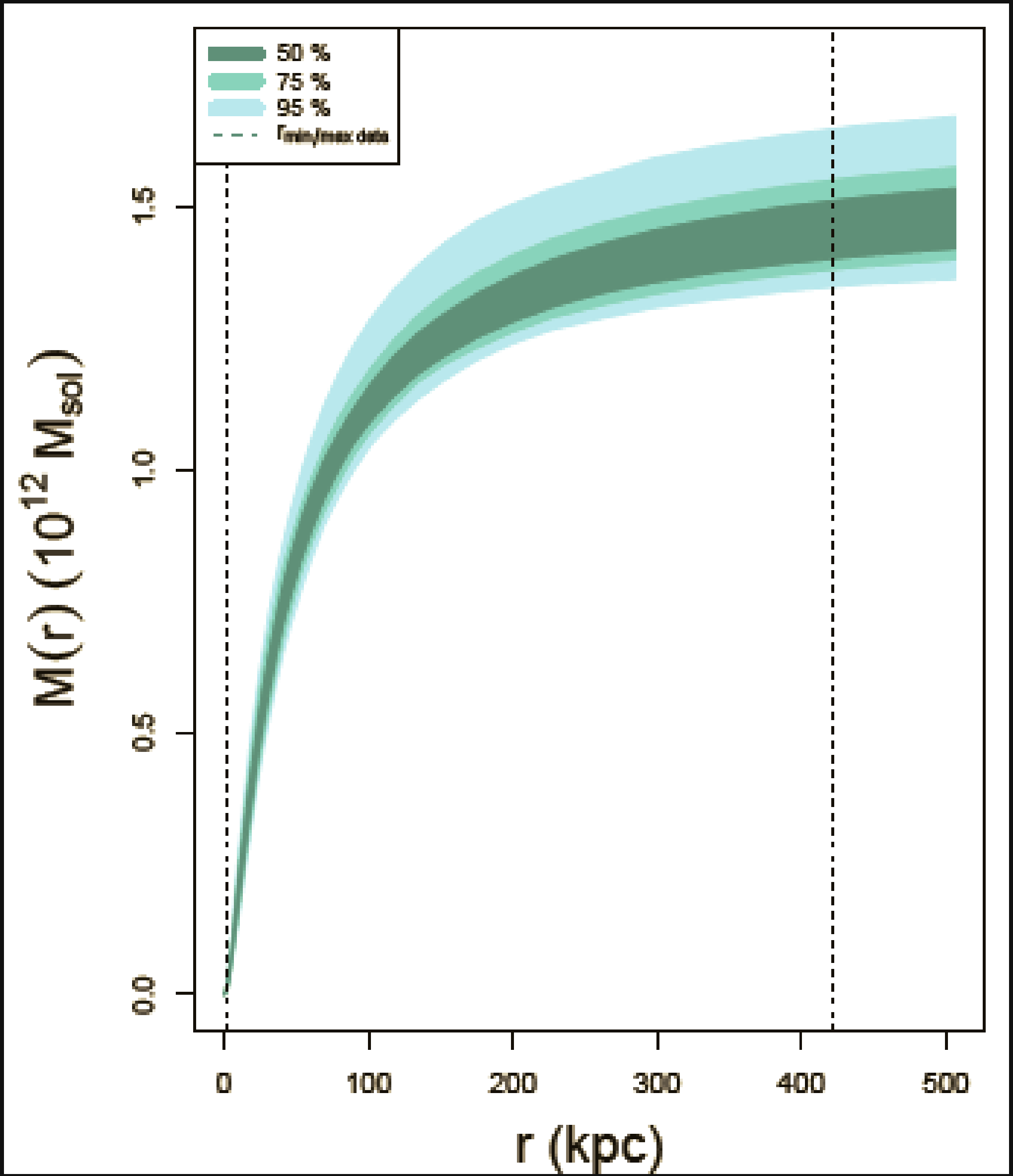

Future Work

Poster #12

- Apply the NFW model (Approximate Bayesian Computation?)
- Incorporate uncertainties via a hierarchical model
- Looking forward
  - other galaxies
  - galaxy clusters
  - GAIA

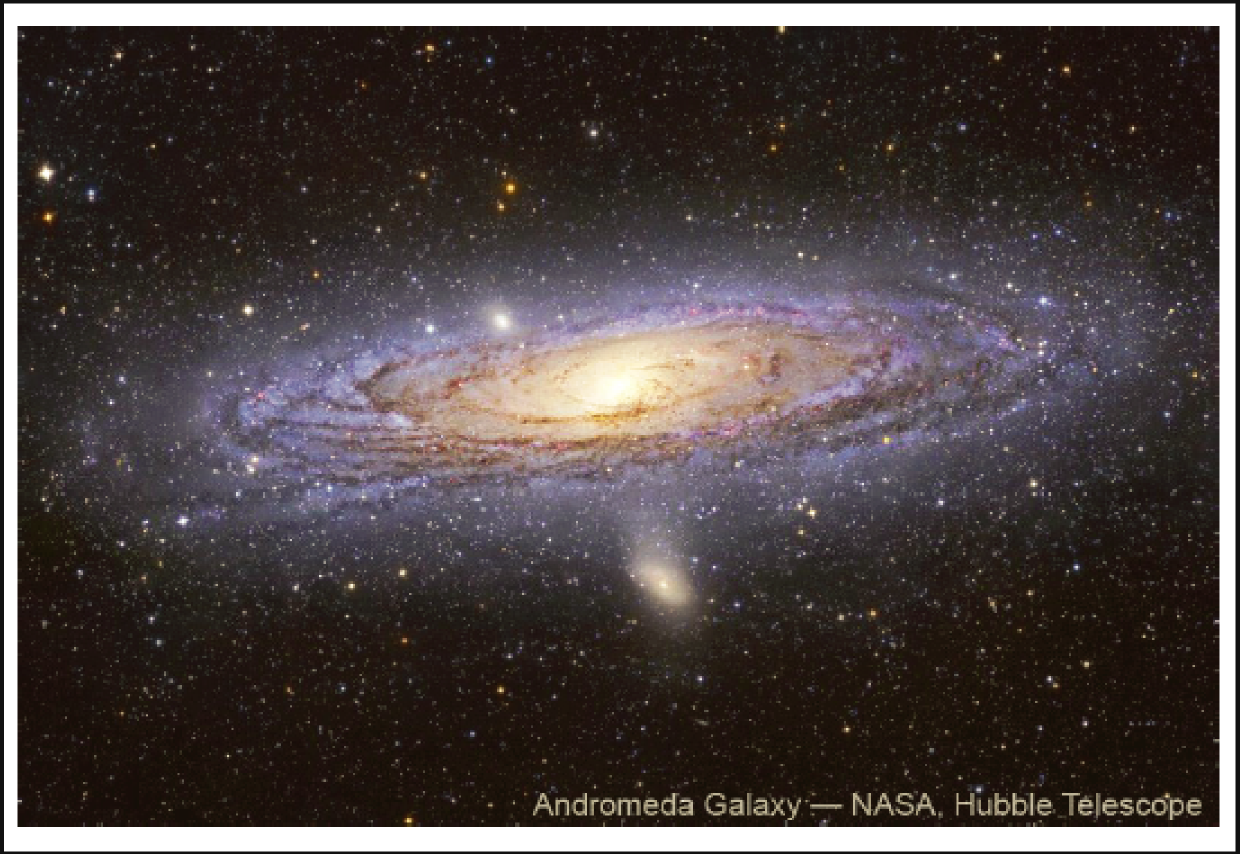

Thank you!

Lithium evolution in POP II pre-main sequence stars with overshoot and accretion

Xiaoting FU

Alessandro Bressan & Paolo Molaro, Paola Marigo

Oct. 14, 2014.
RASPUTIN, ESO

xtfu@sissa.it

ma per seguir virtute e canoscenza
SISSA

Lithium problem

Li abundance in POP II dwarfs (**A(Li)=2.26 dex**)

2.26 dex

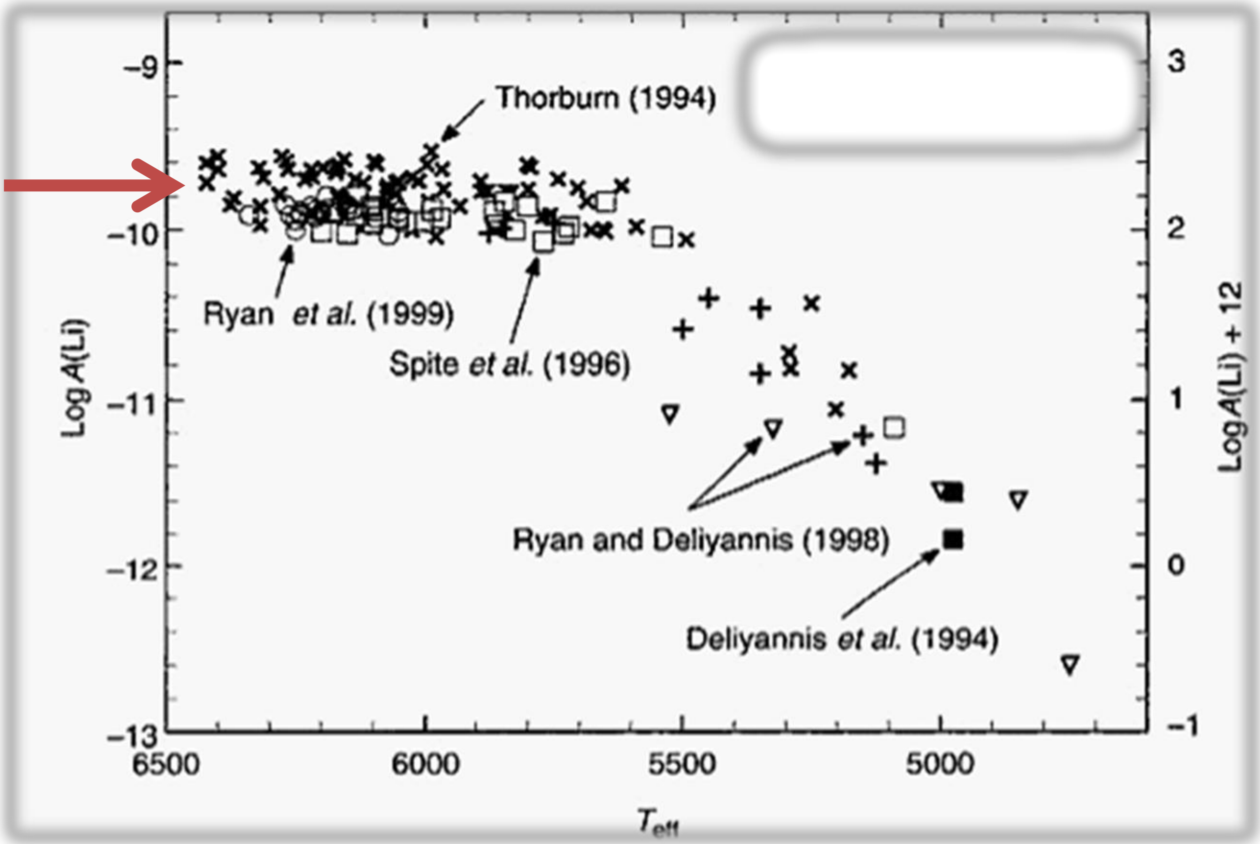

Gray, David. 2005

Lithium problem

Li abundance in POP II dwarfs (**A(Li)=2.26 dex**)
is **a factor of three lower**
than the value of primordial Li predicted by the Big Bang nucleosynthesis
(**A(Li) = 2.72 dex**)

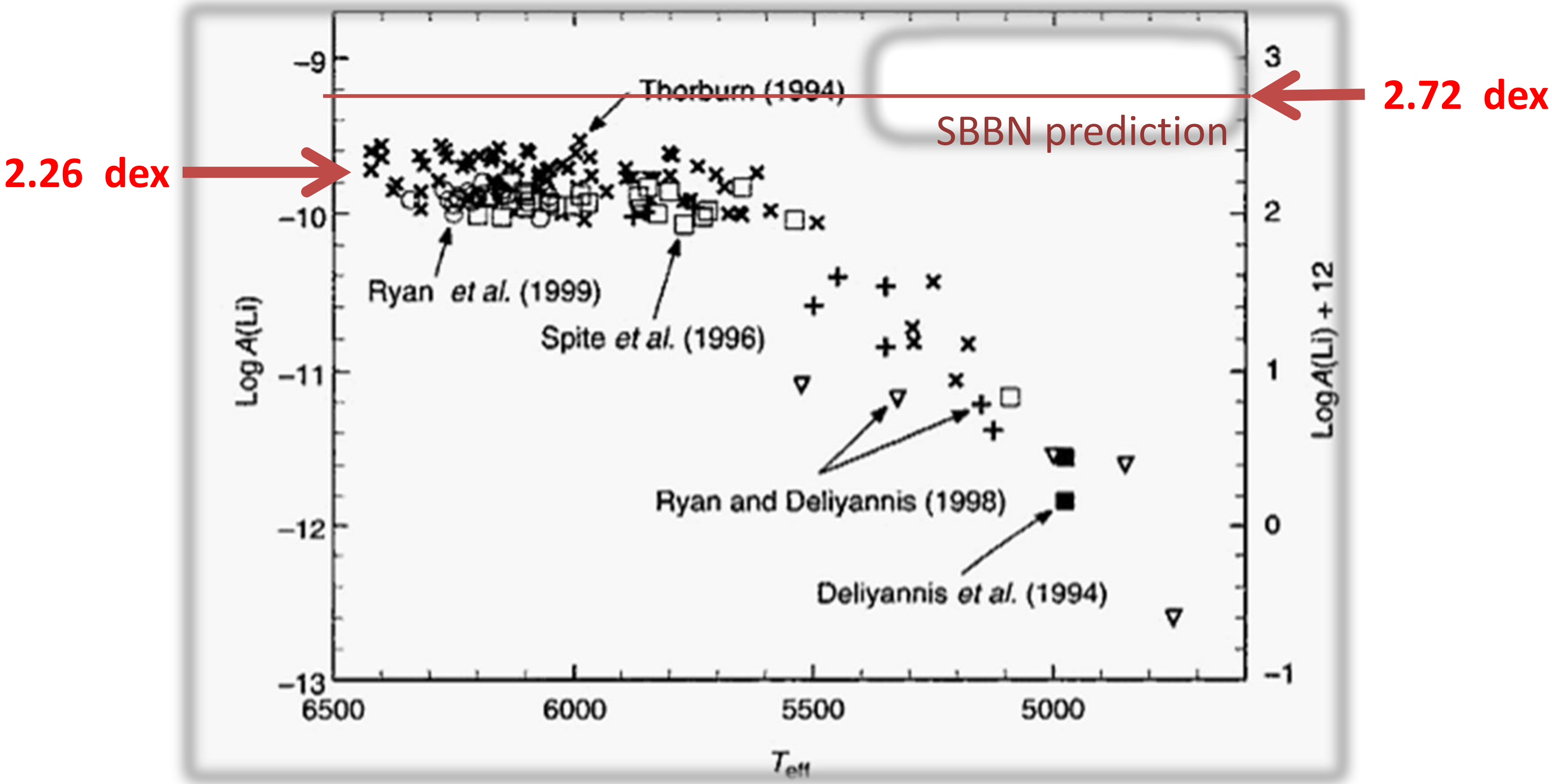

Gray, David. 2005

A self-regulation mechanism considering

Overshoot, accretion, and **EUV photo-evaporation**

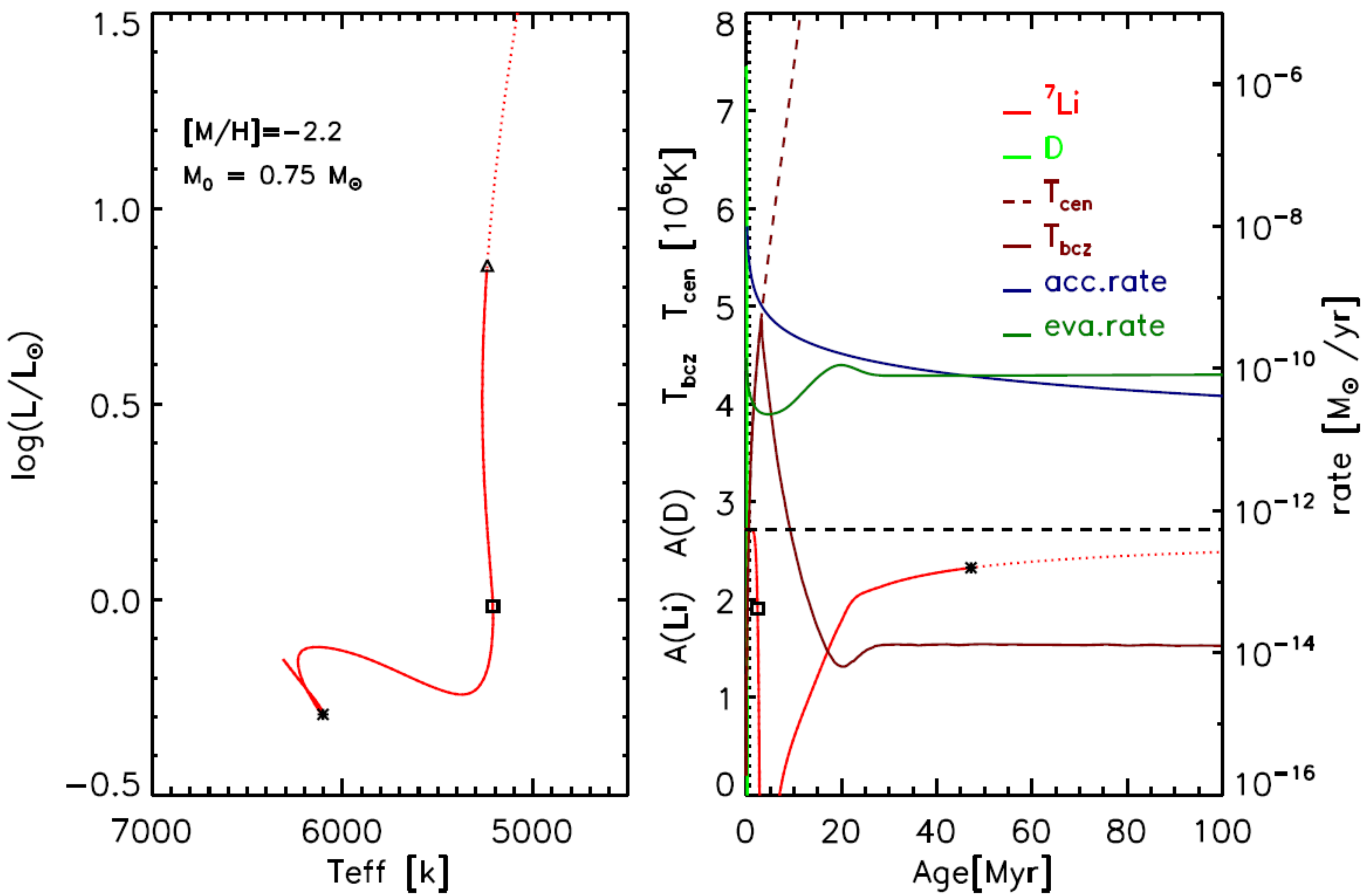

Fu et al. in prep

- **Envelope overshoot**

$$\Lambda_e = 0.3 + (1.5 - 0.3) * f_{cz}$$

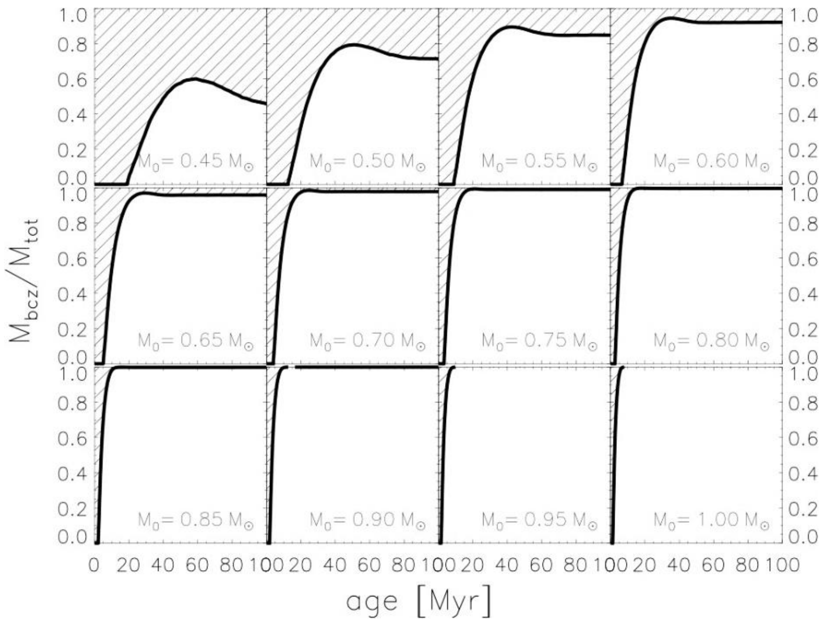

- **accretion**

$$\dot{M}_{acc} = 10^{-8}(t/t_{start})^{-0.85}$$

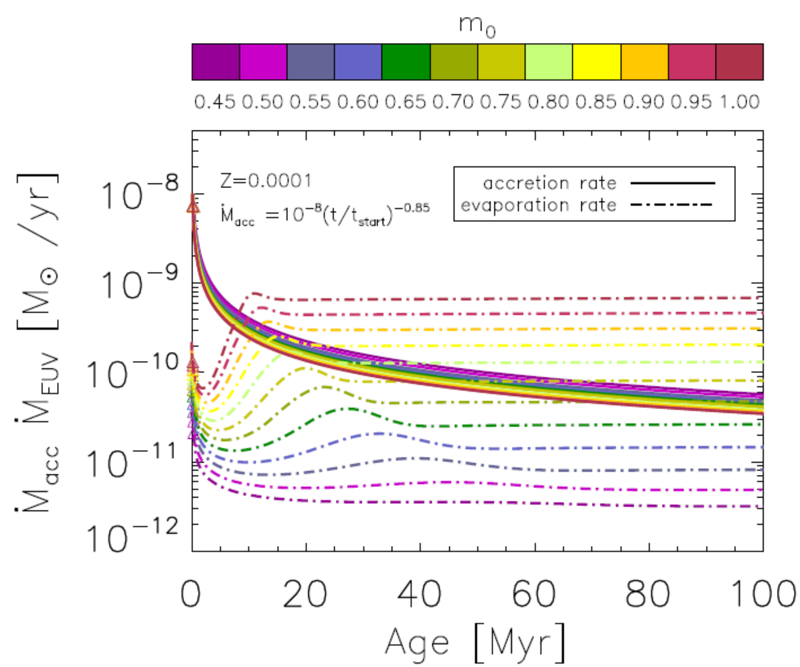

- **EUV photo-evaporation**

$$\dot{M}_{EUV} \sim 4 \times 10^{-10} \left(\frac{\Phi_{EUV}}{10^{41} s^{-1}}\right)^{0.5} \left(\frac{M_*}{M_\odot}\right)^{0.5} \quad M_\odot \; yr^{-1}$$

(Dullemond et al. 2007)

results

stars with initial mass 0.7-0.9 $M_{\odot}$
produce the Spite Plateau

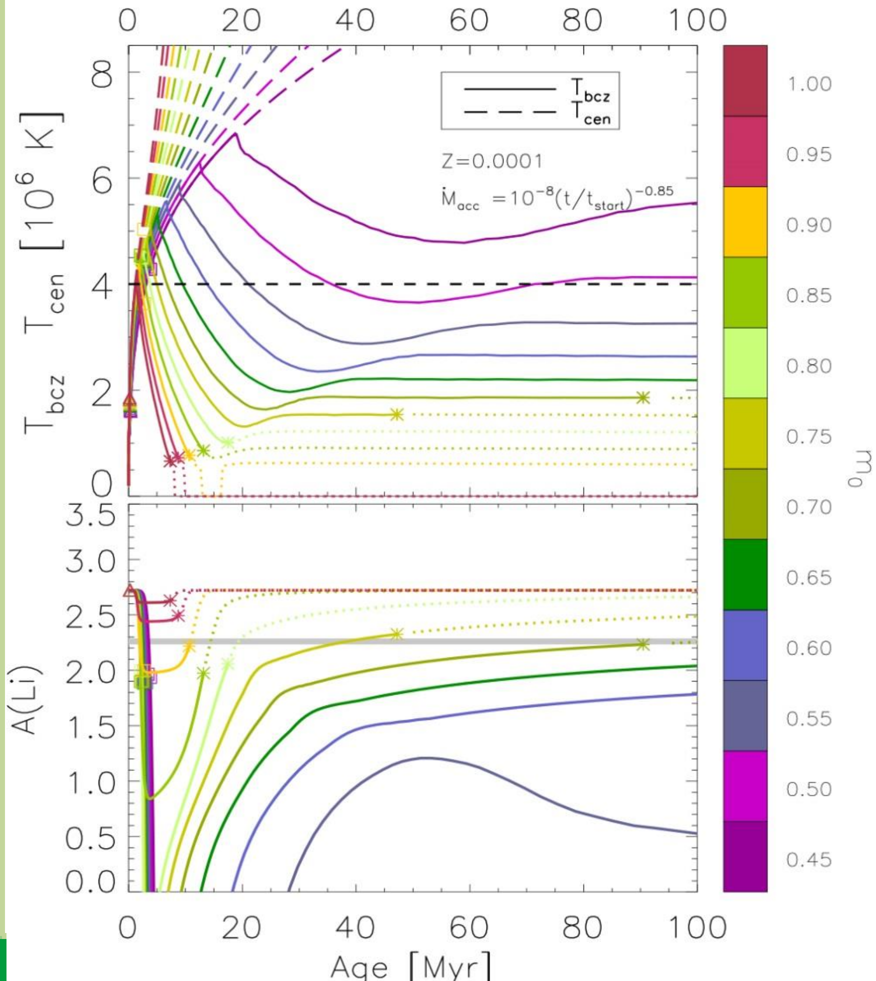

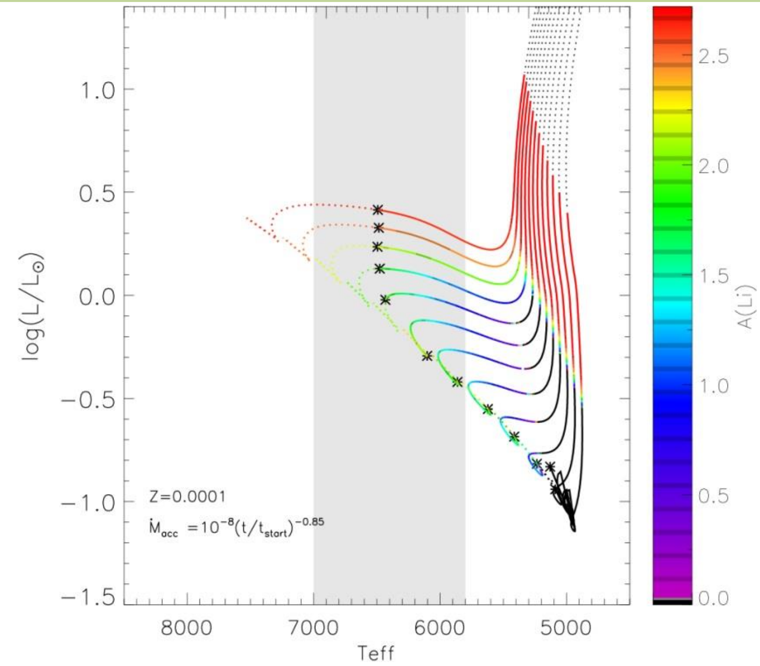

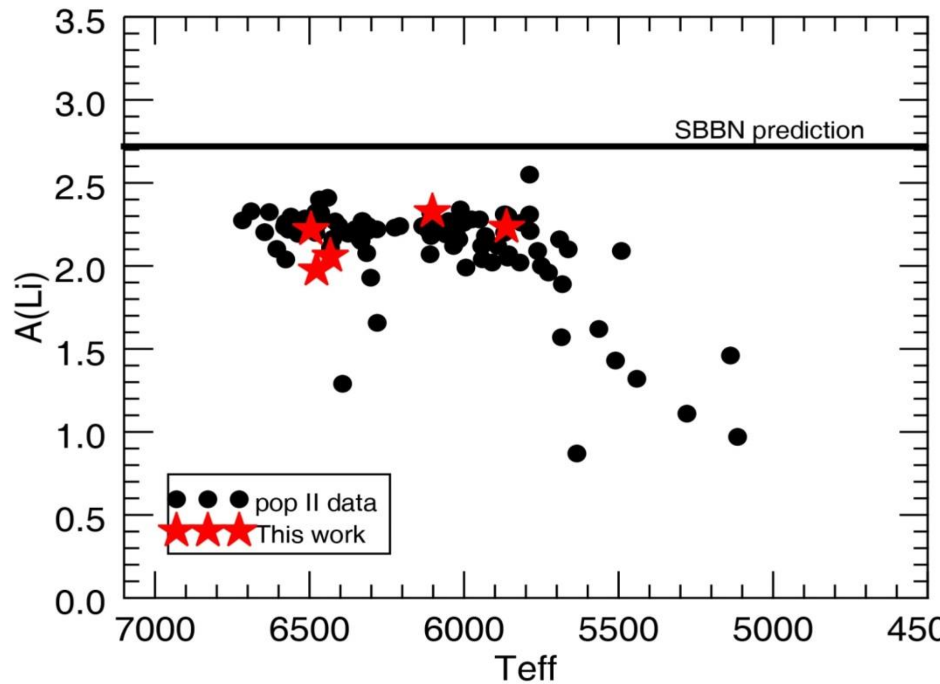

Our model could also explain:

- Low lithium abundance in the planet host stars;
- Li disparities in binary stars;
- Li abundance at very low metallicity and outliers.

RASPUTIN: Resolved And unresolved Stellar PopUlaTIoNs

FIRST APPLICATION OF LINE-DEPTH RATIOS TO DETERMINE STELLAR EFFECTIVE TEMPERATURES WITH H-BAND SPECTRA

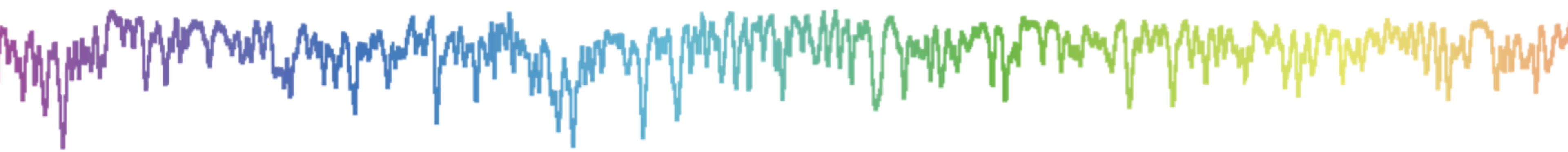

Kei Fukue (The University of Tokyo)

Noriyuki Matsunaga, Ryo Yamamoto, Chikako Yasui, Satoshi Hamano, Naoto Kobayashi (The University of Tokyo), Takuji Tujimoto(NAOJ), Sohei Kondo, Yuji Ikeda (Kyoto Sangyo University), Giuseppe Bono (University of Rome Tor Vergata), Laura Inno (ESO)

Line-depth Ratios

- The effective temperature
  - Fundamental stellar parameter for abundance analysis.
- Spectral line-depth ratios
  - Empirical determination without relying on any stellar models or accuracy of linelist.
  - Reddening-free indicator for determination of Teff.

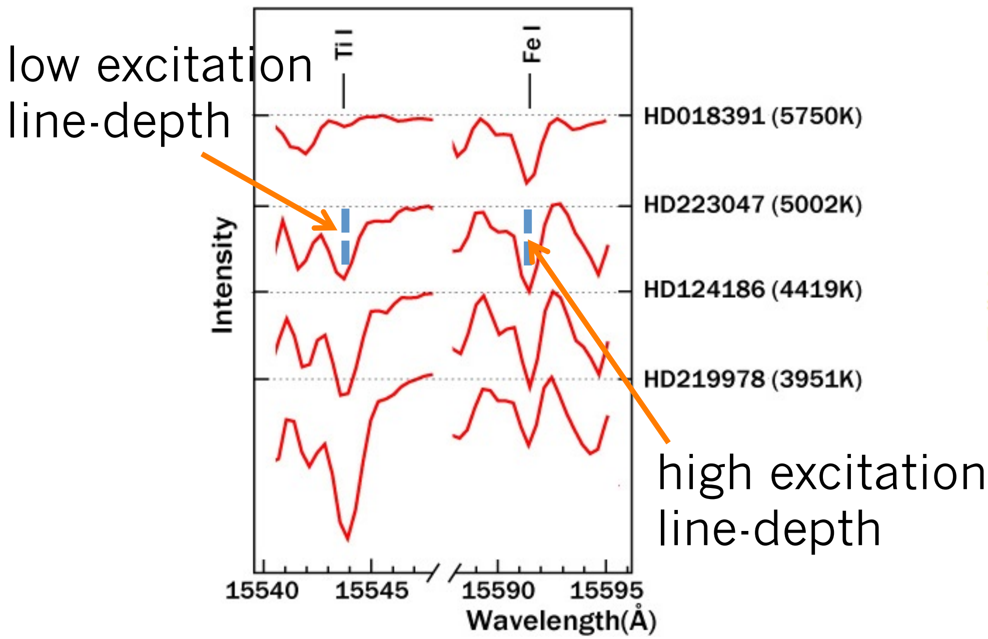

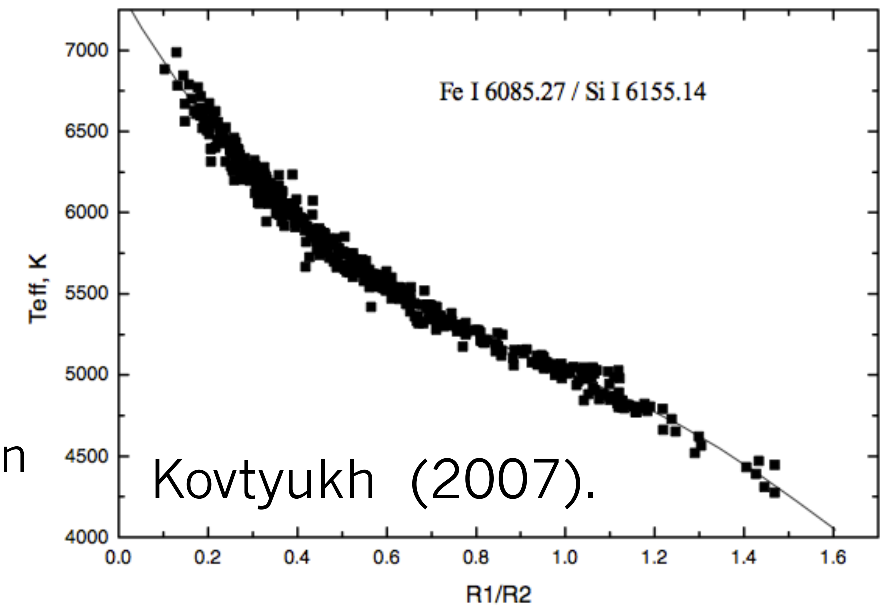

Kovtyukh (2007).

Observation

- Target
  - 12 calibration star
  - Temperature range : 4000 – 6000 K
- Instrument : SUBARU/IRCS
  - Wavelength : H-band (1.46-1.79um)
  - Wavelength Resolution : R=20,000

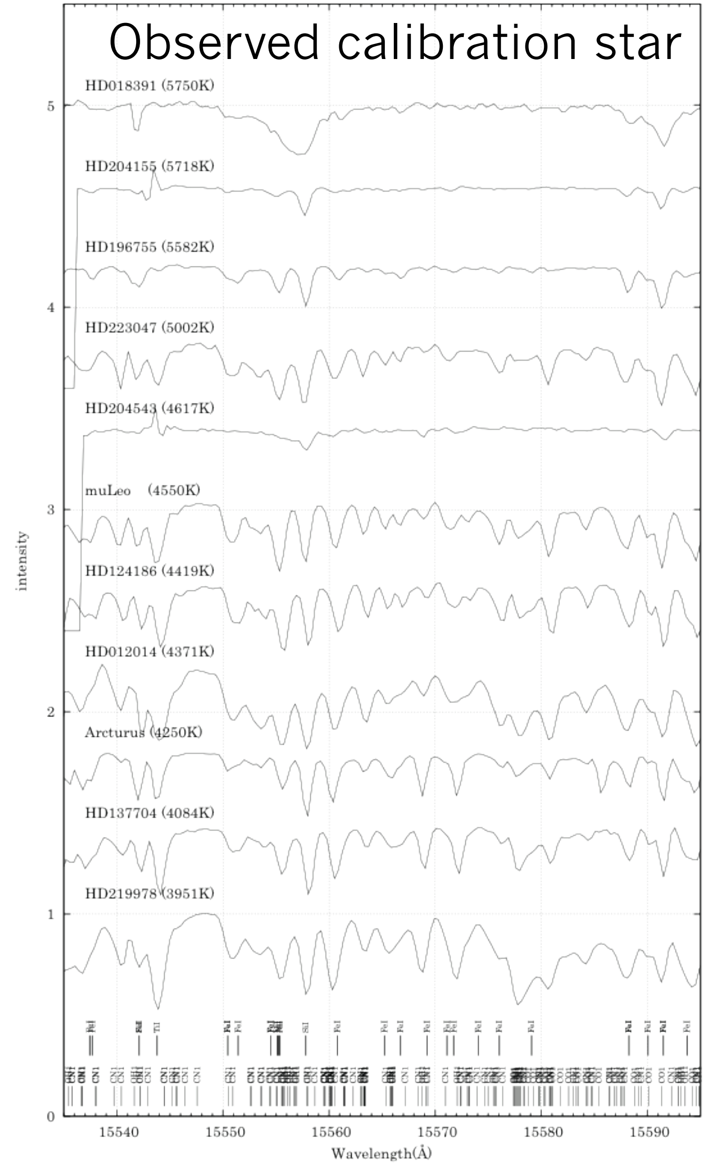

Establishing Temperature Scale

- We measured FeI,SiI,TiI, and more lines.
- We found 7 linear relations with tight correlation
  - uncertainty ~ ±50 K (using all relations)

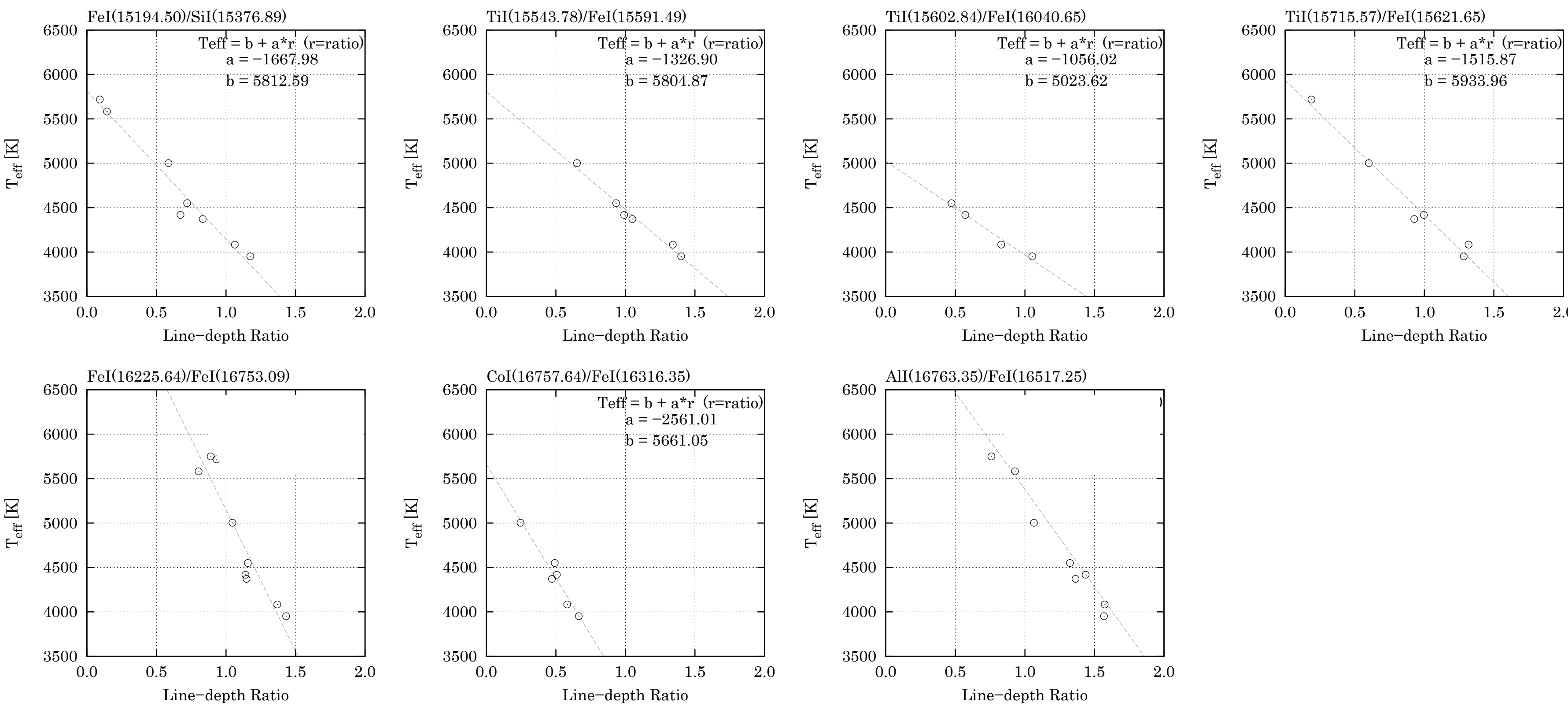

First Application to Galactic Center Cepheids

- Target : cepheids in the Galactic Center
  - new discovered cepheids (Matsunaga et al. 2011)
  - highly reddening objects
- Derived temperature of a cepheid is ～4800K.

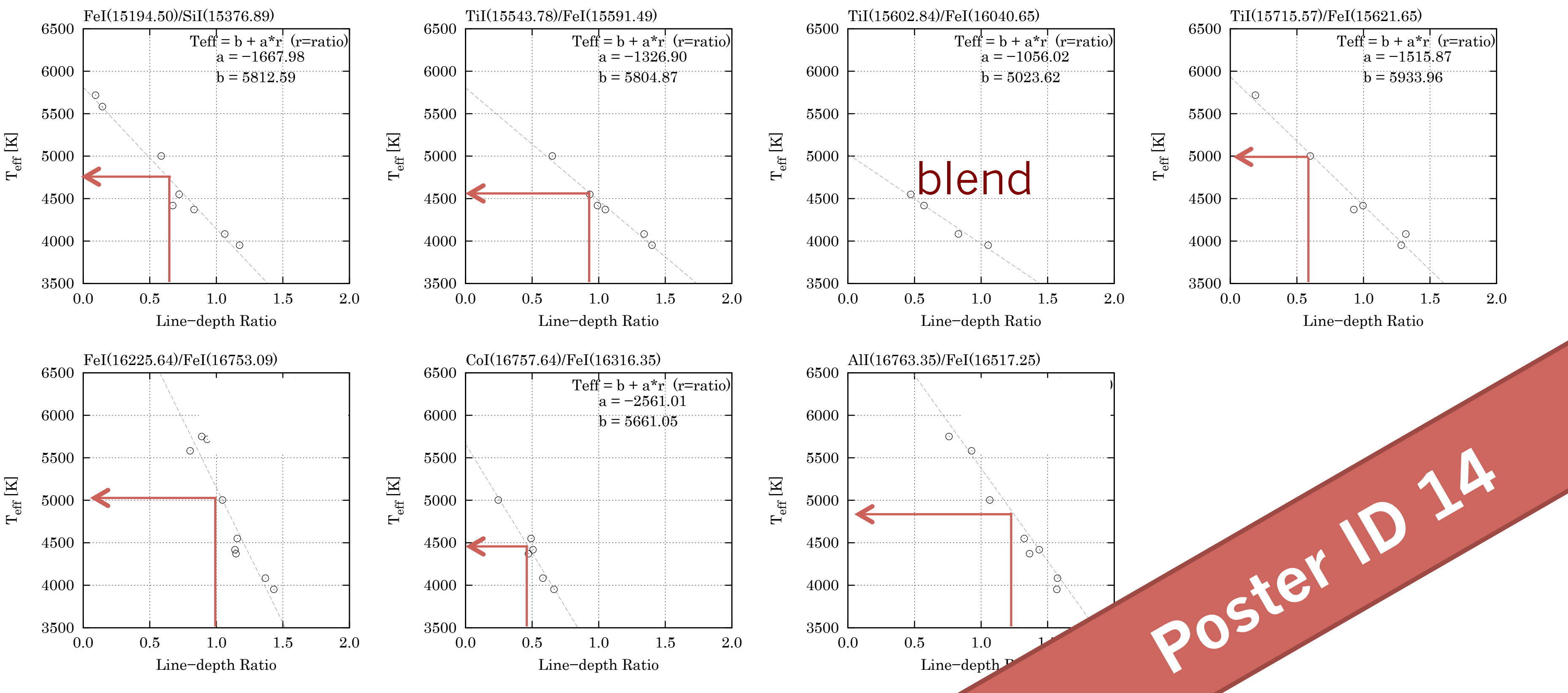

Poster ID 14

The star formation history of NGC 6822

(Poster 15)

Federica Fusco

R. Buonanno, S. L. Hidalgo, A. Aparicio, A. Pietrinferni, G. Bono, M. Monelli, and S. Cassisi

NGC 6822 – data set

Derive the accurate star formation history of the Local Group dwarf irregular galaxy NGC 6822

Data from the ACS onboard on the *Hubble Space Telescope* (P.I. Cannon).
All the fields have the same f.o.v. of 202”x202”.

	NGC 6822
Type	dIrr
$(m\text{-}M)_0$	23.54 ± 0.05
[Fe/H]	-0.9 ± 0.3

Field	Filter	Total exp time (s)	No. images
1 6	F475W	886	2
	F814W	1346	2
2 3 4 5	F475W	1119	2
	F814W	1118	2

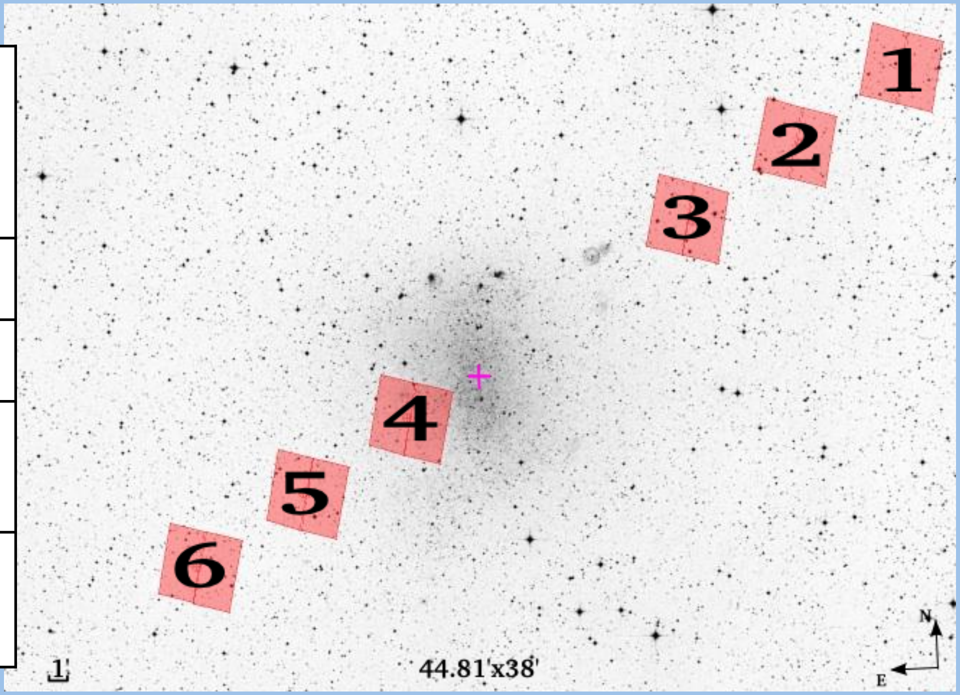

NGC 6822 centre (α , δ)=(19h44m56.6s, -14d47m21s)

NGC 6822 - CMDs

The photometry was performed using DAOPHOT/ALLSTAR/ALLFRAME.

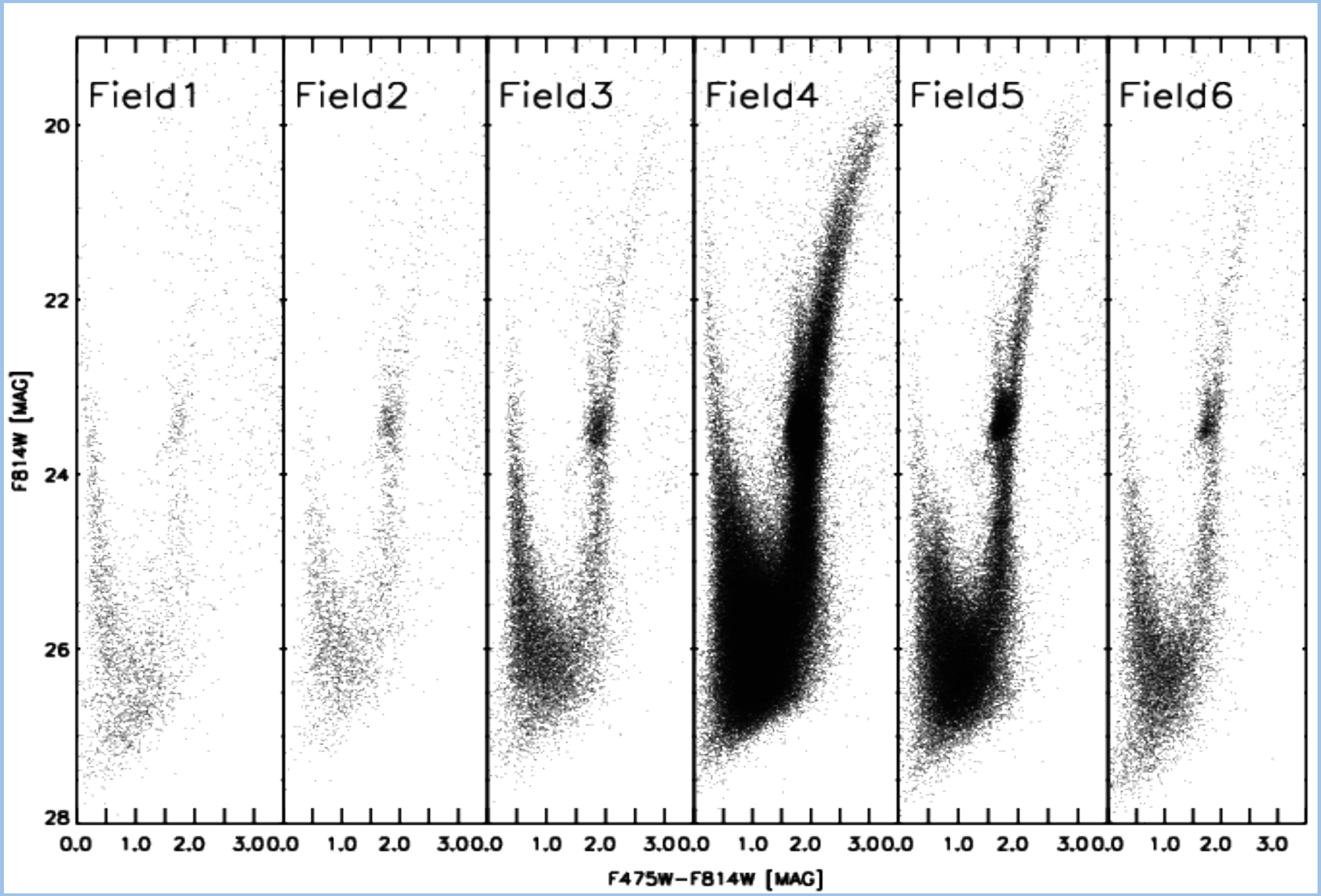

Fusco et al. 2012; Fusco et al. 2014

The SFH of NGC 6822

The SFHs and AMRs are derived using IAC-pop/MinnIAC packages

(Aparicio & Hidalgo 2009; Hidalgo et al. 2011)

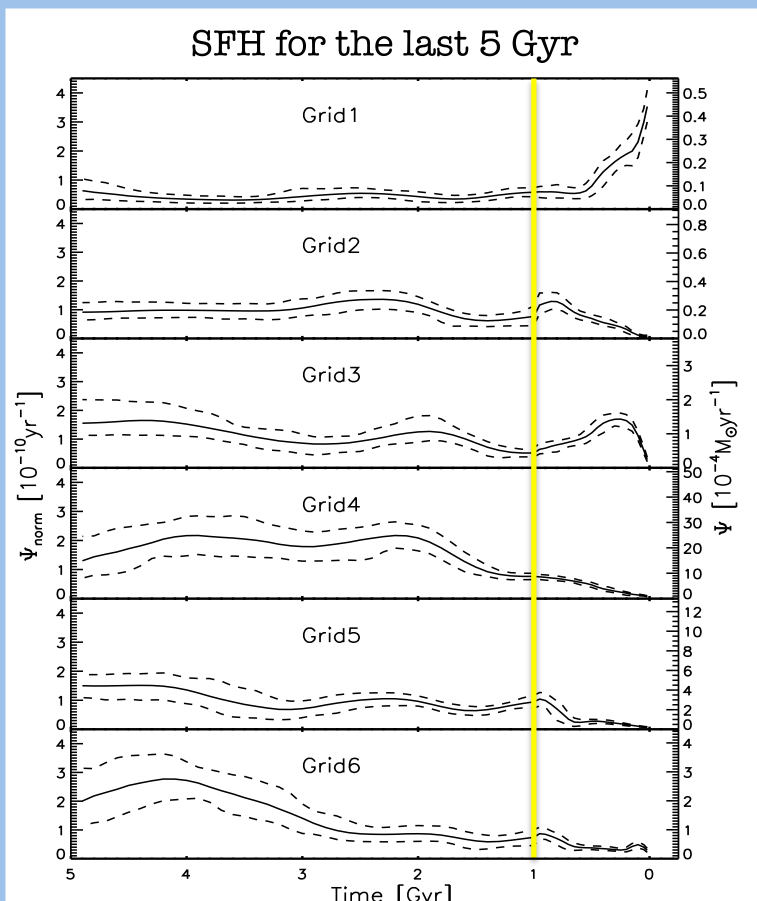

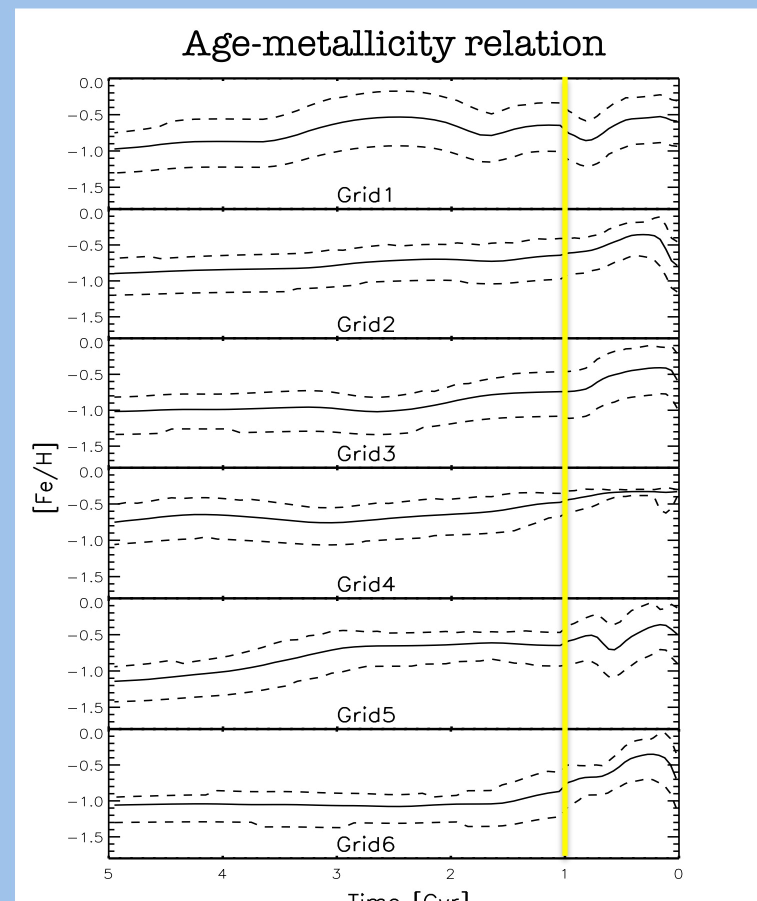

Fusco et al. 2014

Radial properties

- Clear exponential profiles are disclosed in all the cases

- Exception: Grids 1 and 3 show young populations that largely exceed the ones of the surrounding fields

- The scale length r_0 remain constant if we exclude the regions of the most recent SF

- Possible hint of the presence of incipient spiral arms

The integral of $\Psi(t)$ for two time intervals as a function of the galactocentric distance

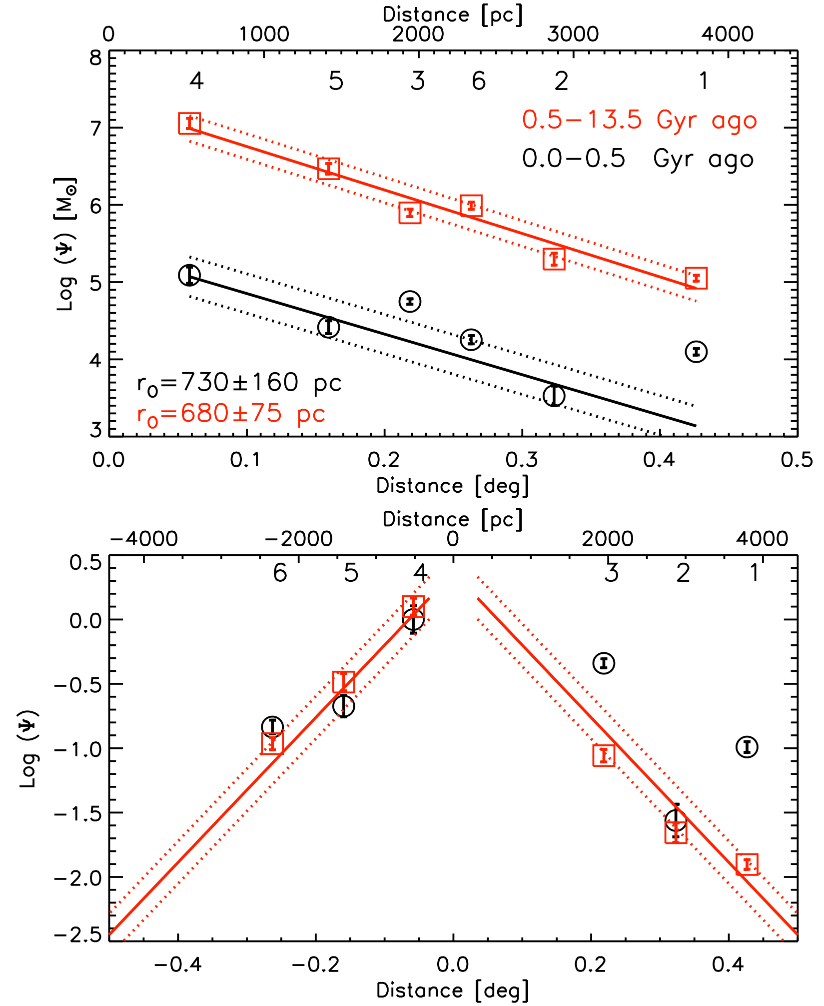

Fusco et al. 2014

Conclusions

- I derived the SFH and AMR for NGC 6822
- The outermost field shows an enhancement in the SFR at very recent epochs, and no change in the metallicity
- The young population has some peculiarity in the cases of Grids 1 and 3

The Stellar Halo of NGC 253

L. Greggio, M. Rejkuba, O.A. Gonzalez, M. Arnaboldi, E. Iodice, M. Irwin, M.J. Neeser, J. Emerson, 2014, AA 562, A73

NGC 253: a bright Spiral galaxy M_B = -20 member of the Sculptor group
From ACS data the distance is D = 3.47 Mpc derived from the I mag. of the RGB Tip

J-band VISTA image (SV data) + previous pointings
The NW side is mapped for the first time.

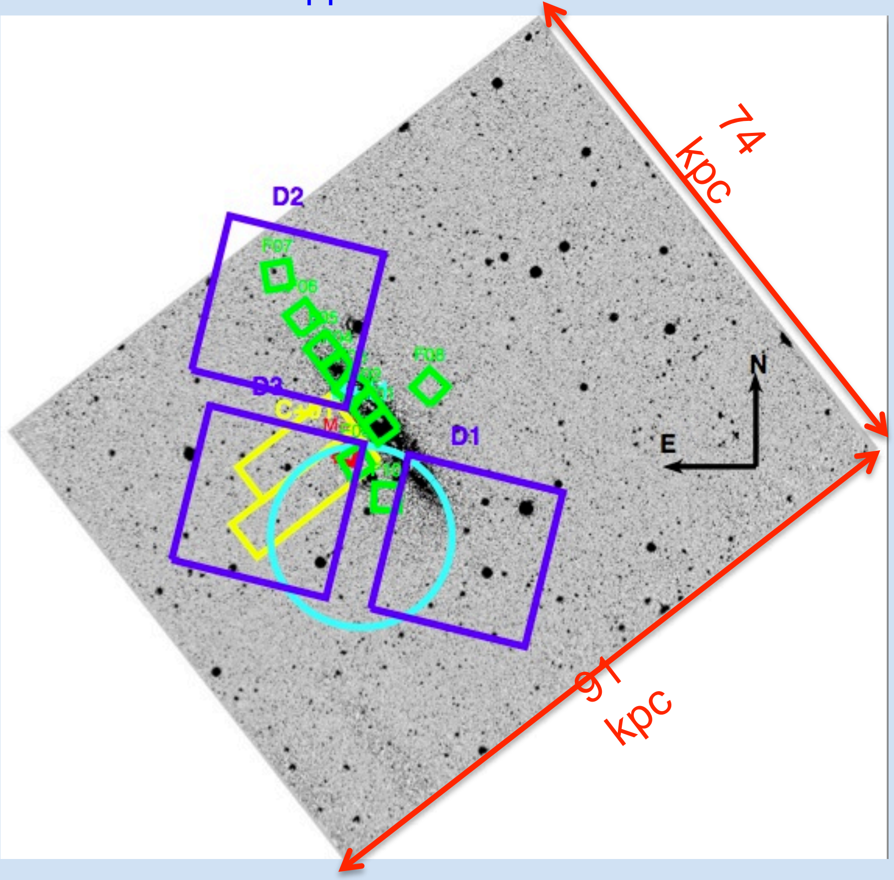

CMD of the bona fide stars:
the photometry down to J~23.5; Z ~ 24.5
samples upper magnitude of the RGB

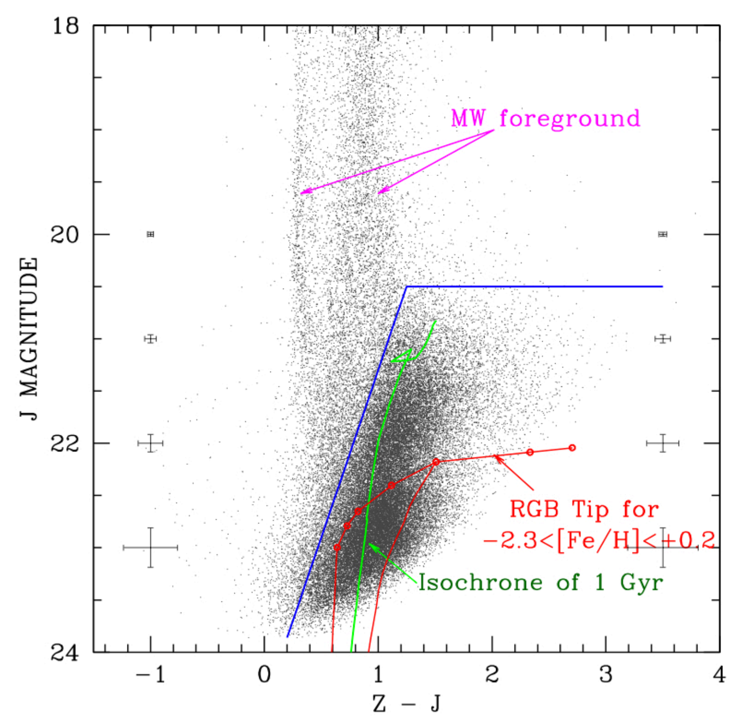

NGC 253 members are found below and to the red of the blue line

Spatially resolved CMD of bona fide stars

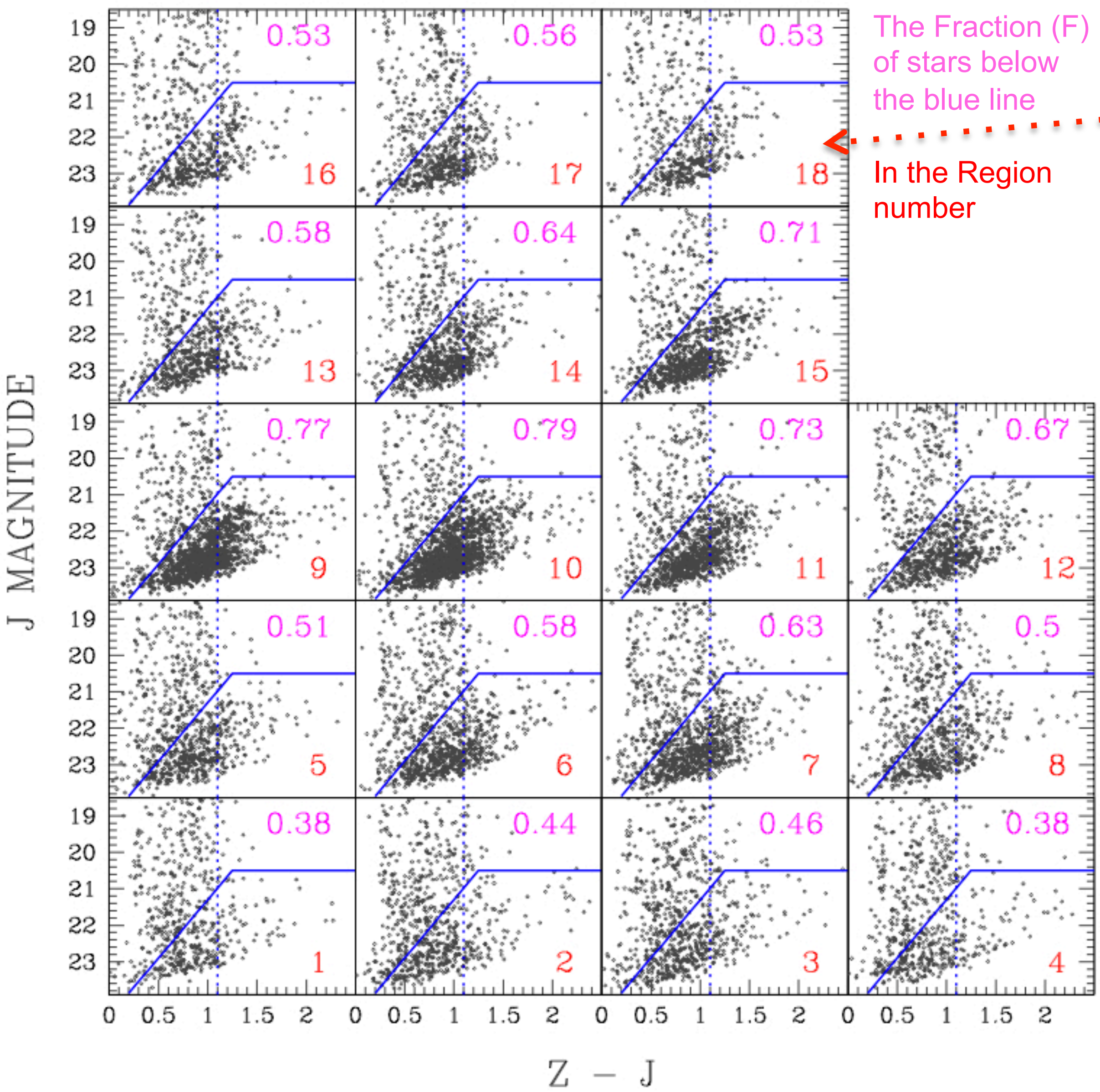

The Fraction (F) of stars below the blue line

In the Region number

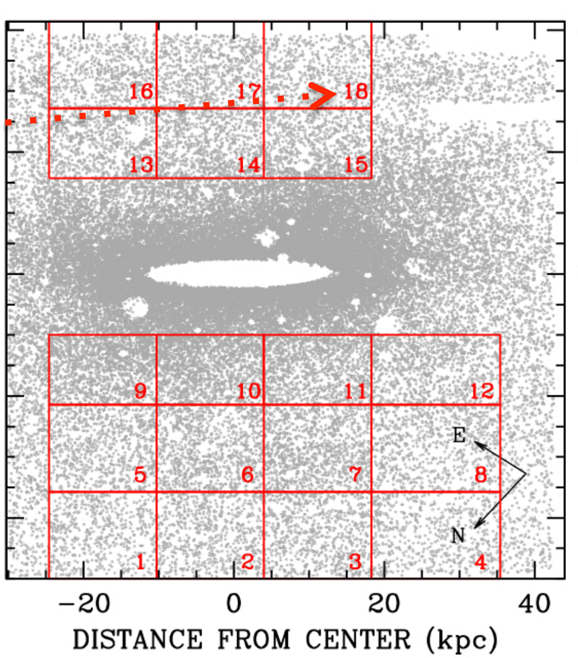

F increases towards the disk as the population of NGC 253 members gets more prominent

In regions 1 to 4 F is still above the expected foreground (~0.3)

NGC 253 members are found up to 50 kpc from the disk

Star counts of NGC 253 members

Profile along the minor axis

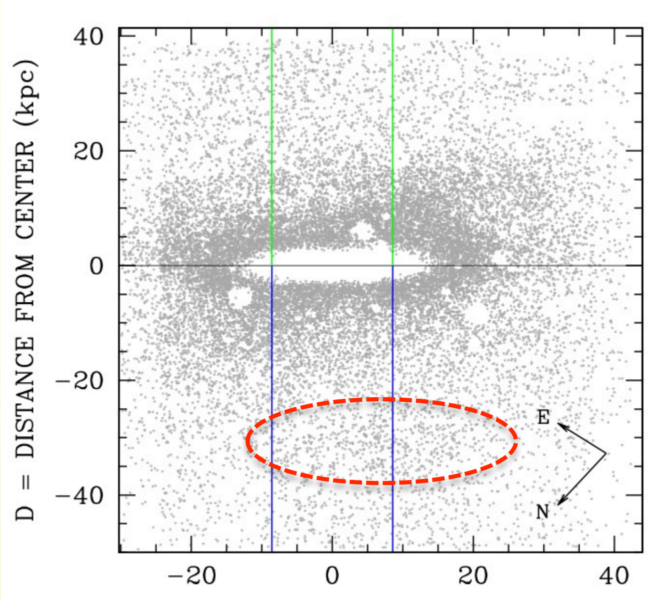

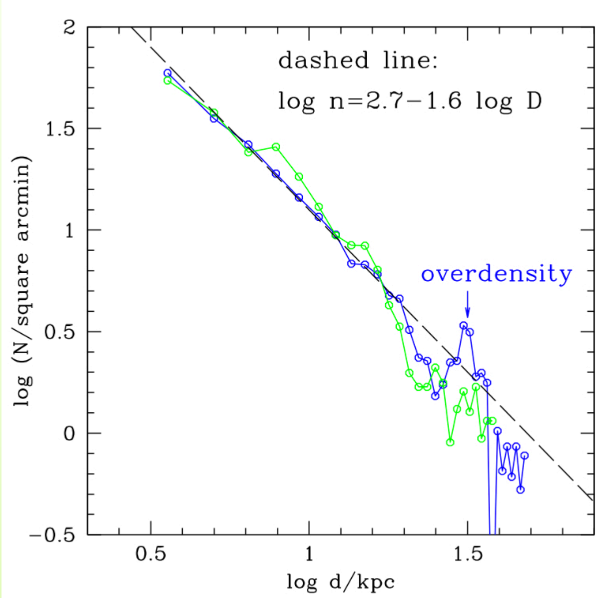

Isodensity contours

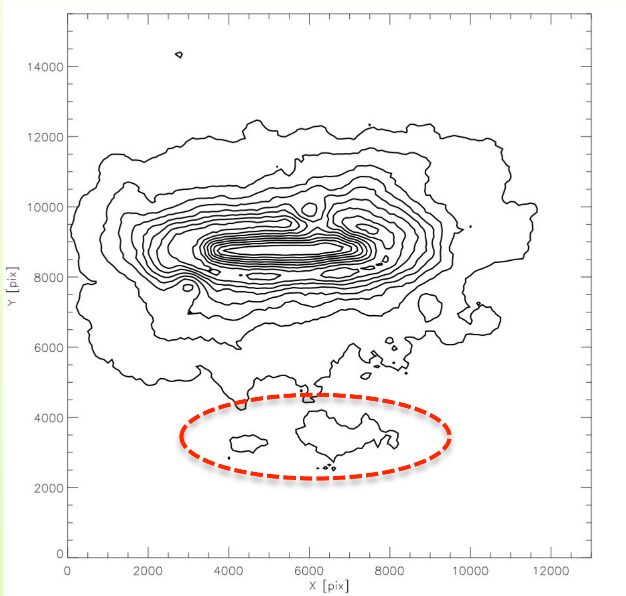

Results:

✓An overdensity is revealed in the outer halo, likely the relic of an accretion event

✓A smooth stellar halo is detected up to 50 kpc from the disk

✓The inner halo shows flattened contours

a widespread population of AGB stars is found up to 30 kpc from the disk

more to be found in the paper

wealth of information is gained with wide field and deep imaging of nearby galaxies

The VMC Survey

Maria-Rosa Cioni, Martin Groenewegen, & The VMC Team

The VMC Survey

VMC pointings

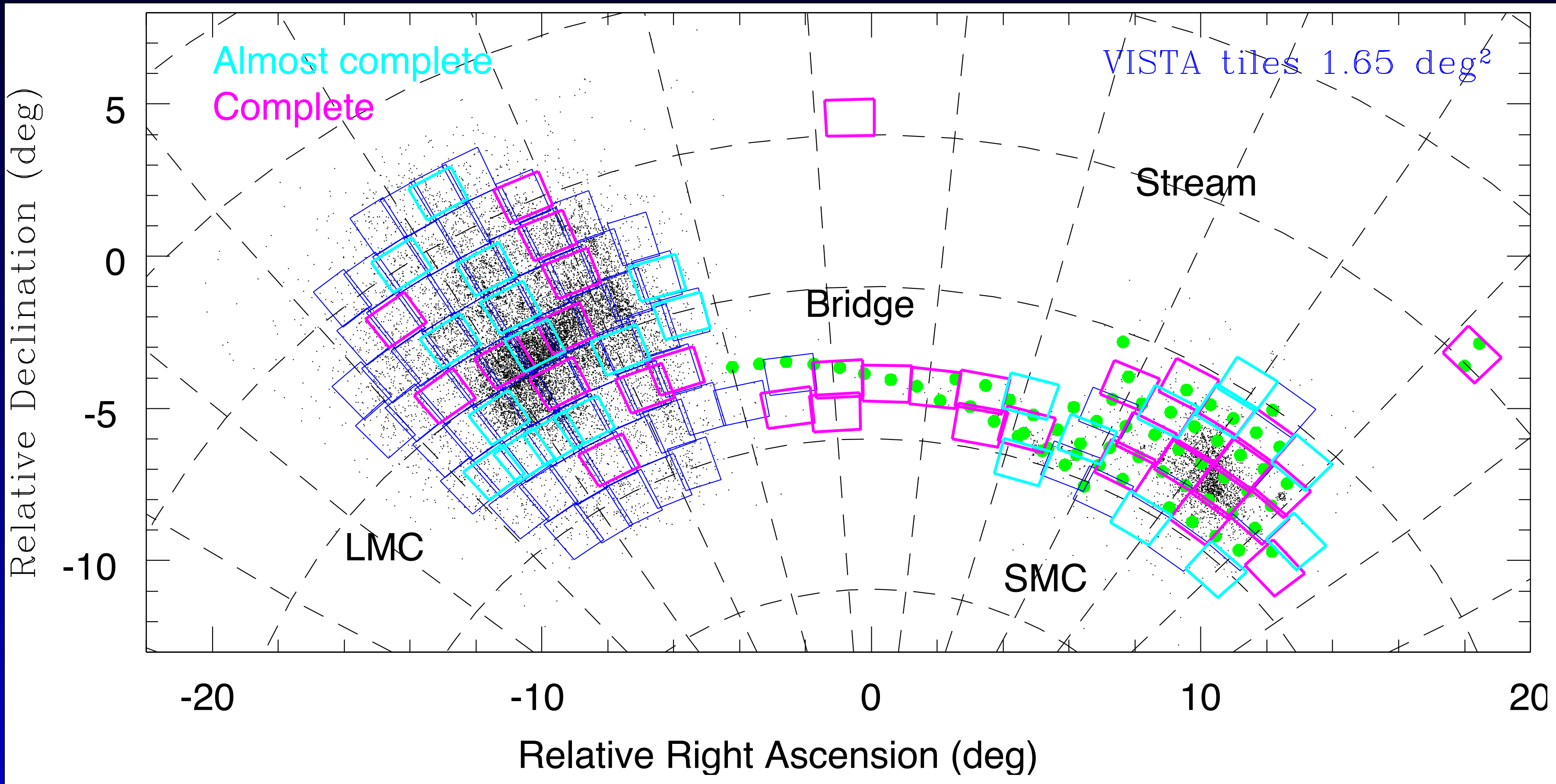

- VST pointings within STEP GTO

VMC

VMC = VISTA Magellanic Cloud Survey

PI. Maria-Rosa Cioni (University of Potsdam, Leibniz-Institut für Astrophysik Potsdam, University of Hertfordshire)

- One of 6 Public Surveys selected by ESO
- Survey in YJK_s of LMC, SMC, Bridge & Stream
- Total area 170 sq.degrees = 110 "tiles"
- 1900 hours allocated
- Started in November 2009, projected end early-2018. Currently 56% complete.
- Already 13 refereed papers, 1 submitted
- DR3 available as of 8 Oct. 2014

VMC: science goals

Primary:

- Determine spatially resolved SFH and AMR
- Interaction of MCs (and with our Galaxy)
- 3D picture: RC, TRGB, RR Lyrae and Cepheids

Secondary:

- Evolved stars (AGB, post-AGB, PNe)
- Clusters
- Quasars
- Proper motion

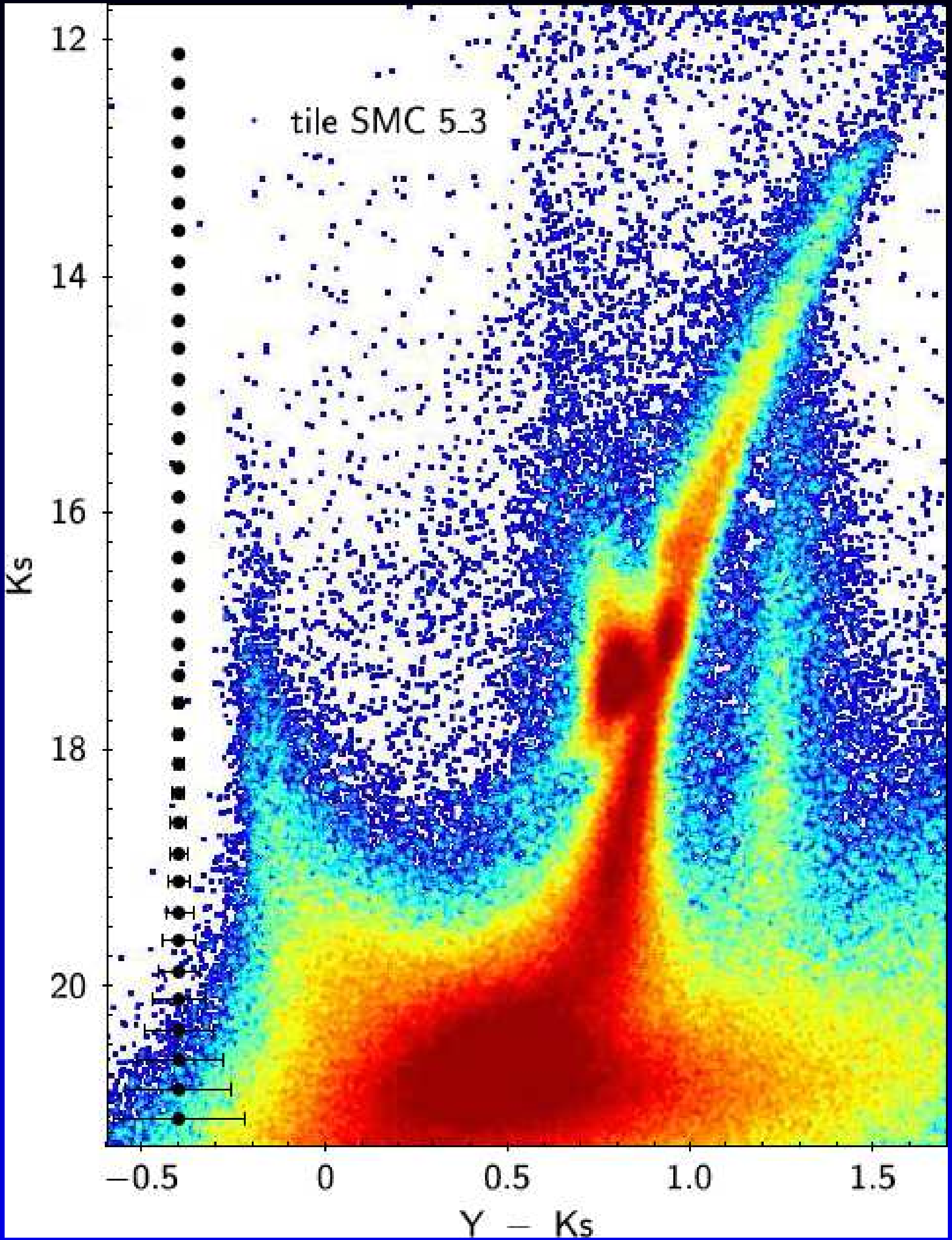

Derive SFH and AMR from deep CMDs.

Variability studies

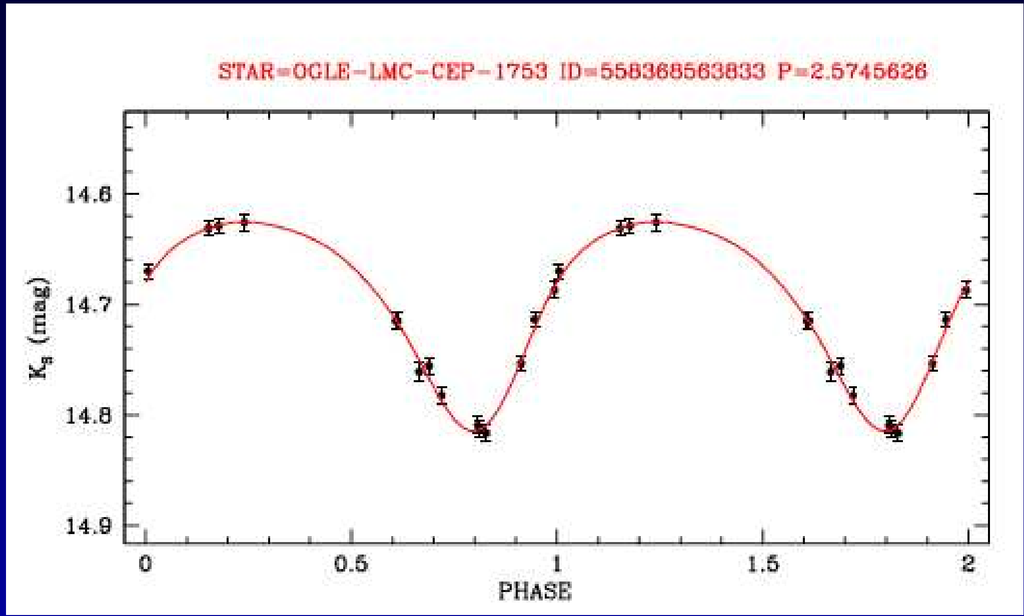

12 epochs in K_s, typically over 1 year, are ideal for studies of RR Lyrae and Cepheids (Period known from OGLE).

On Optical and NIR Selection of Young Clusters in Grand-Design Spirals

Preben Grosbøl, ESO
Horacio Dottori, UFRGS

2014-10-13/P5D
ESO, Garching

<u>Outline:</u>

- Main issues
- HST vs. HAWK-I comparison
- Result and conclusions

Young NIR clusters and Issues

- Young clusters seen in NIR
  - ✔ Massive, very young, highly extinct clusters
  - ✔ Mainly in arm regions of grand-design spirals
- Issue
  - ✔ Not seen in HST data
- Possible reasons
  - ✗ Resolution effects
  - ✗ Extinction – visual vs. NIR
  - ✗ Only in grand-design spirals
- Check by detailed comparison
  - ✔ HST images vs. HAWK-I K-maps

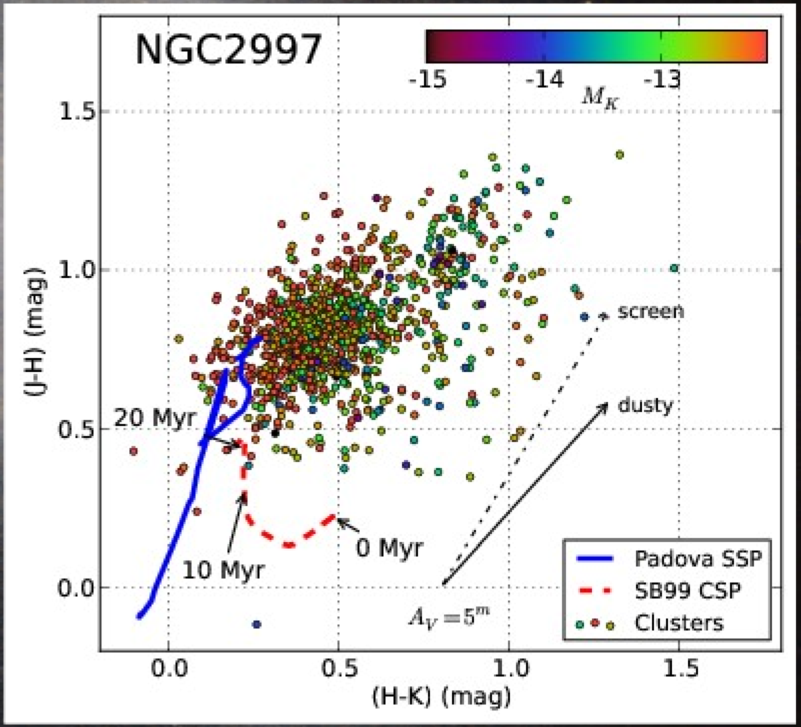

Visual vs. NIR Colors

NGC 1300

HST

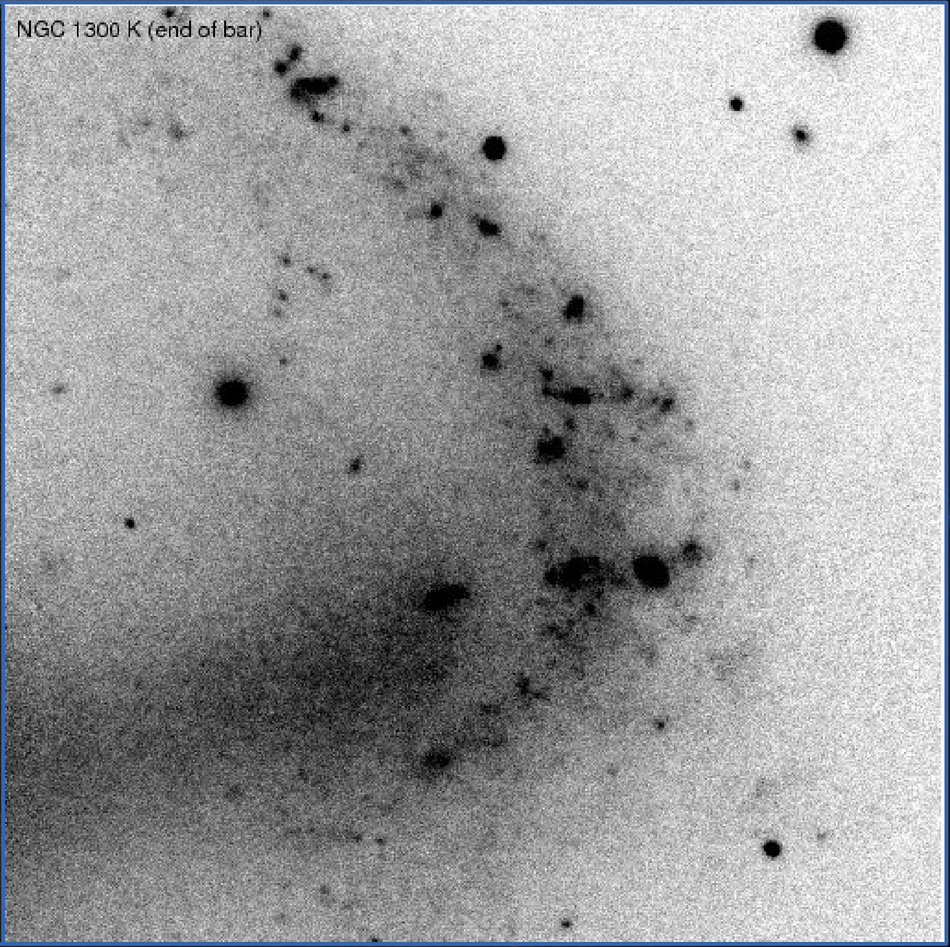

VLT HAWK-I Ks band

HST vs. HAWK-I comparison

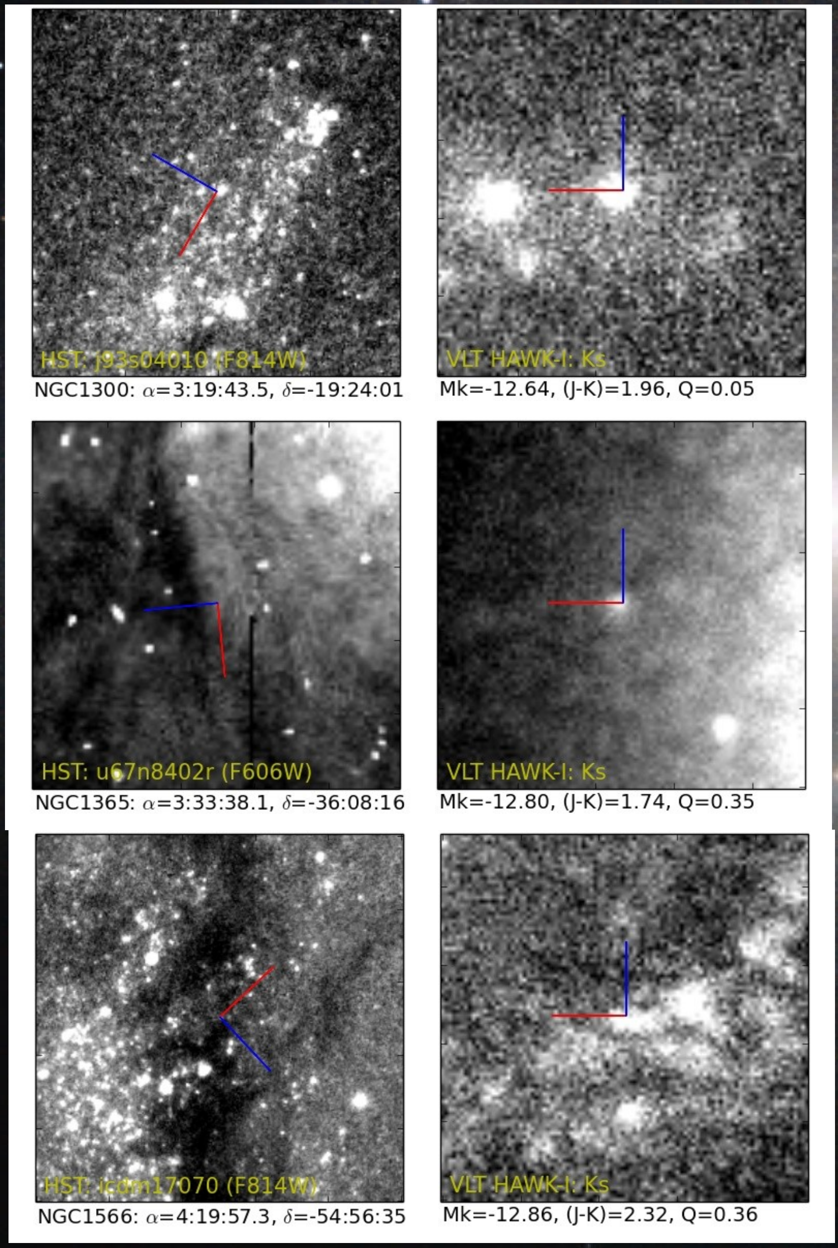

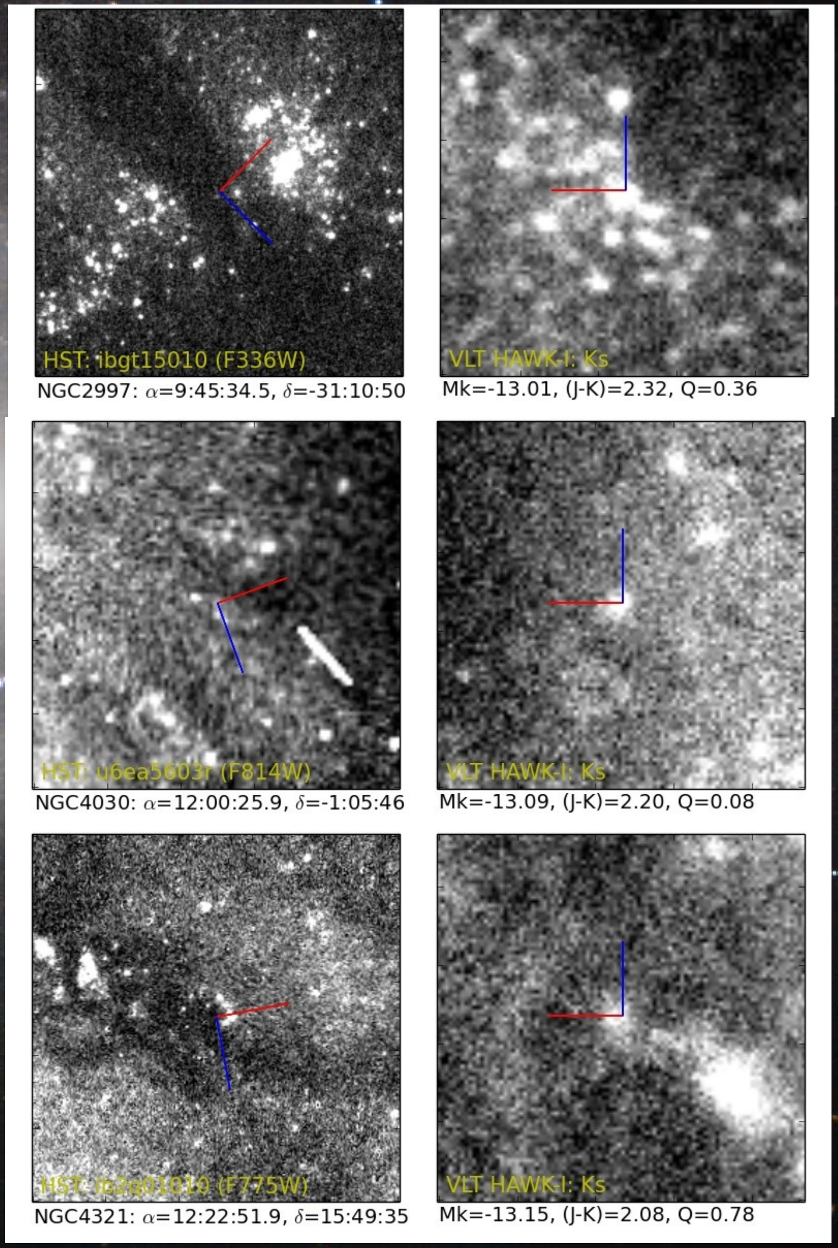

Results and Conclusions

- Results of comparison
  - Majority (i.e. >70%) of very young, massive cluster complexes are located near dust or in dust lanes on HST images

Galaxy	HST drz	Fields	Sources	Dust lane	No dust	Shallow	Bkg
NGC 1300	10	2	17	9	1	0	7
NGC 1365	110	7	17	14	1	2	0
NGC 1566	42	3	39	27	4	5	3
NGC 2997	22	5	20	17	0	3	0
NGC 4030	6	2	7	7	0	0	0
NGC 4321	111	11	42	32	0	10	0
NGC 7424	8	3	14	3	2	8	1
Total	303	33	156	109	8	28	11

- Conclusions
  - The very young, massive cluster complexes seen in NIR are too extinct to be observed in visual bands e.g. by HST
  - Resolution is NOT the major issue (slight reddening of (H-K) may occur)
  - Sample available cannot determine if the very massive clusters are mainly seen in grand-design spirals due the stronger perturbations in their arms

Understanding obscuration in star forming galaxies

Aleksandra Hamanowicz, A.Prof. Andrew Hopkins,
Dr Sarah Brough, Dr Matthew Owers

Poster:20

Warsaw University Observatory, Australian Astronomical Observatory

14 October 2014

Balmer Decrement and galaxy mass

MOTIVATION:

1. Tracking the history of star formation in galaxies
2. Comparing evolution in time of dust mass in galaxies (Dunne et al. 2011), with evolution of obscuration
3. Determining relation (if any exist) between Balmer Decrement and dust mass in star forming galaxies

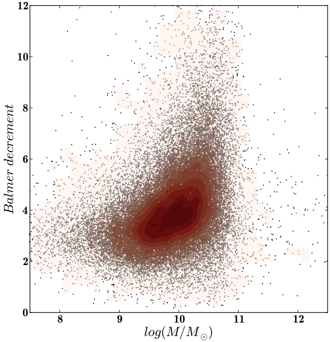

Mass -limited samples

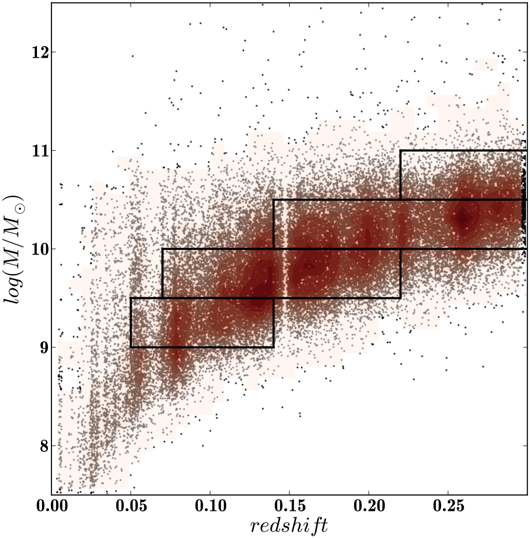

Balmer Decrement evolution with redshift

(a) Evolution of obscuration in galaxies

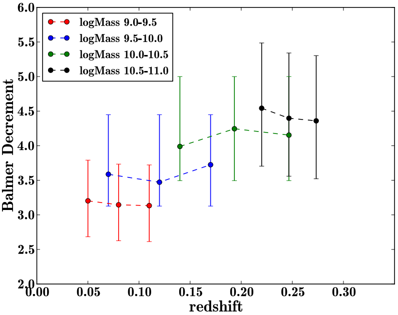

(b) Evolution of obscuration considering galaxy "final mass"

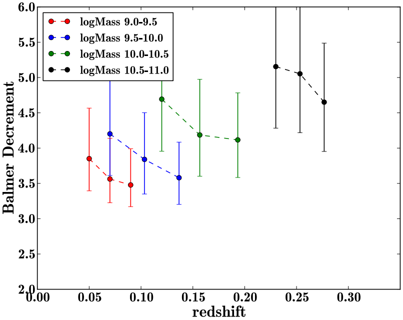

Conclusions

- Consistent with earlier work (Sobral et al., 2011; Gunawardhana et al., 2012) we find a strong relationship between galaxy mass and obscuration and demonstrate that this relationship evolves little, if at all, over $0 < z < 0.3$.
- Using the galaxy "final mass" estimates, we demonstrate the increase in the level of obscuration for a galaxy as it evolves.
- We now plan to compare Balmer decrement and dust masses directly using the formalism of Tuffs et al., (2004) and Popescu et al., (2011) to quantitatively explore the link between dust content and obscuration.

How to measure the initial mass function with high precision

Nikolay Podorvanyuk[1]
Igor Chilingarian[2,1]
Ivan Katkov[1]
[1]Sternberg Astronomical Institute, Moscow State University (Russia)
[2]Smithsonian Astrophysical Observatory, Harvard-Smithsonian Center for Astrophysics (USA)

RASPUTIN, ESO, 2014

A new method for new estimates

- We developed a new technique for the determination of the low-mass slope (α_1; $M_* < 0.5M_\odot$) of the present day stellar mass function (PDMF) using the pixel space fitting of integrated light spectra

We need IMF = PDFM!!!

- This technique can be used to constrain the IMF of stellar systems with relaxation timescales exceeding the Hubble time (e.g., globular clusters where a mass segregation have not yet finished)

- It could be used for objects with older stellar populations (t > 8 Gyr) where massive stars affecting the variable high-end IMF slope have already evolved into stellar remnants, for example, massive elliptical galaxies

An extension of NBURSTS

- Our technique was developed as an extension of the NBURSTS package (Chilingarian et al. 2007a,b) -- an approach to determine the parametrized line of-sight velocity distribution (LOSVD) and star formation history (SFH) of unresolved stellar populations by means of the **full spectral fitting** in the pixel space.

An extension of NBURST

We provide two versions of the technique:

(1) a fully unconstrained determination of the age, metallicity and α_1

(2) a constrained fitting by imposing the externally determined mass-to-light ratio (M/L) of the stellar population.

Monte-Carlo simulation

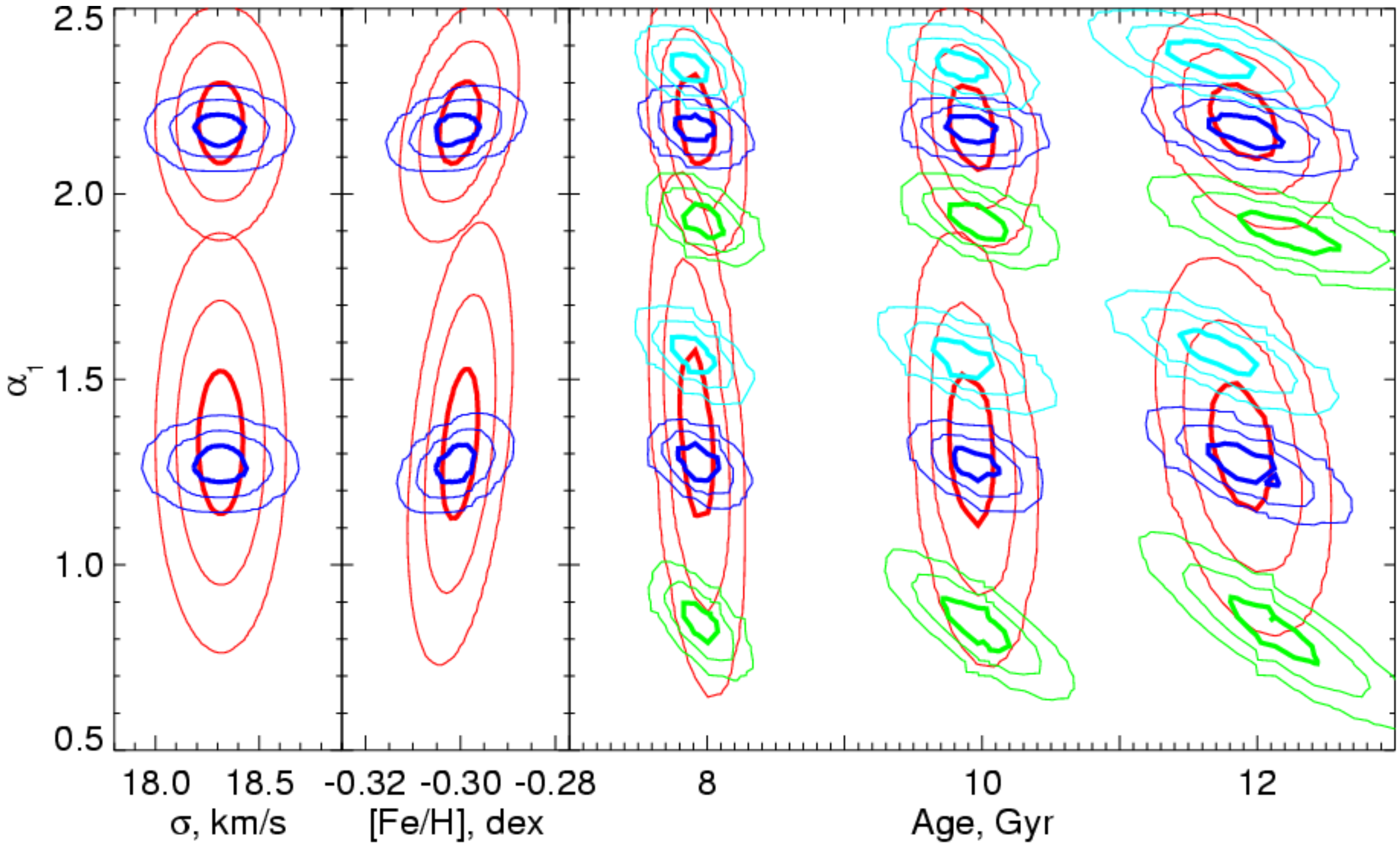

(a) age, metallicity and α_1 can be precisely determined by applying the unconstrained version of the code to high signal-to-noise datasets (S/N=100, R = 7000 yield α_1~0.1);

(b) the M/L constraint significantly improves the precision and reduces the degeneracies, however its systematic errors will cause biased α_1 estimates

The distribution of α_1-sensitive information

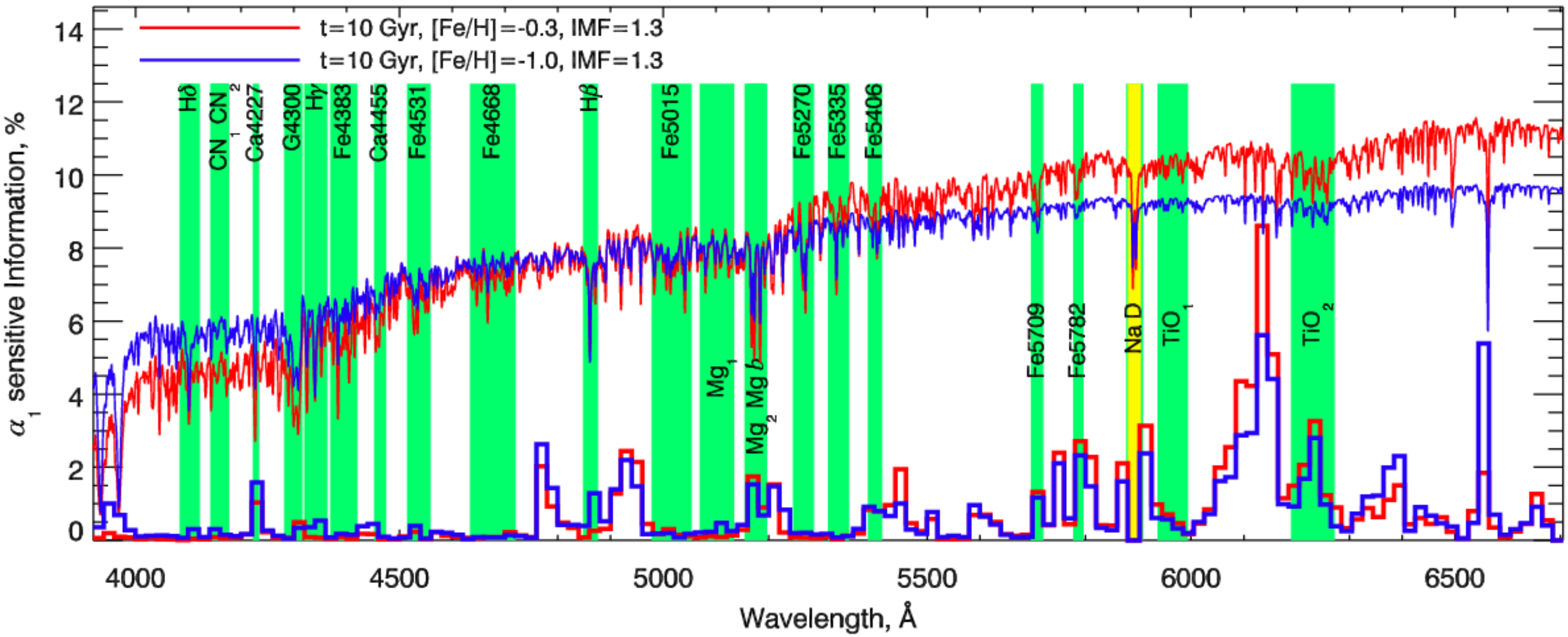

IMF-sensitive information is not associated with Lick indices

Most of the IMF-sensitive spectral regions are those containing numerous but relatively faint absorption lines sensitive to the surface gravity in the atmospheres of late type (GKM) stars. These lines associated with CaI, VI, CoI, NiI and TiI absorption lines

Real data: galactic GC

(1) intermediate resolution (R=1300) Galactic GC spectra from Schiavon et al. (2005) obtained at the 4 m Blanco telescope at CTIO in the wavelength range 3900< λ <6500 A

None of the clusters had t_{rel} > 4 Gyr, and those spectra were integrated and extracted only in the cluster core region.

We could not obtain any reliable estimates of α_1 values in these objects but only use them to evaluate statistical errors of the techniques for spectra of such a type. The statistical uncertainties of the first version of our technique turned to be about α_1~0.3–0.5. Fixing the M/L values reduced them down to 0.15.

Real data: UCD

Intermediate resolution (R=1500–2000) high signal-to-noise ratio spectra (3900< λ <6800 A) of Fornax and Virgo cluster UCDs obtained with Gemini GMOS-N/GMOS-S

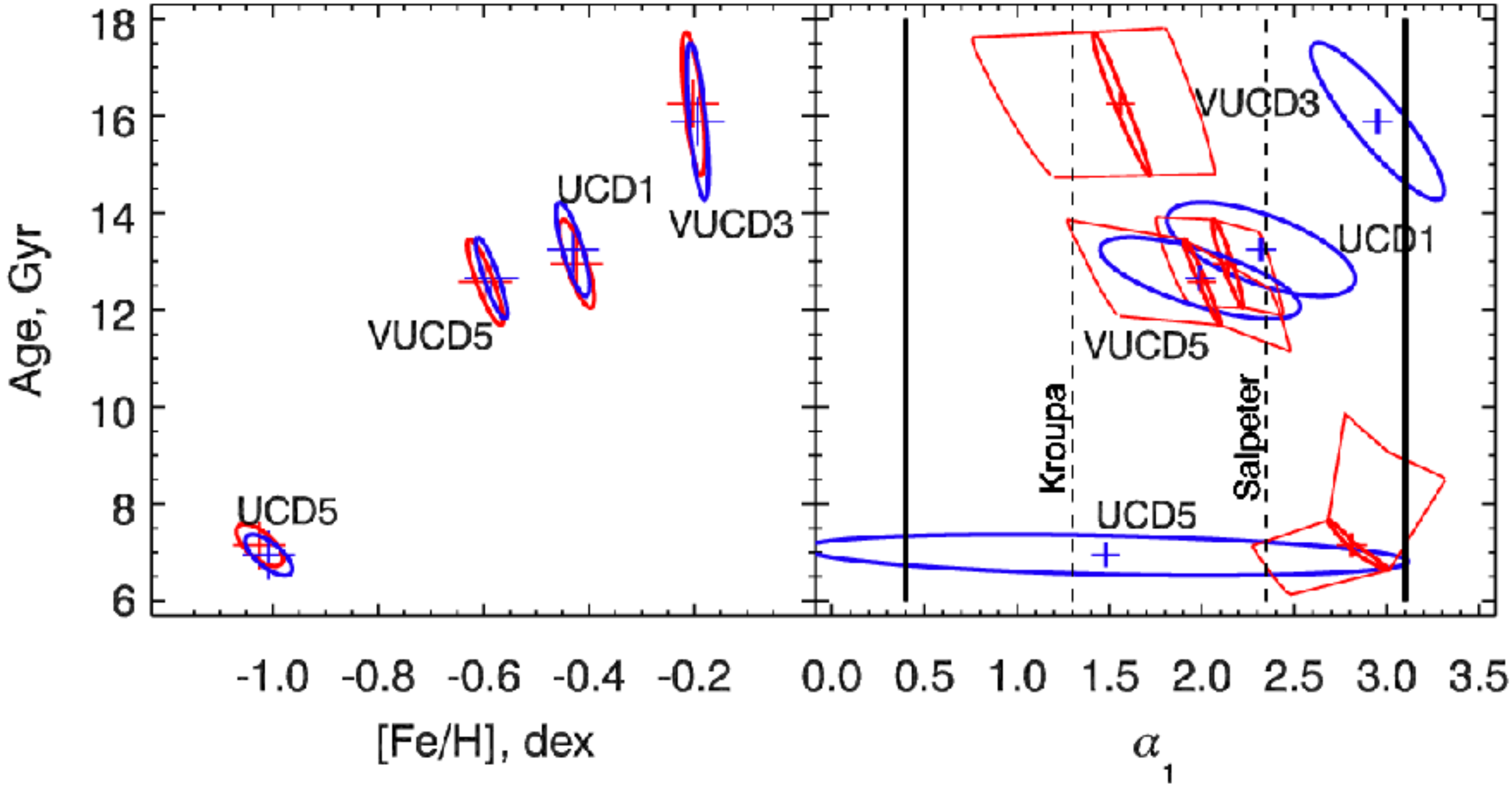

Read data: 1000 massive elliptical galaxies

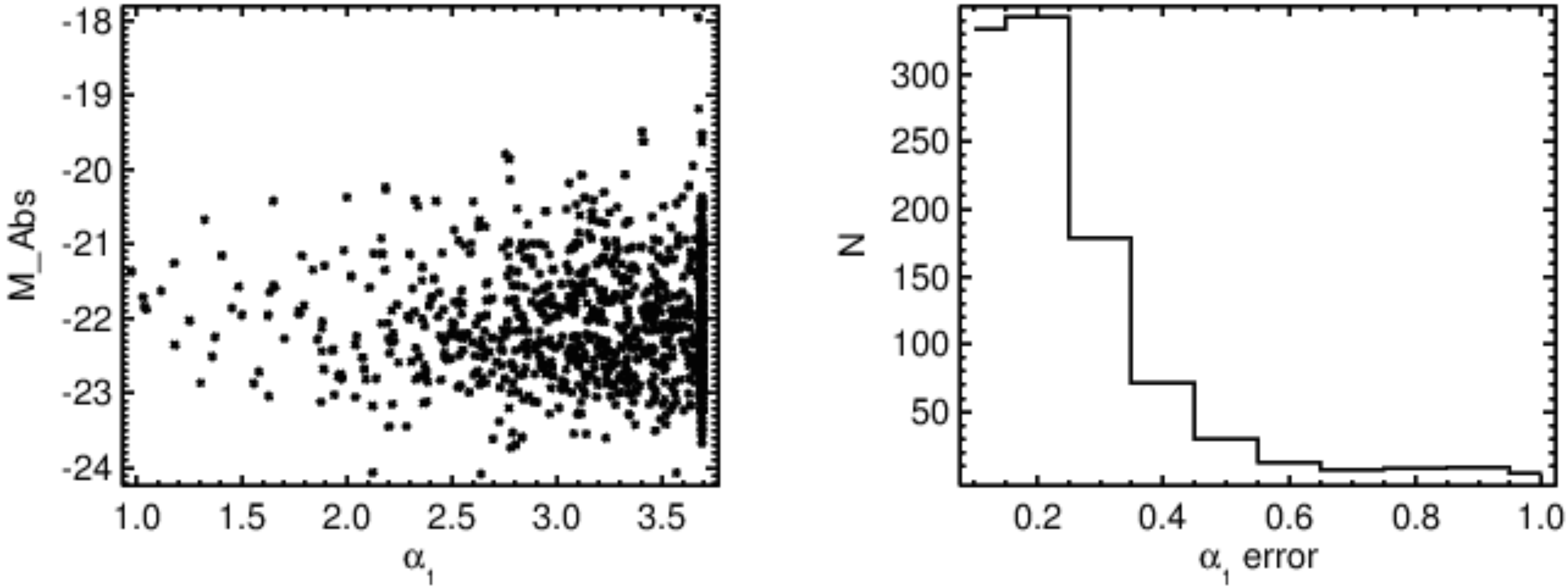

Determination of the low-mass IMF slope using unconstrain version of our technique for 1000 giant elliptical galaxies form SDSS: the low-mass IMF for the most of objects is bottom-heavy (α_1 ~ 3.0…3.5). The most of these estimates has α_1 error 0.1…0.3.

KEYPOINT: We do not see any evidence that the low mass IMF slope in giant ellipticals depends on their mass how it was reported in Cappellari et al. (2012, Nature, 484, 485)

Thank you for attention!

Podorvanyuk N., Chilingarian I., Katkov I.,

A new technique for the determination of the initial mass function in unresolved stellar populations. MNRAS, 2013, 432 (4): 2632-2638. arXiv:1303.0897

Have a nice evening!